

Fall 2010

Nonlinear control strategy for a cost effective myoelectric prosthetic hand

Cristian Federico Pasluosta

Follow this and additional works at: <https://digitalcommons.latech.edu/dissertations>

 Part of the [Biomedical Engineering and Bioengineering Commons](#), and the [Robotics Commons](#)

NONLINEAR CONTROL STRATEGY FOR A COST EFFECTIVE
MYOELECTRIC PROSTHETIC HAND

by

Cristian Federico Pasluosta, BS.

A Dissertation Presented in Partial Fulfillment
of the Requirements for the Degree
Doctor of Philosophy

COLLEGE OF ENGINEERING AND SCIENCE
LOUISIANA TECH UNIVERSITY

November, 2010

UMI Number: 3438520

All rights reserved

INFORMATION TO ALL USERS

The quality of this reproduction is dependent upon the quality of the copy submitted.

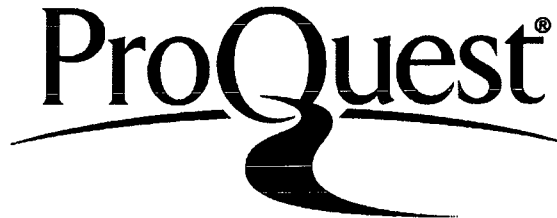
In the unlikely event that the author did not send a complete manuscript and there are missing pages, these will be noted. Also, if material had to be removed, a note will indicate the deletion.



UMI 3438520

Copyright 2011 by ProQuest LLC.

All rights reserved. This edition of the work is protected against unauthorized copying under Title 17, United States Code.



ProQuest LLC
789 East Eisenhower Parkway
P.O. Box 1346
Ann Arbor, MI 48106-1346

LOUISIANA TECH UNIVERSITY

THE GRADUATE SCHOOL

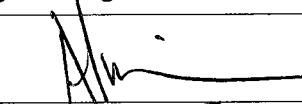
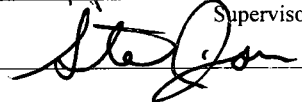
09/15/2010

Date

We hereby recommend that the dissertation prepared under our supervision
by Cristian Federico Pasluosta

entitled NONLINEAR CONTROL STRATEGY FOR A COST EFFECTIVE
MYOELECTRIC PROSTHETIC HAND

be accepted in partial fulfillment of the requirements for the Degree of
Doctor of Philosophy in Biomedical Engineering


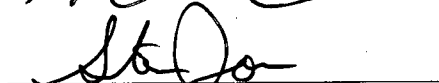

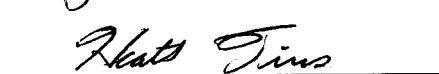



Supervisor of Dissertation Research


Head of Department

Department

Recommendation concurred in:

Advisory Committee

Approved: 
Director of Graduate Studies

Approved: 
Dean of the Graduate School


Dean of the College

ABSTRACT

The loss of a limb tremendously impacts the life of the affected individual. In the past decades, researchers have been developing artificial limbs that may return some of the missing functions and cosmetics. However, the development of dexterous mechanisms capable of mimicking the function of the human hand is a complex venture. Even though myoelectric prostheses have advanced, several issues remain to be solved before an artificial limb may be comparable to its human counterpart. Moreover, the high cost of advanced limbs prevents their widespread use among the low-income population.

This dissertation presents a strategy for the low-level of control of a cost effective robotic hand for prosthetic applications. The main purpose of this work is to reduce the high cost associated with limb replacement. The presented strategy uses an electromyographic signal classifier, which detects user intent by classifying 4 different wrist movements. This information is supplied as 4 different pre-shapes of the robotic hand to the low-level of control for safely and effectively performing the grasping tasks. Two proof-of-concept prototypes were implemented, consisting on five-finger underactuated hands driven by inexpensive DC motors and equipped with low-cost sensors. To overcome the limitations and nonlinearities of inexpensive components, a multi-stage control methodology was designed for modulating the grasping force based on slippage detection and nonlinear force control.


A multi-stage control methodology for modulating the grasping force based on slippage detection and nonlinear force control was designed. The two main stages of the control strategy are the force control stage and the detection stage. The control strategy uses the force control stage to maintain a constant level of force over the object. The results of the experiments performed over this stage showed a rising time of less than 1 second, force overshoot of less than 1 N and steady state error of less than 0.15 N. The detection stage is used to monitor any sliding of the object from the hand. The experiments performed over this stage demonstrated a delay in the slip detection process of less than 200 milliseconds. The initial force, and the amount of force incremented after sliding is detected, were adjusted to reduce object displacement. Experiments were then performed to test the control strategy on situations often encountered in the ADL. The results showed that the control strategy was able to detect the dynamic changes in mass of the object and to successfully adjust the grasping force to prevent the object from dropping.

The evaluation of the proposed control strategy suggests that this methodology can overcome the limitation of inexpensive sensors and actuators. Therefore, this control strategy may reduce the cost of current myoelectric prosthesis. We believe that the work presented here is a major step towards the development of a cost effective myoelectric prosthetic hand.

APPROVAL FOR SCHOLARLY DISSEMINATION

The author grants to the Prescott Memorial Library of Louisiana Tech University the right to reproduce, by appropriate methods, upon request, any or all portions of this Dissertation. It is understood that "proper request" consists of the agreement, on the part of the requesting party, that said reproduction is for his personal use and that subsequent reproduction will not occur without written approval of the author of this Dissertation. Further, any portions of the Dissertation used in books, papers, and other works must be appropriately referenced to this Dissertation.

Finally, the author of this Dissertation reserves the right to publish freely, in the literature, at any time, any or all portions of this Dissertation.

Author 

Date 10/19/10

TABLE OF CONTENTS

ABSTRACT	III
LIST OF TABLES.....	X
LIST OF FIGURES	XI
ACKNOWLEDGEMENTS	XVI
CHAPTER 1 INTRODUCTION.....	1
1.1 Statement of the Problem	1
1.2 Research Need	5
1.3 Overview of the Prosthetic Hand Project	5
1.4 Project Goals.....	7
1.4.1 <i>General Goal</i>	7
1.4.2 <i>Specific Goals</i>	8
1.5 Overview of the Control Strategy Design	8
1.5.1 <i>Pre-shape Stage Controlled by EMG Signals</i>	9
1.5.2 <i>Force Control and Detection Stages</i>	13
1.5.3 <i>Control Strategy Implementation</i>	13
1.6 Overview of the Testing Methodology.....	14
CHAPTER 2 LITERATURE REVIEW.....	16
2.1 The Human Hand and its Control.....	17

2.1.1	<i>The Structure, Actuators and Receptors of the Human Hand</i>	17
2.1.2	<i>Control of the Dexterous Manipulation of the Human Hand</i>	23
2.2	Upper Limb Amputation and its Replacement	26
2.2.1	<i>Upper Limb Amputation: Surgery and Level Classification</i>	26
2.2.2	<i>Upper Limb Replacement</i>	27
2.3	State of the Art in Advanced Upper-Limb Prostheses	31
2.3.1	<i>Mechanical Design</i>	31
2.3.2	<i>Sensory Systems</i>	40
2.4	Control Strategies in Advanced Upper-Limb Prosthesis.....	45
2.4.1	<i>Open Loop</i>	45
2.4.2	<i>Closed Loop Systems with Feedback to the User</i>	46
2.4.3	<i>Closed Loop Systems with Feedback to the Control System</i>	47
2.4.4	<i>Hybrid Closed Loop Control Systems</i>	50
2.5	Low-Cost Approaches	52
CHAPTER 3 MECHATRONIC DESIGN OF THE PROTOTYPE.....		54
3.1	Mechanical Design	55
3.1.1	<i>Preliminary Finger Design</i>	55
3.1.2	<i>First Generation Prototype</i>	57
3.1.3	<i>Second Generation Prototype</i>	59
3.1.4	<i>Grasping Patterns</i>	62
3.2	Electronic Design	63
3.3	Preliminary Cost Analysis.....	68

CHAPTER 4 FORCE CONTROL STAGE	70
4.1 Hypothesis	72
4.2 Force Control Design.....	72
4.2.1 <i>Neural Network-Based Modeling</i>	72
4.2.2 <i>System Identification</i>	77
4.2.3 <i>Optimization Algorithm</i>	80
4.3 Preliminary Simulation.....	83
4.3.1 <i>Methodology</i>	83
4.3.2 <i>Results</i>	84
4.4 Evaluation over the Prototype	86
4.4.1 <i>Methodology</i>	86
4.4.2 <i>Results</i>	89
4.5 Discussion.....	94
CHAPTER 5 DETECTION STAGE	96
5.1 Hypothesis	97
5.2 Slippage Detection Algorithm.....	97
5.3 Preliminary Evaluation	98
5.3.1 <i>Methodology</i>	98
5.3.2 <i>Results</i>	99
5.4 Quantitative Evaluation	101
5.4.1 <i>Methodology</i>	101
5.4.2 <i>Results</i>	103
5.5 Discussion.....	106

CHAPTER 6 EVALUATION AND ADJUSTMENT.....	108
6.1 Hypothesis.....	109
6.2 Evaluation of the Equilibrium between Fingers and Objects.....	109
6.2.1 <i>Methodology</i>	109
6.2.2 <i>Results</i>	111
6.3 Adjusting of the Control Strategy.....	113
6.3.1 <i>Modifications</i>	115
6.3.2 <i>Methodology</i>	115
6.3.3 <i>Results</i>	117
6.4 Evaluation of the response to force disturbance.....	119
6.4.1 <i>Methodology</i>	119
6.4.2 <i>Results</i>	121
6.5 Discussion.....	126
CHAPTER 7 CONCLUSIONS AND FUTURE WORK.....	129
7.1 Conclusions.....	129
7.2 Ongoing and Future Work.....	131
7.2.1 <i>Ongoing Improvements on the Prototype</i>	131
7.2.2 <i>Future Improvements on the Control Strategy</i>	132
7.2.3 <i>Future Implementation of the Control Strategy on Microcontrollers</i>	133
APPENDIX A.....	135
APPENDIX B.....	150
REFERENCES.....	154

LIST OF TABLES

Table 1-1: Percentage use of the main grasp configurations in ADL [16].	10
Table 1-2: Four movements are classified from EMG signals and they are interpreted as five possible pre-shapes configuration plus an open hand state.	11
Table 2-1: Insertion and function of the extrinsic muscles of the hand (from [21]).	20
Table 2-2: Insertion and function of the intrinsic muscles of the hand (from [21]).	21
Table 2-3: Sensory receptors classification and function.	23
Table 2-4: Characteristics of different types of prostheses.	28
Table 3-1: Preliminary cost analysis of the prototype.	69
Table 4-1: Objects used in the experiments.	87
Table 5-1: Objects used in the preliminary slip experiments.	99
Table 5-2: Objects used in the quantitative slip experiments.	103
Table 6-1: Different objects that were used for the grasping experiments and their approximate weights and dimensions.	110
Table 6-2: Result from the grasping experiments.	113
Table 6-3: Factors and levels of the factorial design.	117

LIST OF FIGURES

Figure 1-1: Block diagram of the overall project.	6
Figure 1-2: Block diagram of the control strategy.	9
Figure 1-3: Classification of the main grasp patterns (from [16]).	10
Figure 1-4: Flow chart of the control algorithm.	12
Figure 1-5: Block diagram of the hardware architecture and the software of the controller.	14
Figure 2-1: Upper limb mechanical model (from [22]).	18
Figure 2-2: Predictive sensory control of the motor system (following [29]).	25
Figure 2-3: Amputation levels (from [32]).	27
Figure 2-4: Adaptation of an underactuated system to the shape of an object (from [34]).	32
Figure 2-5: Left: CyberHand (from [48]). Right: SmartHand (from [6]).	33
Figure 2-6: Silicon hand (from [44]).	34
Figure 2-7: Southampton REMEDI hand (from [50]).	35
Figure 2-8: The SensorHand ¹ ™ Speed from Otto Bock (from [51]).	36
Figure 2-9: Female and male version of the DARPA program five-fingered hand (from [52]).	37
Figure 2-10: The i-LIMB from Touch Bionics (from [5]).	38
Figure 2-11: Gas-actuated prosthetic arm (from [47]).	39

Figure 2-12: Prosthetic hand with shape memory alloy actuators (from [37]).	40
Figure 2-13: Sensory substitution in prosthetics (from [53]).	41
Figure 2-14: Sample of an array-based force sensor scheme [55].	42
Figure 2-15: Fluid-based biomimetic tactile sensor (from [58]).	43
Figure 2-16: Thick-film multifunction sensor (from [62]).	44
Figure 2-17: Different control strategies of upper-limb prosthetic devices.	45
Figure 2-18: Control strategy scheme (from [18]).	48
Figure 2-19: Control scheme of a grip control using a biomimetic fluid-based sensor (from [80]).	50
Figure 2-20: Hybrid control system with feedback to both the user and the control system (from [85]).	51
Figure 2-21: Body-powered low-cost prosthetic hand (modified from [86]).	52
Figure 2-22: Gloveless endoskeletal low-cost prosthetic hand (from [87]).	53
Figure 3-1: Underactuated finger.	56
Figure 3-2: Schematics of three different positions for testing the force sensor.	57
Figure 3-3: First hand generation. CAD model (left). Actual prototype (right).	58
Figure 3-4: CAD model of the second generation prototype.	60
Figure 3-5: Fabrication of the silicone glove.	61
Figure 3-6: Hand prototype wearing the silicone glove.	62
Figure 3-7: Grasping patterns produced by the prototype (modified from [89]).	63
Figure 3-8: Circuit boards.	64
Figure 3-9: Signal conditioning circuit.	65
Figure 3-10: Calibration setup.	66

Figure 3-11: 4th polynomial fitting for the calibration of the FSR circuit.	66
Figure 3-12: PWM circuit.....	67
Figure 3-13: Circuit used to switch the direction of rotation of the motors.	68
Figure 4-1: Block diagram of the force control system.....	71
Figure 4-2: Feedforward neural network topology (modified from [103])......	73
Figure 4-3: Diagram of the Neural Network model.	78
Figure 4-4: Physical model of underactuated finger and the motor-pulley system.....	83
Figure 4-5: Control system outputs (red line) for different joint angles (θ in radians) and reference signal (blue line).....	85
Figure 4-6: Response to a disturbance.....	85
Figure 4-7: Experiment setup.	87
Figure 4-8: Typical step response of a second order system.	88
Figure 4-9: Sample of the signals recorded during the experiments.	89
Figure 4-10: Average closing and rise time for each object.....	90
Figure 4-11: Average overshoot results for each object.....	91
Figure 4-12: Average steady state error for each object.....	92
Figure 4-13: Average percentage of time in which the motor was on for each object.....	93
Figure 4-14: Sample of the 2 minutes experiment.	94
Figure 4-15: Results for the two minutes trial.....	94
Figure 5-1: Different grasping patterns for the slippage experiments.....	98
Figure 5-2: Force signal obtained from the index finger while holding a small bottle. Derivative of the force and setting of the threshold.....	100
Figure 5-3: Setup of the slip detection experiments.	102

Figure 5-4: Example of the results obtained during the slip detection experiments.	104
Figure 5-5: Cumulative probability function as a function of the detection delay values, parameterized with respect to each threshold value.	105
Figure 5-6: Detection delay for 80% of the experiments.	106
Figure 6-1: Support device designed to assist during the different tests. It contains 4 buttons that simulate the four possible outputs from the EMG classifier....	111
Figure 6-2: Some of the objects used in the static experiments.	112
Figure 6-3: Cylindrical experiments setup.	116
Figure 6-4: Box plot of the displacement vs. step size and initial force.....	118
Figure 6-5: Iteration plot for the displacement results..	118
Figure 6-6: Tip experiments setup.....	120
Figure 6-7: Torque experiment setup.	121
Figure 6-8: The force sensor output along with the reference and force control signals are shown.....	123
Figure 6-9: Average displacement of the cylindrical hold experiments.....	124
Figure 6-10: Average displacement of the tip grasping experiments.....	125
Figure 6-11: Average rotational displacement of the torque experiments.	126
Figure 7-1: New improved prototype.	131
Figure 7-2: Arduino platform (from [114]).	134
Figure A-1: Front panel of the control strategy.....	136
Figure A-2: Block diagram: Grasping type selection.....	137
Figure A-3: Block diagram: Whole Pre-shape stage.....	138
Figure A-4: Block diagram: Detail of Pre-shape stage.....	139

Figure A-5: Block diagram: Whole Force Control and Detection stage.	140
Figure A-6: Block diagram: Detail of the Force Control and Detection stage.	141
Figure A-7: Block diagram: Release stage.	142
Figure A-8: Block diagram: Detail of the Release stage.	143
Figure A-9: Front Panel of the Force Control stage of the index finger.	144
Figure A-10: Block Diagram of the Force Control stage of the index finger.	145
Figure A-11: Front Panel of the Force Control stage of the middle finger.	146
Figure A-12: Block Diagram of the Force Control stage of the middle finger.	147
Figure A-13: Front Panel of the Force Control stage of the thumb.	148
Figure A-14: Block Diagram of the Force Control stage of the thumb.	149

ACKNOWLEDGEMENTS

First of all, I want to thank my wife for her tirelessly support during all these years. I would not be able to obtain this degree if it had not been for her. Thank you Mari for all your love, patience and comprehension.

I want to thank my parents for being part of this journey, for supporting me in the tough times and for always being there any time I needed them. Thank you Dad and Mom. I want to thank my sisters and my brother-in-law. They always were very supportive and they helped me to reduce the distance to home. Thank you Caro, Eli and Carlos. I also want to thank my wife's family for their support and affection.

I would like to thank all my friends for encouraging me during all this time. Specially, I want to thank my best friend Juan Fontana, for being my partner in this project and for always being so patient and comprehensive. I also want to thank Dr. Pedro Derosa and Dr. Daniela Mainardi for their friendship and continued support.

I want to thank all of the members of my committee, my advisor Dr. Alan Chiu, Dr. Eric Guilbeau, Dr. Steven Jones, Dr. Stan Cronk and Dr. Heath Tims. Dr. Chiu helped me on this work by making available all the materials needed to develop the project and by always offering good advise in all the stages during my time here at Louisiana Tech. Dr. Tims assisted me on the design and the mechanical aspects of the prototypes. Dr. Cronk helped me during the early stage of my studies here in Louisiana Tech. Dr. Guilbeau and Dr. Jones helped me to improve the writing of this dissertation.

Every member of my committee gave me very valuable feedback to improve and expand this project.

I want to thank the College of Engineering and Science for its continued financial support during all these years as a teaching assistant at Louisiana Tech University. I want also to acknowledge to the NIH and the Board of Regents grants.

Finally, I want to thank God, source and foundation of everything.

CHAPTER 1

INTRODUCTION

1.1 Statement of the Problem

The hand is an amazing component of the human body. It represents one of the most important tools that human beings have to perform the majority of the activities of daily living (ADL). It allows humans to explore the surrounding environment and to interact and communicate with other human beings. These features are fulfilled by the tremendous dexterity and sensory information that a human hand contains. Consequently, the loss of a limb drastically reduces an individual's functionality and social interaction. Accordingly, the task of replacing a human hand with an artificial one is a great challenge that involves the efforts of researchers from multiple disciplines.

The loss of a limb produces a tremendous psychological, social and economical impact in the affected individual. The amputee is psychologically affected by the inability to perform common ADL, which may include personal hygiene or dressing. Moreover, in the case of trauma amputation the individual does not have a chance of preparing for this abrupt change in her or his life [1]. Once an amputation occurs, it lasts forever and has no cure.

There is also a social impact related to the missing of a limb since the reincorporation to society, with limited functionality and deteriorated cosmetic appearance, is a challenging task. Upper-limb amputees are at a disadvantage relative to lower-limb amputees because it is easier to notice an upper-limb prosthesis than a lower one [1]. Even though lower-limb amputations are 20 times more frequent than the upper-limb amputations, the damage produced by an upper limb amputation generally has a stronger impact [2]. Finally, replacement of an absent limb with an artificial limb, which may restore some functionality, is expensive. This cost may prevent low-income amputees from accessing this kind of technology.

Limb replacement is a complex process from the engineering point of view. A system that mimics the behavior and dexterity of a natural hand must accurately control many degrees of freedom (DoF) to produce stable grasping in order to hold and manipulate objects of varied weights and geometries.

In the past decades researchers have worked to develop externally powered artificial limbs that can satisfy the needs of people who have suffered amputations as a result of wars, traumatic accidents, congenital defects, cancer, infections, or circulatory diseases. Moreover, upper-limb replacement is an interesting problem because of the importance of dexterity in human hands and the engineering challenge it presents. However, about 35% of the affected people do not use their prosthetic devices regularly [3] for several reasons, including the psychological effort necessary to control these devices, the low level of dexterity provided, and the high cost. Respondents to an internet survey performed by Pylatiuk et al. [4] indicated low satisfaction with the weight and grasping velocity of prosthesis and a need to have the devices perform activities such as

handicrafts, personal hygiene, using cutlery, operating electronic devices and dressing. Other desired features were force feedback systems and independent movement of the principal fingers (thumb and index) and the wrist.

Therefore, in order to increase the acceptability of a myo-controlled prosthetic device some conditions must be met. First, the device must be easy to use and adaptable to different users to reduce psychological effort and avoid muscle fatigue. Second, the device must control enough DoFs to permit various grasping configurations, which may allow it to perform the most frequent ADL. Finally, electromechanical considerations, like weight, dimensions and power consumption, must be acceptable to the user. Many of these criteria have been addressed by new advanced prosthesis like the i-Limb (commercially available from Touch Bionics [5]), the SmartHand (an European project [6]) and the Revolutionizing Prosthetic project from the Defense Advance Research Project Agency (DARPA) [7]. However, the high cost associated with the replacement of the missing limb has not been strongly addressed. The device must be affordable by the low-income population. In developing countries low cost becomes essential, and a less dexterous but inexpensive device may be much more acceptable than a complex but costly one.

In the United States, approximately 1.7 million people live with limb loss, and it is projected that by the year 2050 this number will be doubled [8]. It is also estimated that one out of every 200 people in the U.S. has had an amputation [9]. There is an average of over 130,000 hospital discharges for amputation per year and upper-limb amputations accounted for 3 percent of all dysvascular limb loss discharges. In general, a prosthetic arm or a leg above the knee usually costs between \$10,000 and \$15,000. Some have a

cost of \$35,000 or more. The i-Limb costs between \$60,000 and \$150,000 depending on the length of the amputation. Although these devices are generally covered with no cap by Medicare and Medicaid, most private insurance companies have limits between \$500 and \$3,000 for prostheses. In addition, an amputee may have a lifetime limit of \$10,000 and one prosthetic [10]. The Annual Census Bureau estimates that 47 million people, or 15.8 percent of the United States population, were without health insurance during the year 2006. Every year, 25,000 people in the U.S. have entire arm amputations and 61,000 people have partial hand amputations.

In developing countries, cost is a key factor that may determine whether prostheses are accessible to the amputee population. One possibility for people in developing countries for accessing to a low-cost prosthesis is to appeal to aid organizations such as the International Committee of the Red Cross. However even this organization cannot manufacture a prosthetic device for less than \$1,000 [11]. A survey performed in India on 71 traumatic upper-limb amputees [12] used a Prosthetic Rehabilitation Score system to determine the main reasons of dissatisfaction in the use of body-powered prosthesis. The assessment indicates that the second most important reason is the high cost associated with maintenance and replacement of the device [12]. A field survey conducted in Vietnam [13] indicates that although prostheses on average are used 12 hours a day, many amputees were not able to continue with the same job after the amputation. Moreover, only 49% of the surveyed participants work outside their homes and only 58% hold the same job they had before the amputation.

1.2 Research Need

The development of a cost effective and easy-to-use dexterous prosthetic device is needed for the amputee community. Such a device must have an appropriate control strategy to compensate for the low-cost mechanical and electronic systems. Children and adults who suffer from upper-limb loss and limb deformities as a result of trauma, congenital defects, cancer, infection and circulatory disease leading to amputation will be the target users. This research is especially appealing and needed for low income families, people with inadequate insurance coverage here in the United States, or in developing countries.

1.3 Overview of the Prosthetic Hand Project

This dissertation is part of a multi-systems project aimed towards the development of a low-cost prosthetic hand controlled by electromyographic (EMG) signals in a functional approach. A block diagram of the whole project is presented in Figure 1-1. The project is divided into four main sub-parts: the EMG signal classification system (or high level of control), the control strategy (or low level of control), a vibrotactile feedback system (high level of feedback) and the prototype of the hand.

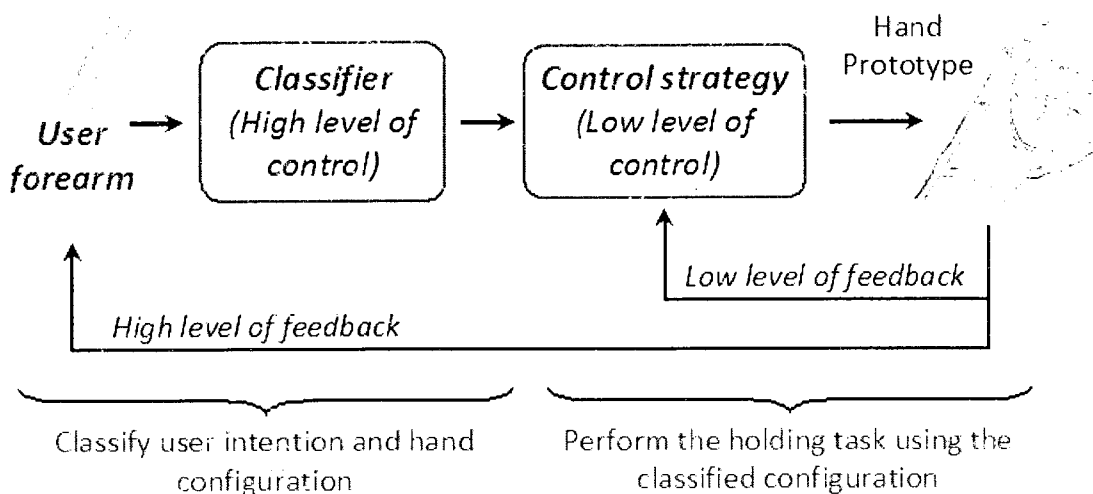


Figure 1-1: Block diagram of the overall project.

Surface EMG signals recorded from the forearm are classified to determine the intention of the user to open/close the hand and to determine the initial pre-shaping of the hand. This stage is referred here as the high level of control of the hand. After the pre-shape is chosen, the control strategy is turned on, and it is able to automatically modulate the grasping to conform to different shapes and weights of the objects. This automated sequence is referred as the low level of control of the hand. As a result, the high level of control is performed by the user and the low level is performed automatic by the prosthetic device.

The major advantage of this methodology is that the user only needs to control the hand at the high level, that is, the user decides when to close/open the hand and the grasp configuration. The user does not need to continuously monitoring the device after the grasp selection. The automation decreases drastically the psychological effort of the user and leads to a more natural and easier control of the device.

The system also contains two levels of feedback. Low-level feedback is a group of signals that are fed back to the automatic controller, while high-level feedback is another group that is fed back to the user to provide a sense of touch or spatial orientation. In each case, the signals may be a subset of grasping force, joint position, slippage, velocity, acceleration, or other measurable variables. Some signals may be fed back through both the low-level and high-level loops.

A proof-of-concept prototype of a five fingered prosthetic hand was designed and fabricated to serve as a flexible platform to implement and evaluate the different levels of control of the hand. The control strategy for the low level of control is the main focus of this dissertation.

1.4 Project Goals

1.4.1 *General Goal*

We claim that useful prosthetic devices can be designed using inexpensive sensors and actuators if the applied control technique is able to deal with the problems associated with the low-cost technology. We will develop a new generation of prosthesis that will be accessible to people with low incomes. The device will also provide functionality that will allow the user to perform most of the ADL. Therefore, the main goal of this dissertation is to develop a control strategy for a new dexterous cost effective prosthetic hand.

1.4.2 *Specific Goals*

The overall goals of this research are to:

- a) Design a prototype of a low-cost robotic underactuated prosthetic hand to serve as a platform to evaluate the performance of the proposed proof-of-concept control strategy.
- b) Develop and evaluate a slip detection algorithm to assist in the grasping task of an underactuated low-cost robotic hand that does not include specialized sensors.
- c) Develop and evaluate a force control system to assist in the grasping task of an underactuated finger that does not include expensive sensors and actuators.
- d) Develop and evaluate the proposed control strategy, which integrates objectives b and c, to modulate the grasping force of an underactuated low-cost robotic hand while performing activities commonly encountered in daily living.

1.5 Overview of the Control Strategy Design

A control strategy for automatically driving the fingers of the prototype was designed and implemented, in which the index, thumb and middle fingers are controlled independently and identically by the same algorithm, consisting on three main stages: a pre-shape stage, a force control stage and a detection stage (see Figure 1-2). A brief introduction to each of these stages is outlined in the following subsections.

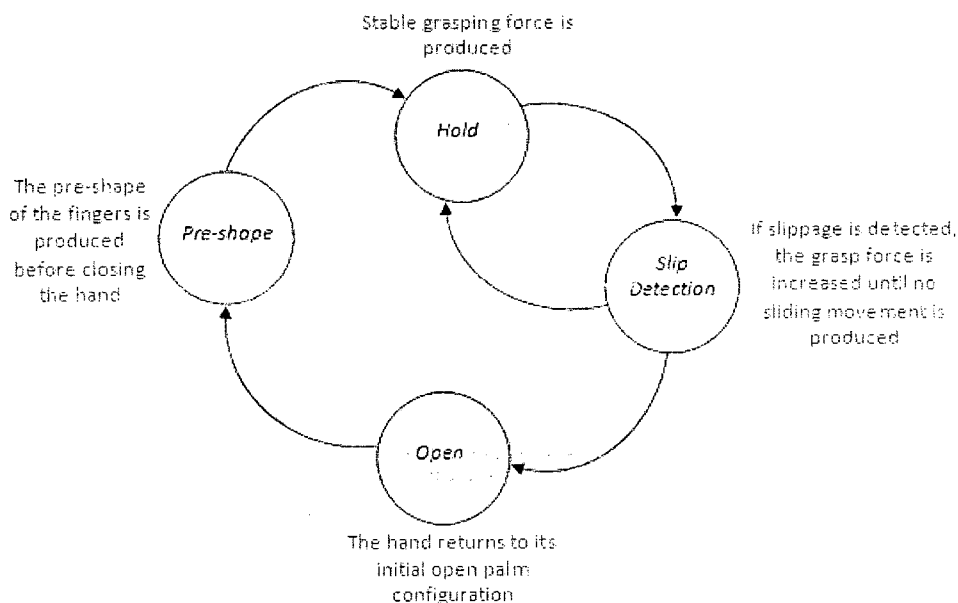


Figure 1-2: Block diagram of the control strategy.

1.5.1 *Pre-shape Stage Controlled by EMG Signals*

Surface electrodes are placed in strategically selected locations of the residual limb in order to record and obtain as much information as possible from electromyographic (EMG) signals. Wavelet transform is used for extraction of time-frequency features and Support Vector Machine (SVM) is applied as the classification technique (for more details refer to [14]). Four desired movements are classified and used as inputs to the control strategy. The four movements are interpreted as five possible pre-shapes of the hand plus an open hand configuration. In this way the user is able to command the prosthesis and decide the adequate pre-shape of the hand depending on the geometry and weight of the object. The event of choosing the grasp configuration is usually referred as the high-level of control in dexterous manipulation [15].

The five pre-shape configuration were selected from the eight main grasp configurations (see Figure 1-3) [16]. Sollerman and Ejeskär reported their percentage of use in ADL [16], which are shown in Table 1-1.

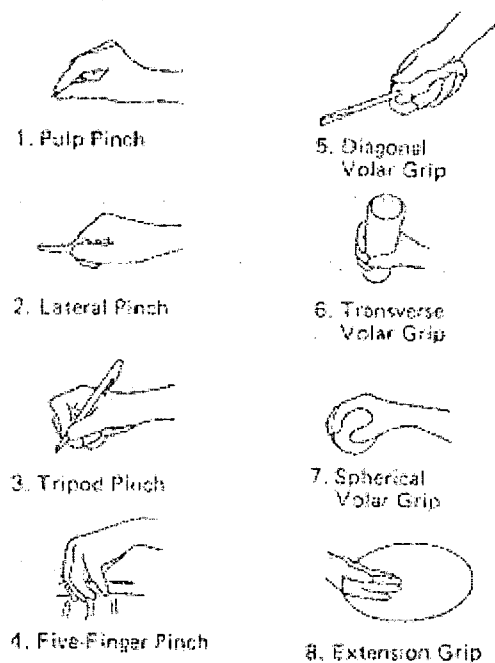


Figure 1-3: Classification of the main grasp patterns (from [16]).

Table 1-1: Percentage use of the main grasp configurations in ADL [16].

Grasp Configuration	%
Pulp pinch	20
Lateral pinch	20
Tripod pinch	10
Five-finger pinch	15
Diagonal volar grip	15
Transverse volar grip	14
Spherical volar grip	4
Extension grip	2

The first six configurations in Table 1-1 represent 94% of grasping events. We selected five of these configurations, *transverse volar grip (cylindrical)*, *spherical*, *lateral pinch*, *tripod pinch*, and *pulp pinch (thumb-index pinch)*. We then defined pre-shapes that are appropriate to the given configuration.

Figure 1-4 is a flow chart of the control algorithm. The hand remains idle until the input signals from the EMG classifier initiate the desired grasp configuration. Table 1-2 shows the four possible outputs from the EMG classifier and the respective class. When class 1 is selected, three grasp configurations are possible: *cylindrical*, *spherical* or *lateral pinch*. This class activates all five fingers to close at the same time and produces either *cylindrical* or *spherical* grasping, depending on the geometry of the object. Extension grip can also be achieved in this configuration. Moreover, if the thumb is shifted to the lateral position, a *lateral pinch* grasp will be obtained. If class 2 is selected, the *Thumb-index pinch* configuration is performed, where only the thumb and index fingers are active while the rest of the fingers remain in their open configuration. The thumb is positioned to allow the closing index finger to reach its tip, forming a pinch. Alternatively, when class 3 is selected, the hand switches to *Tripod* grasping in which the hand reaches a tripod configuration. Finally, when class 4 is selected the hand switches to *open palm* configuration and the fingers remain inactive until another classes is selected.

Table 1-2: Four movements are classified from EMG signals and they are interpreted as five possible pre-shapes configuration plus an open hand state.

Classified Movements	Grasp Type
Class 1	Cylindrical/Spherical/Lateral
Class 2	Tip (thumb-index pinch)
Class 3	Tripod
Class 4	Open

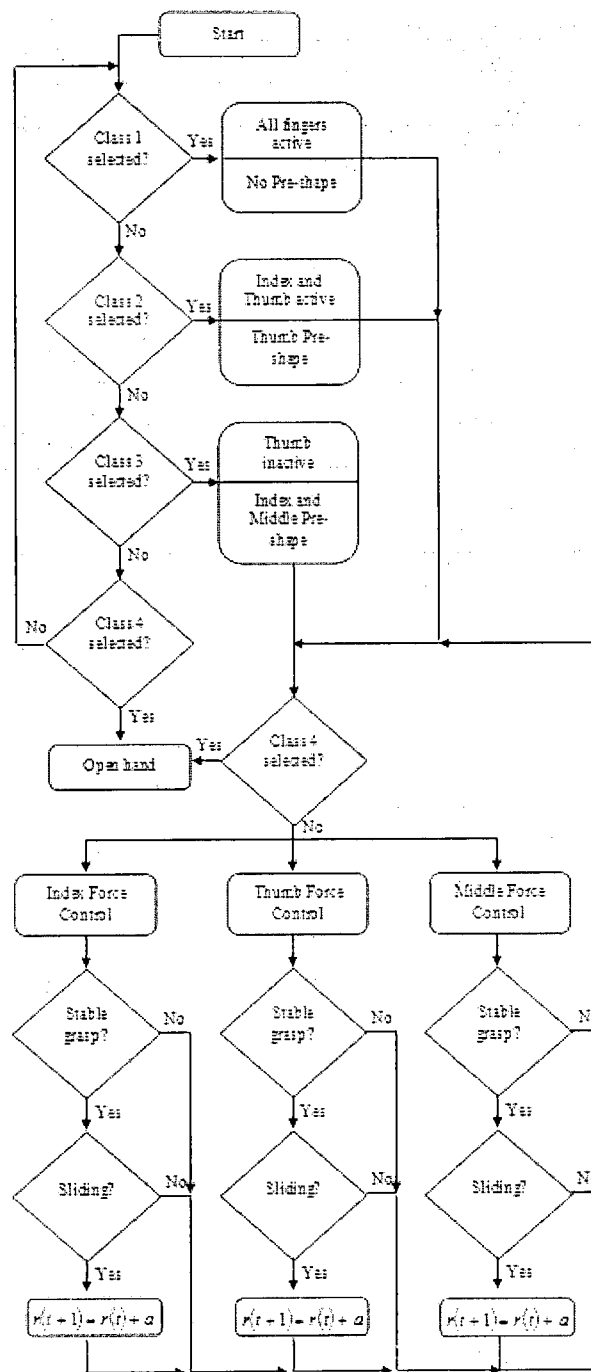


Figure 1-4: Flow chart of the control algorithm.

1.5.2 *Force Control and Detection Stages*

Once the grasping configuration is selected, the force control and the detection stages are activated, and they work in conjunction with each other. In the force control stage, the nonlinear model predictive control (NMPC) technique is implemented to maintain a pre-determined level of force. When the grasping motion is stabilized, the system alternates between the force control state and the detection state, in which any sliding or unintended movement of the object can be monitored. When these movements are detected, the level of force exerted by the fingers is modulated discretely, ensuring that the grasping procedure is secure (see Figure 1-4). The force control and detection stages often belong to the low-level of control defined in dexterous manipulation [15]. Control methodologies similar to the one described here have been proposed by researchers in the area of prosthesis during the past [17-20], however the use of NMPC in prosthetic hands has not yet been found in the literature.

1.5.3 *Control Strategy Implementation*

To implement the control strategy, software and hardware were designed to serve as a flexible platform for the developing of the project. The hardware contains the motor drivers, the position and force sensors, the signal conditioning system and the data acquisition boards. The software part is divided in the real time controller (control strategy) and offline training. The controller is implemented in LabVIEW (National Instruments) and Matlab (The MathWorks) is used for its training stage. Figure 1-5 shows the block diagram of the hardware architecture and the software of the controller.

Each of these parts will be explained in more detail in the following sections. The complete implementation is described in Appendices A and B.

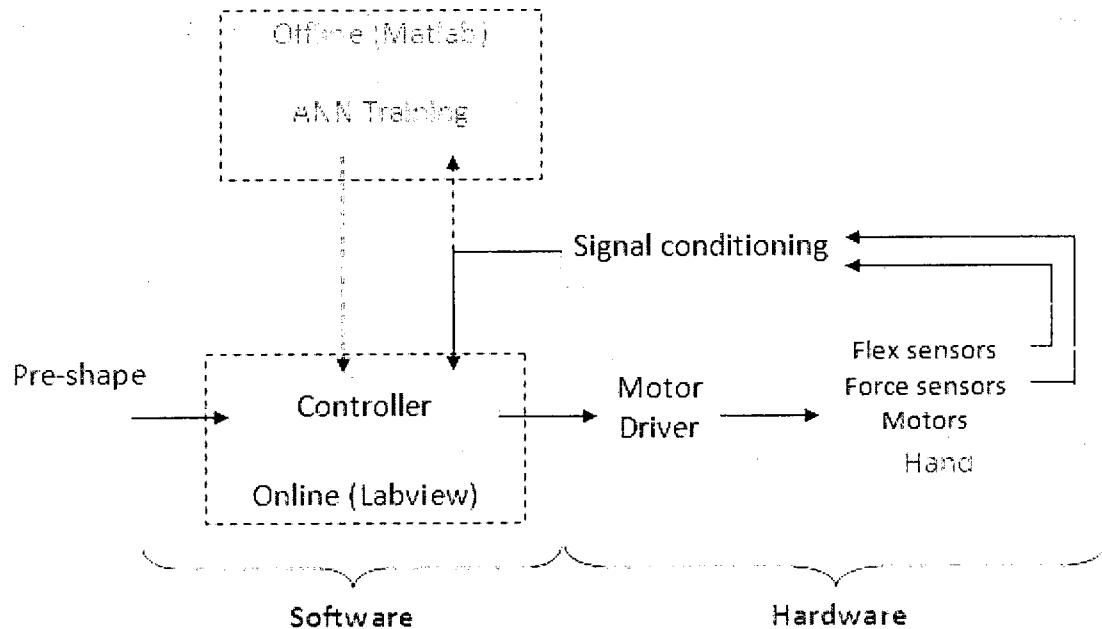


Figure 1-5: Block diagram of the hardware architecture and the software of the controller.

1.6 Overview of the Testing Methodology

Since the proposed control strategy is composed of multiple subsystems, the testing methodology was divided in several steps and grouped into two main evaluation stages. During the first stage of evaluation, the main subsystems were tested separately (force control and detection systems). Experiments were conducted to evaluate their individual performance and assess their compatibility in a combined system. In the second stage of evaluation, both subsystems were combined along with the pre-shape stage in order to complete the control strategy. Experiments were then conducted to evaluate the ability of the hand (and consequently the performance of the control

strategy) to securely grasp several objects. In the next stage, the parameters of the control strategy were optimized to minimize the slippage of the object from the hand. Finally, the capability of the hand to adapt to situations potentially encountered in ADL was evaluated. During this stage, experiments involving induced external forces over the grasped object were conducted to evaluate the dynamic response of the hand.

CHAPTER 2

LITERATURE REVIEW

The human hand is a marvelous biological device designed not only to grasp and manipulate objects, but also to serve as an exploratory and communicative tool. It is able to produce both precision and power grasp, with amazing closing velocity and grasping force control, which end up with a huge flexibility and adaptation to different scenarios. This is achieved thanks to three main factors: the design of the *skeletal structure* of the hand; the *redundancy in the actuators and sensors* (muscles and receptors); and the *neural control strategy* of the central nervous system (CNS).

Historically, researches from many areas have been working in order to mimic the structure and control of the human hand. The replacement of a missing limb has been of huge interest by the academy and industry researchers due to the necessity of the amputee population for better prosthetic devices. A review of the existing technologies in prosthetics is presented in this chapter along with a short review of the human hand characteristics and its control by the nervous system. Finally, some current low-cost approaches are presented at the end of the chapter.

The aim of this review is to gather information about the state of the art in advanced myoelectric upper-limb prosthetic devices and to define what is needed to improve them and to reduce their cost.

2.1 The Human Hand and its Control

2.1.1 *The Structure, Actuators and Receptors of the Human Hand*

The human hand skeleton contains 27 bones that arrange in three groups: the wrist bones or carpus bones (8 bones), the palm or metacarpus bones (5 bones) and the phalanges or bones of the fingers (14 bones) [21]. Each of the four fingers has 3 phalanges and the thumb has two. Beside the articulations that the human hand has at the carpus and metacarpus level, it has 3 articulations at each finger and two at the thumb. The fingers articulate as follows: the first row of phalanges articulate at one end with the metacarpals and at the other end with the second row of phalanges, which articulate with the third row of phalanges. For the thumb the first phalange articulates with the metacarpal bone and with the second phalange [21].

Figure 2-1 presents a model of the upper limb structure (according with A. Morecki [22]). According to this model, the human arm contains 27 DoF; in which 22 DoF belong to only the hand. Changmock et al. [23] summarize the mechanical equivalent of the human hand joints with a total of 21 DoF, in which the thumb is considered to contain 5 DoF. The existence of a thumb and the possibility of its opposition are unique features of the human hand that enable dexterous grasping and object manipulation. Without the opposition of the thumb a minimum of 30 percentage of the hand efficiency is lost [24].

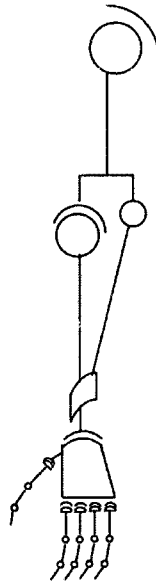


Figure 2-1: Upper limb mechanical model (from [22]).

The skeletal structure of the human hand is actuated by the voluntary muscles. They consist of a fleshy part attached to one bone that ends in a cordlike structure, called tendon, which passes over the connecting joint and attaches to the adjoined bone [24]. The muscles can shorten their length (referred as muscle contraction) to produce motion by pulling the tendon [24]. The tendons allow reduced muscle volume at each joint, which assists to the free movement of the bones.

The muscles that move the human hand are usually divided into extrinsic and intrinsic. The former are the hand muscles located at the forearm and the latter are the hand muscles located inside of it. Table 2-1 and Table 2-2 present the insertion and function of the extrinsic and intrinsic muscles, respectively. The extrinsic muscles produce mainly the flexion/extension, abduction/adduction and pronation/supination of the hand; however some of them are used especially for flexing and extending the fingers. The intrinsic muscles are more specialized for the flexion/extension of the fingers

as well as for its abduction/adduction. It was suggested that the intrinsic muscles are used to stabilize the fingers and for fine manipulation, while the extrinsic muscles are used for grasping heavy objects [25]. Five special intrinsic muscles are dedicated to the thumb and three to the little finger.

Table 2-1: Insertion and function of the extrinsic muscles of the hand (from [21]).

Name	Insertion	Function
Pronator teres	Middle of the lateral surface of the radius	Pronates the hand
Flexor carpi radialis	Second metacarpal	Flexes the hand and helps to abduct
Palmaris longus	Flexor retinaculum	Flexes the hand
Flexor carpi ulnaris	Pisiform bone	Flexes and adduct the hand
Flexor digitorum sublimus	2nd phalanx of the fingers	Flexes the 1st and 2nd phalanx of the fingers
Flexor pollicis longus	Base of the distal phalanx of the thumb	Flexes thumb 2nd phalanx and flexes, adducts the metacarpal
Flexor digitorum profundus	Base of the last phalanx of the fingers	Flexes the last phalanx of the fingers
Pronator quadratus	Border, palmar and surface area prox. to ulnar notch of the radius	Pronates the hand
Extensor carpi radialis longus	Base of the 2nd metacarpals	Extends the hand and abducts the hand
Extensor carpi radialis brevis	Base of the 3rd metacarpals	Extends the hand
Extensor carpi ulnaris	Base of the 5th metacarpals	Extends and adducts the hand
Extensor digitorum communis	2nd and 3rd phalanges of the fingers	Extends the fingers and the wrist
Extensor digiti minimi	1st phalanx of the little finger	Extends the little finger
Supinator brevis	Radius	Supinates the hand
Abductor pollicis longus	Base of the 1st metacarpal	Abducts the thumb and the wrist
Extensor pollicis brevis	Base of the 1st phalanx of the thumb	Extends the 1st phalanx of the thumb and abducts the hand
Extensor pollicis longus	Base of the thumb last phalanx	Extends the 2nd phalanx of the thumb and abducts the hand
Extensor indicis proprius	The tendon of the Extensor digitorum communis of index	Extends and adducts the index

Table 2-2: Insertion and function of the intrinsic muscles of the hand (from [21]).

	Name	Insertion	Function
Thenar	Abductor pollicis brevis	Base of the 1st phalanx of the thumb	Abducts the thumb
	Opponens pollicis	Metacarpal bone of the thumb	Abducts, flexes and rotates the metacarpal of the thumb
	Flexor pollicis brevis	Base of the proximal phalanx of the thumb	Flexes and adducts the thumb
	Adductor obliquus pollicis	Base of the proximal phalanx of the thumb	Adducts the thumb
	Adductor transversus pollicis	Base of the 1st phalanx of the thumb	Adducts the thumb
Hypothenar	Palmaris brevis	Ulnar border of the palm	Draws the skin at the ulnar side of the palm toward the middle of the palm
	Abductor digiti minimi	Base of the 1st phalanx of the little finger and to the ulnar border of the aponeurosis of the Extensor digiti minimi	Abducts the little finger and flexes its proximal phalanx
	Flexor digiti minimi brevis	Base of the 1st phalanx of the little finger	Flexes the little finger
	Opponens digiti minimi	Metacarpal bone of the little finger	Abducts, flexes and rotates the 5th metacarpal
Intermediate	Lumbricales	The tendinous expansion of the Extensor digitorum	Flex the metacarpophalangeal joints and extend the two distal phalanges
	Interossei dorsales	Base of the proximal phalanges and into the aponeuroses of the tendons of the Extensor digitorum	Abduct the fingers, flex the metacarpophalangeal joint and extend the two distal phalanges
	Interossei palmares	Base of the 1st phalanx and aponeurotic expansion of the Extensor communis tendon to the same finger	Adduct the fingers, flex the metacarpophalangeal joint and extend the two distal phalanges

A determined movement of the hand is usually produced by the action of two or more muscles. For example, the flexion of the wrist is achieved by the flexor carpi ulnaris, flexor carpi radialis and the palmaris longus muscles. Moreover, in order to flex the fingers the extensor muscles of the wrist contract to avoid its flexion [21]. This redundancy in the actuators of the hand is a complex problem from the control point of view and it represents one of the key elements for the dexterous manipulation of the human hand. Weghe et al. developed an anatomically-corrected test bed to analyze the neural control of the human hand movements [26]. In one of their works, they focused on muscle redundancy in precise manipulation [27], in which the control of six muscles (3 intrinsic and 3 extrinsic) was analyzed for the index finger. They hypothesize that the intrinsic muscles are used more frequently in fine manipulation than the extrinsic ones since they have a smaller force “gain” (smaller arm moment).

The human hand contains around 17,000 receptors that gather information about the outside and the inside environment of the hand. Table 2-3 shows the sensory receptors found in the human hand along with their functions. They can be classified according to the stimuli they detect as *tactile*, *thermoreceptors*, *nociceptors* and *proprioceptors*. Tactile receptors sense outside mechanical information such as touch, pressure, and vibration. Thermoreceptors detect temperature changes. Nociceptors are pain receptors and can detect mechanical, chemical and thermal damage of tissue. Finally, proprioceptors measure inside mechanical events like joint angulations, and muscle and tendon stretch. The redundancy in receptors is important to provide feedback to the central nervous system. This information is vastly used for coordinating the motor functions of the hand.

Table 2-3: Sensory receptors classification and function.

Sensory Receptors		
Classification	Name	Function
Tactile	Free nerve endings	Detect touch and pressure
	Meissner's corpuscles	Detect movement of objects over the surface, low frequency vibrations and assist in texture recognition
	Merkel's discs	Detect continuous touch of objects against the skin and assist in texture recognition
	Hair end-organs	Detect movement of objects on the surface
	Ruffini's end-organs	Detect prolonged touch and pressure and assist in joint rotation detection
	Pacinian corpuscles	Detect tissue vibrations and other rapid changes in tissues
Thermoreceptors	Cold receptors	Detect changes in temperatures between 10°C and 40°C (peak at 24°C)
	Warmth receptors	Detect changes in temperatures between 30°C and 50°C (peak at 45°C)
Nociceptors	Thermal	Detect freezing cold and burning hot temperatures (below 10°C and above 45°C)
	Mechanical	Detect mechanical damage of tissues
	Chemical	Detect chemical damage of tissues
Proprioceptors	Muscle spindles	Measure muscle length
	Deep joint receptors	Measure joint angulations
	Golgi tendon receptors	Measure tendon tension

2.1.2 Control of the Dexterous Manipulation of the Human Hand

Each skeletal muscle fiber is innervated by myelinated nerves that originate from large motor neurons in the spinal cord forming a neuromuscular junction [28]. The motor nerves control the muscles contraction through the spreading of action potentials. The motor control of each skeletal muscle of the human body is divided in different levels. Each level accomplishes different functions to assist in the execution of the different movements, and most of the time, they are organized hierarchically. Three specific levels

are encountered in the motor control of the nervous system: the spinal level, the hindbrain level and the motor cortex level.

In the spinal level, programmed motion patterns are encountered that assist in the performing of automatic movements such as pain-associated reflexes or the combination of different muscle contractions for walking. These motion patterns are controlled by higher levels of control, which dictate when they have to be activated or inhibited [28]. The hindbrain level assists in the motor control of tasks associated with muscle tone control for maintaining body equilibrium and for the specific task of standing [28]. The motor cortex level controls most of the voluntary movements by controlling the signals of the spinal level. It sends parallel commands to initiate different patterns in the spinal cord, and it can even bypass the Spinal level if necessary [28].

Two associated brain structures, the cerebellum and the basal ganglia, are also important in the motor control. The cerebellum functions with the spinal level to rapidly increase the stretch reflex when an unexpected load is detected. It also assists in maintaining the equilibrium of the body as well as in movement planning of smooth and rapid changes from one direction to another. The basal ganglia helps to produce unconscious planned sequential movements such as writing, throwing a ball or typing [28].

The dexterous manipulation of the human hand is the product of the fine control of the nervous system of the different muscles of the hand. The key component of this control is prediction [29, 30]. Figure 2-2 shows a descriptive diagram of the control strategy used by the nervous system during object manipulation. The object is first recognized by visual or haptic information. This triggers internal parametric models of object dynamics, created during the learning process, which determines the commands

that have to be sent to the muscles to perform a determined manipulation task. At the same time, these models contain information of the predictive sensory information that should be received given the observed object. This information is then compared to the sensory information received from the tactile receptors of the hand. If a mismatch is found (presence or absence of a determined sensory signal), the muscle commands are updated as well as the internal models [29].

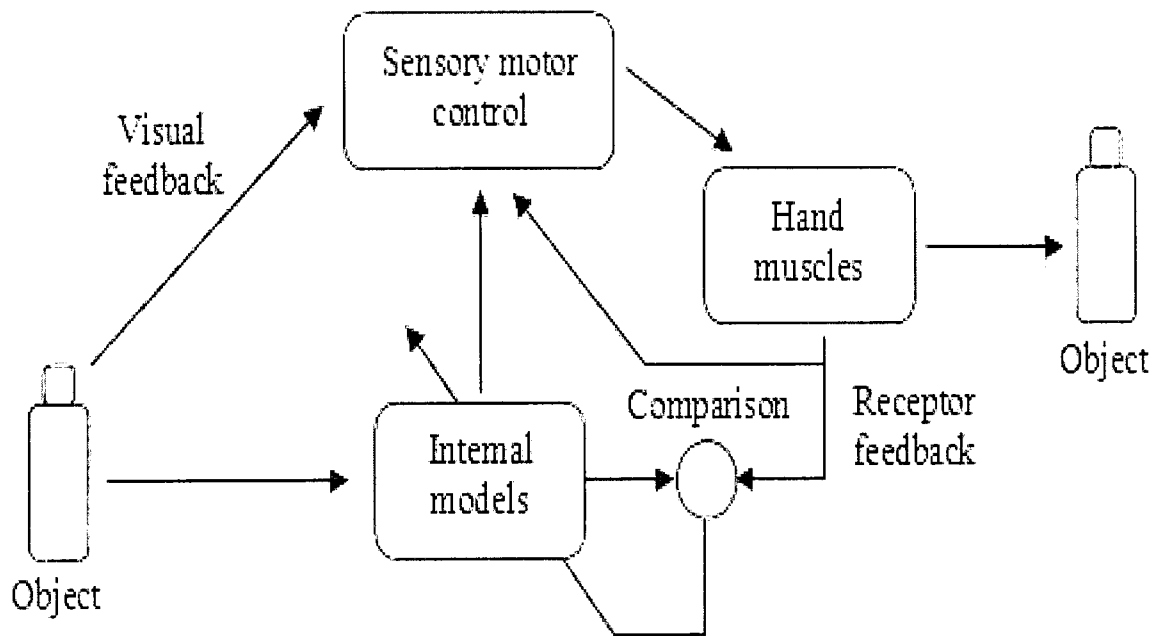


Figure 2-2: Predictive sensory control of the motor system (following [29]).

Note that a closed loop appears in the control of the manipulation task. However, the feedback information is used to monitor the task progress and not to directly control the task. This happens mainly because of the large time delay (100 ms) associated with the conduction and processing of the sensory information as well as with muscle activation, which would limit the time response of the hand [29, 30].

During multidigit manipulation (as well as in two-digit manipulation), the nervous system attempts to minimize the normal force exerted by the fingertips over the surface of the grasped object, while preventing slippage. That is, the normal force increase parallel with the load force, exceeding (minimally) the minimum force level to ensure grasping stability [31].

2.2 Upper Limb Amputation and its Replacement

2.2.1 *Upper Limb Amputation: Surgery and Level Classification*

The initial surgical therapy as well as the initial occupational therapy plays an important first step for the future use of the residual limb [1]. One of the most efficient surgical techniques is to attach the residual limb to the bone. This gives support for fitting the prosthesis and makes it easier to contract the muscles. Besides the surgery, issues such as wound care, scar management, residual limb shaping and edema control are important and need to be correctly addressed in order to minimize the impact of the amputation [1]. The length of the residual limb is also important and needs to be taken into account since the fitting of any prosthesis depends also on this factor.

Different amputation levels are described in Figure 2-3. The degree of motion depends on the location of the amputation. Transradial level (below elbow) is the most common in upper limb amputation. It allows good distribution of the forces and the easy fitting of prosthetic devices [1]. Elbow disarticulation is one of the most complicated level of amputation since it limits the elbow motion, which translates to prosthetic length issues and deterioration of cosmetics [1]. In transhumeral (above elbow) amputation level, the length of the residual limb is important because it determines the amount of space available to fit a prosthesis that has an artificial elbow [1]. Finally, higher levels of

amputation present more challenging issues for prosthesis fitting such as weight, appearance and heat dissipation [1].

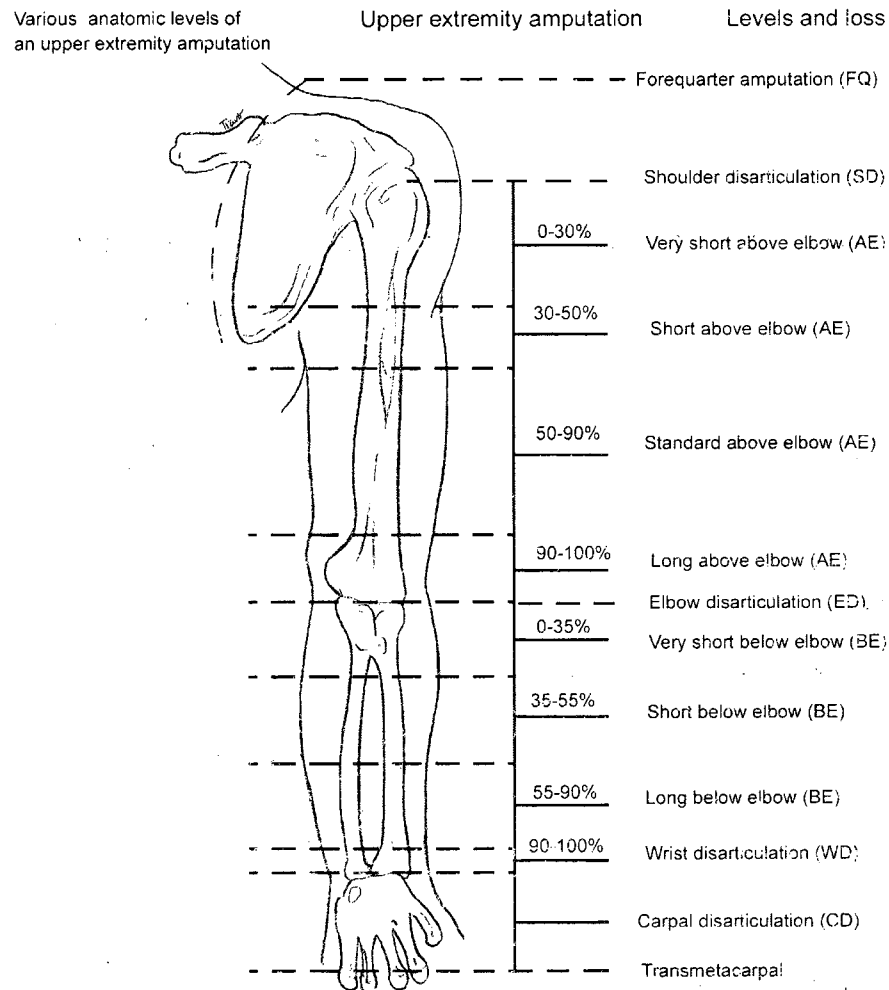


Figure 2-3: Amputation levels [32].

2.2.2 Upper Limb Replacement

The replacement of an upper limb is a complex task since the high dexterity of the hand and arm systems, the space and weight constraints, the cosmetic appearance and the psychological factors implicit in this task, which specifically depend and vary from one

amputee to another. A prosthesis is a device intended to return some of the function and physical appearance of a missing limb.

Several types of prostheses are available that allow the user to recover some natural functions. They are summarized in Table 2-4. The selection of a given prosthesis depends on the user's condition, preferences and objectives. In some cases, an amputee may be best served by no prosthesis at all. Therefore, the early stage of the patient assessment is very important for the amputee.

Table 2-4: Characteristics of different types of prostheses.

Type	Cost	Control effort	Function	Cosmetics	Weight	Feedback
Cosmetic	High	Very low	Least	Best	Light	No
Body-powered	Moderate	Moderate	Moderate	Least	Moderate	Highest
Electrically powered	Highest	Least	Highest	Moderate	Heaviest	Limited
Hybrid	Moderate	Moderate	High	Moderate	Heavy	Moderate
Activity-specific	-	Moderate	High	Poor	Moderate	No

Cosmetic (or passive) prostheses mainly mimic the appearance of the remaining limb but lack the ability to grasp. However, their use demands low effort and minimum maintenance. Active prostheses, divided in body-powered, electrically powered and hybrid, offer more functional characteristics at the cost of incrementing the weight and reducing the cosmetics.

Body-powered prostheses are mechanical devices that are actuated by motion of some part of the amputee body. This body motion is translated to a motion of the prosthesis, such as open/close of the hand or flexion/extension of the elbow, by means of a cable. They are the most common prosthetic device in the United States [1]. The main drawback of these devices is the limited range of motion given by the harness. However, they offer a high level of sensory feedback, which is very appreciated by the amputee population.

Externally powered prostheses use an electric source (a battery) to power electric motors, which actuate the prosthesis. The most common way that the user commands the prosthesis is by surface EMG electrode, but other input devices, such as switches, servos, linear transducers, potentiometers and touch pads, are also used to control the prosthetic device [1]. The advantages of these devices are the ease of control and lack of a need for a harness and in most of the cases the grasping force is increased with respect to the body-powered counterpart. Some disadvantages are the cost, weight and limitation in sensory feedback [32].

The hybrid option is a mixture between the body-powered prostheses and the externally powered devices. The most common combination is the use of a body-powered elbow with an electric hand and wrist [1]. Another option is an electric elbow with a body-powered hand. A final option is an activity-specific prosthesis, which is a device optimized to perform some determined activities, such as sports, gardening or repairing tasks. They are well-suited to the specific task but are not generally appropriate for other activities. They also tend to lack cosmetics.

The common components of an upper limb prosthetic device are the socket, the suspension, the control-cable system (for body powered prostheses), the control system with the power supply (for externally powered prostheses), and the terminal device. The socket is the interface between the residual limb and the prosthesis. Usually, it contains two layers: an inner soft layer and a hard outer layer. The inner layer covers the residual limb and the outer one prolongs the prosthesis to mimic the length of the counterpart limb [32]. The suspension is the part of the prosthesis in charge of attaching it to the residual limb. There are three types of suspensions: the harness-based, the self-suspended sockets and the suction sockets. The control-cable system is the mechanism used to control the movements of a body-powered prosthetic device, by translating the movements of others part of the body. These movements are transmitted to the prosthetic device mechanically by a cable system [32]. Some externally powered prostheses use a control system embedded in a microprocessor to control the devices movements. A battery is needed in this case to supply the energy to the microprocessor and to the sensors and actuators. Finally, the terminal device is the most distal part of the prosthesis. It can be divided also into passive and active. The passive terminal device can be divided again for cosmetic and for function. The active terminal devices are more functional than passive but usually less cosmetic [32]. They can be categorized as either hooks or prosthetic hands. Prosthetic hands allow more degrees of freedom and are more cosmetic than hooks. However, hooks are lighter than prosthetic hands. In addition, specific terminal devices are fabricated to match a specific task as mentioned before [32].

2.3 State of the Art in Advanced Upper-Limb Prostheses

2.3.1 *Mechanical Design*

During the past decade, different approaches have been addressed by researchers in industry and the academy in order to meet the mechanical requirements of upper limb prosthetic devices. The key elements of these devices are:

- a) Anthropomorphic size
- b) Light weight
- c) Sufficient DoF
- d) Large grip force
- e) Low control effort
- f) Low noise
- g) Cosmetics

One of the major challenges on the design of dexterous prosthetic hands is to find a balance among large number of DoF, large grip forces, small size actuators and reduced weight. A feasible solution to this problem is the use of underactuated mechanisms.

An underactuated system is one that contains more DoF than actuators. In an underactuated system (e.g. a finger) the torque is generated at one point (its proximal section) and transmitted to the adjoined parts (the phalanges) through either a wire-pulley system or rigid links [33]. While wires reduce the dimensions of the mechanism, the links are more robust and lead to larger grip forces [34]. Mechanical limits and passive elements, such as springs, constrain the system to adapt to the object shape [33].

In addition to having a reduced number of actuators, which reduce the weight and cost, underactuated systems allow a grasping configuration that is adaptable to the shape

of the object is obtained, which produces a more stable grasping configuration [35].

Figure 2-4 shows this concept.

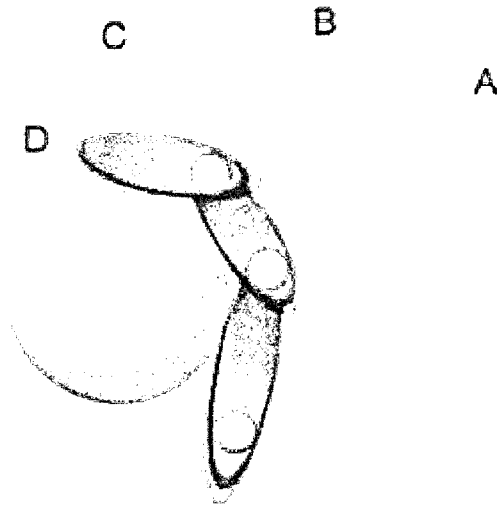


Figure 2-4: Adaptation of an underactuated system to the shape of an object (from [34]).

The underactuation concept has been applied to the design of several upper limb prosthetic devices [19, 34, 36-47]. The CyberHand [19, 48], a five-fingered prosthetic hand that contains 16 DoF and 6 motors, is actuated using a tendon-cable system. One motor per finger drives its 3 phalanges and one motor is used to produce the thumb abduction or adduction. This prosthetic hand is designed to restore not only the function of the missing limb, but also the sense of touch, giving to the amputee the opportunity of feeling what the hand is grasping.

An improved version of the CyberHand, the SmartHand [6, 39, 49], is one of the most advanced prosthetic hands. It also contains 16 DoF, but only 4 motors since the middle, ring and little fingers all move together. All the motors are integrated in the palm of the hand and transmit their torque by an underactuated system similar to its ancestor.



Figure 2-5: Left: CyberHand (from [48]). Right: SmartHand (from [6]).

Another hand that uses the underactuation concept is the HIT/DLR [41, 42]. In this hand, the thumb and index are driven by one motor each one and the other three fingers by another one. The thumb also contains a motor for its opposition. It uses underactuated bars and torsional springs to flex and extend the fingers, which can exert a maximum force of 10 N. The silicone hand [44] is an underactuated system with 10 passive DoF controlled by only one motor. In this design, the springs are replaced by compliant joints since the entire hand is made of silicone (Figure 2-6). A tendon-cable system is used to transmit the power of the motor to the fingers. A similar prosthetic hand design by Kamikawa and Maeno [40] has 15 DoF and only one motor. Grasping force up to 20 N were achieved with finger closing time less than one second.

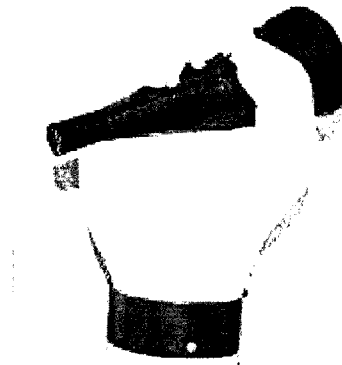


Figure 2-6: Silicon hand (from [44]).

The SPRING hand [34] and the Southampton REMEDI hand [50] are additional underactuated prosthetic systems. The former is a three-fingered hand that contains 8 DoF and one motor. The underactuation is produced by means of a slider, a differential mechanism and a belt-pulley system. The latter is a five-fingered hand actuated with 6 motors (4 for the fingers and two for the thumb). Each finger contains 6 bar linkages (capable of exerting up to 9 N) and a locking system for saving power (see Figure 2-7). Finally, a multifunctional underactuated prosthetic hand with extrinsic actuation is presented by Dalley et al [36]. It contains 16 DoF driven by 5 DC motors using a tendon-cable mechanism and torsional springs located at the joints of each finger. The position of thumb opposition is driven by a DC motor.

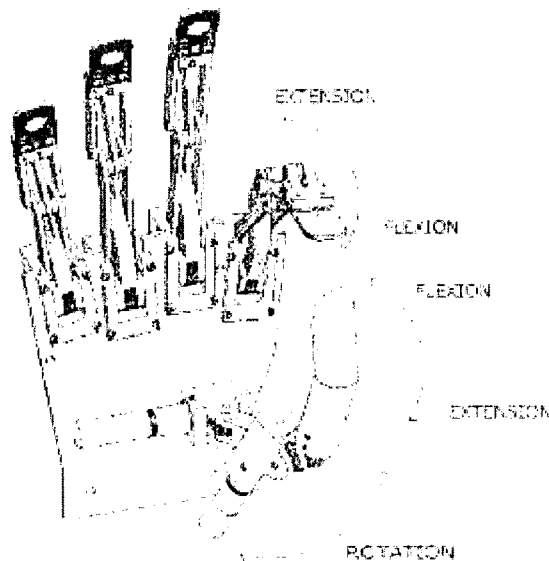


Figure 2-7: Southampton REMEDI hand (from [50]).

In another approach, the use of direct active control of each joint (equal number of DoF than actuators) has been reported [51]. Even though, this approach presents the limitation of less DoF due to the size of the motors (which are not small enough to fit in each joint and at the same time meet the anthropomorphic constraint) they have in general the advantage of larger grasping forces.

An example of this type of mechanism is the commercially available SensorHand™ Speed from the company Otto Bock [51]. It contains 1 DoF controlled with a DC motor that is connected to a clutch. This mechanism allows the switch between a high speed gear ratio and a high torque gear ratio. The SensorHand™ Speed has three active fingers: the thumb, index and middle fingers, which are connected mechanically and move all together. All fingers contain only one bended phalanx and the thumb is in

an opposable fixed position which allows cylindrical and pinch grasping configurations (see Figure 2-8). The maximum grip force achieved with this hand is 100 N.

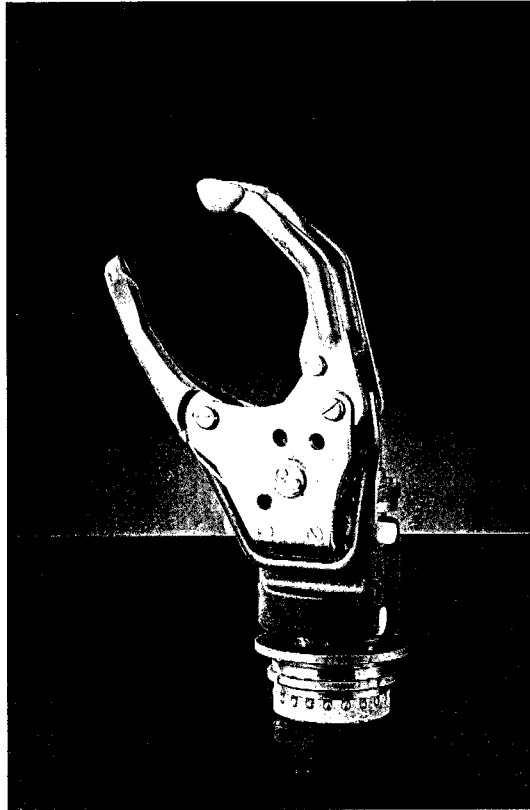


Figure 2-8: The SensorHand™ Speed from Otto Bock (from [51]).

The DARPA project “Revolutionizing Prosthesis” is developing another upper limb prosthesis that uses mostly active mechanisms [7, 52]. The group seeks to develop a new generation of prosthetic arm that will restore the functional and sensing aspect of the missing limb. They have created a five-fingered hand with 18 DoF controlled by 18 compliant DC motors embedded inside the hand and the wrist (Figure 2-9). Each finger has 3 joints with 2 associated motors. The index, ring and little fingers contain abduction or adduction motors and the thumb contain 4 DoF.

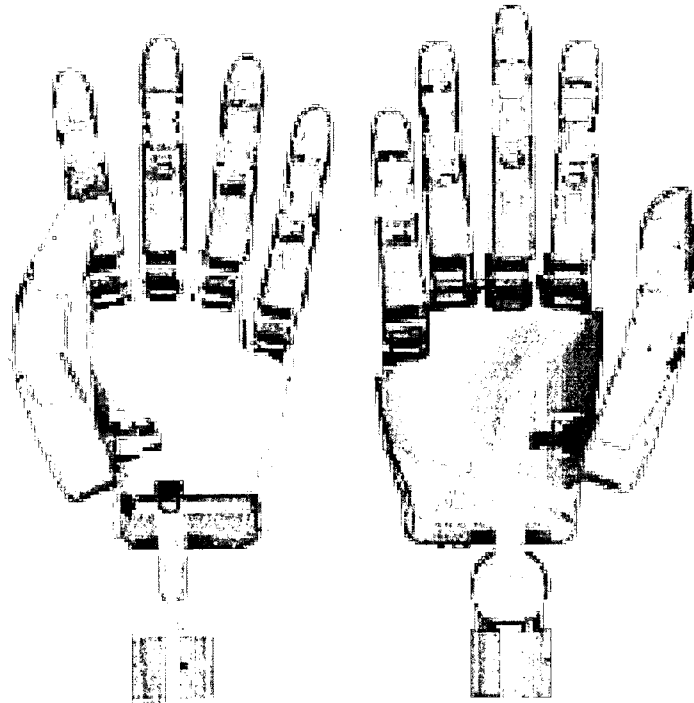


Figure 2-9: Female and male version of the DARPA program five-fingered hand (from [7]).

A new prosthetic hand, commercially available since 2007, which would be in between active and underactuated hand, is the i-LIMB from Touch Bionics [5]. It is one of the most dexterous hands on the market, and consists of a five fingers controlled independently by five DC motors (see Figure 2-10). Each finger contains 2 phalanges, with the distal phalanx bended (simulating a third fixed one). It is made of high-strength plastic in a modular design, which allows the easy interchange of the pieces that constitute the hand. The motion of the DC motors is transmitted by a toothed belt

(underactuation) to the phalanges. The thumb can be manually rotated to produce different grip patterns.



Figure 2-10: The i-LIMB from Touch Bionics (from [5]).

In these approaches, DC motors have been used to drive the mechanisms of the hand. However, researchers have been investigating other options to actuate prosthetic hands. For example, a gas-actuated prosthetic arm has been developed by Fite et al. [47]. This arm contains 21 DoF (17 DoF for the hand) and 9 gas-based pneumatic actuators, from which 5 are dedicated to the hand. The gas used to actuate the arm is monopropellant hydrogen peroxide that is controlled by small-sized servovalves. The hand is underactuated and contains compliant joints given by torsional springs. Figure 2-11 shows a prototype of the gas-actuated arm. The servovalves control the cylinders that perform the motion by pulling tendon-cables routed towards the hand.

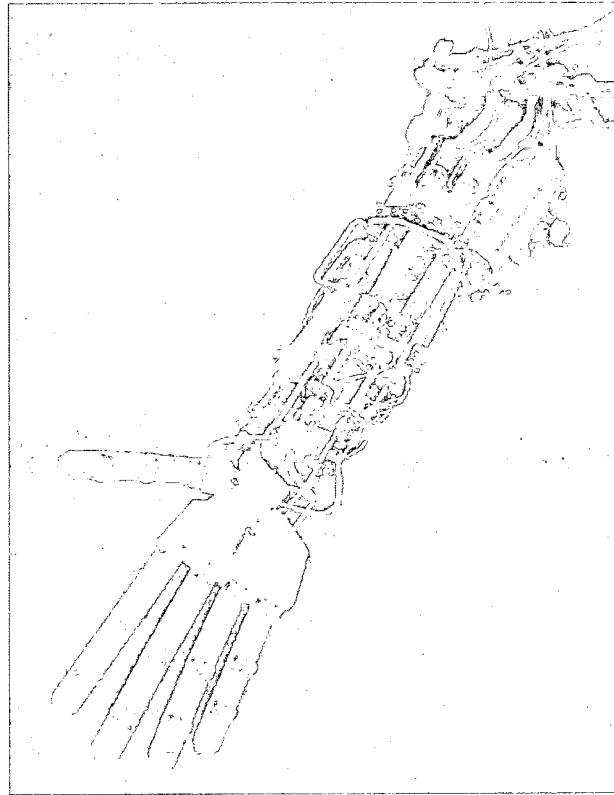


Figure 2-11: Gas-actuated prosthetic arm (from [47]).

Another pneumatic arm was proposed by Takeda et al. [46]. The actuator is made of a rubber balloon that is fed with air through channels and it is covered by a net. When the balloon is inflated (expanded) its length is shortened, which produces a linear motion that is translated to the joints.

A different approach has been addressed by Andrianesis and Tzes [37]. They used a shape memory alloy as the actuator for a prosthetic hand. This alloy contracts when it is heated, and leads to linear motion. One of the advantages of this kind of actuation is that no audible noise is produced. In their work, they developed a 16 DoF prosthetic hand driven by 7 actuators (see Figure 2-12). The actuation mechanism was specially designed to exploit the use of shape alloy wires (in this case Nitinol), which are located in the

forearm of the prosthesis. The wires are heated by an applied current, and the motion is translated by sliding plates. Extension is produced by springs, and a locking mechanism is included to save power consumption.



Figure 2-12: Prosthetic hand with shape memory alloy actuators (from [37]).

2.3.2 Sensory Systems

The sensory system is a key element of the current advanced upper-limb prostheses. In the past decade, prostheses were equipped with only one joint (one DoF) and no sensory feedback. With the advance in sensor technology, new miniature sensors have been developed that make possible integration into reduced spaces such as a fingertip or a phalanx joint. In general, in order to produce dexterous manipulation and stable grasping it is necessary to have some degree of proprioceptive feedback (e.g. joint position) and exteroceptive feedback (such as contact force). Object slip detection is also a very important issue to ensure the secure grasping and object manipulation in ADL.

The sensory information is then fed back either to the control system of the prosthetic device or to the user. Information such as surface temperature, contact force and slippage may be useful for the user to obtain some degree of sense and control over the prosthetic device [53]. This concept is represented in Figure 2-13. The sensors placed

in the prosthesis (a and b) can be used to automatically adjust the grip force (c) or it can be fed to the user by different ways such as the bones (d), the peripheral nerves (e), the skin (f) or by acoustic channels (g).

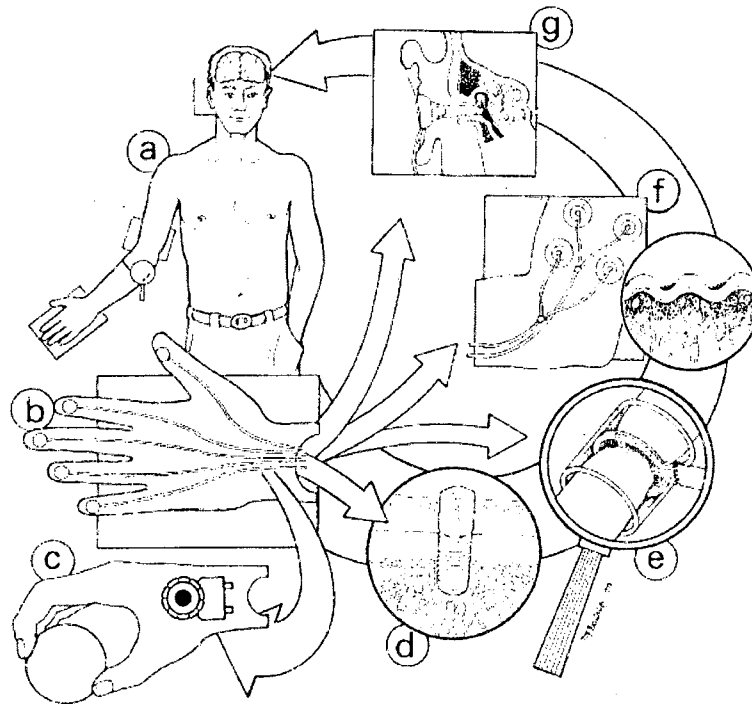


Figure 2-13: Sensory substitution in prosthetics (from [53]).

Several approaches have been used to design and fabricate exteroceptive sensors for prosthetic applications. Tactile/force sensors and slippage sensors are commonly used in prosthetics for exteroceptive feedback. Göer et al. presented a tactile sensor that can measure pressure profiles and vibrations in the sensor surface [54]. In this approach, a commercial array-based pressure profile sensor (DSA 9330/9335) was modified by embedding a piezoelectric PVDF (Polyvinylidene Fluoride) into the sensor. In this way not only the pressure profile is obtained, but also object slip detection is possible. The use of arrays of tactile and force sensors has also been presented in [55], in which a matrix of

64 piezoresistive force sensors were used (similar to Figure 2-14). Moreover, Edin et al. described an array of on-off sensors for the detection of mechanical discrete events [56].

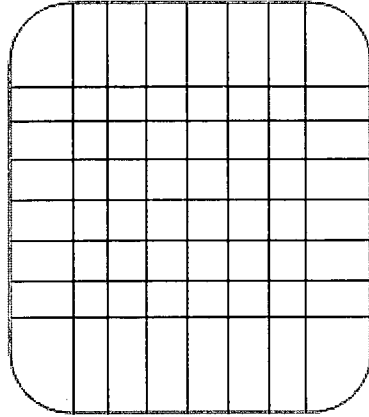


Figure 2-14: Sample of an array-based force sensor scheme [55].

In another direction, the use of fluid-based force sensors has been investigated [57, 58]. This kind of sensor consists of a rigid core surrounded by a fluid, which is contained by a flexible skin. When an external pressure deforms the fluid, the deformation can be measured either by electrodes placed in the rigid core (if the fluid is conductive, then the change in the impedance of the electrode is measured) or by a pressure sensor embedded inside the fluid. This concept is illustrated in Figure 2-15.

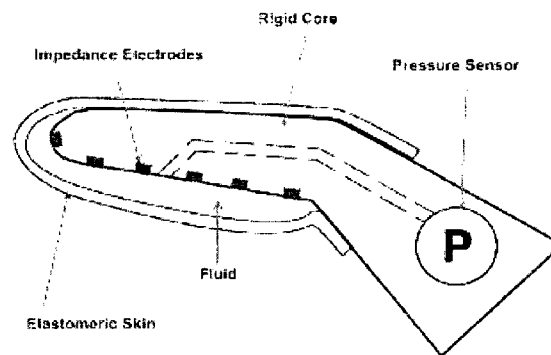


Figure 2-15: Fluid-based biomimetic tactile sensor (from [58]).

The use of micro electromechanical systems (MEMS) to fabricate miniaturized tactile sensors has also been extensively investigated. A 3-axial force sensor that can detect normal and tangential forces was presented by Carrozza et al. in [19]. The same sensor was then embedded in soft compliant flexible packaging that allows it to be used as a slippage detector [59]. A capacitance-based contact force was developed by Chappell and Elliott [60], which consists of two plates separated by an elastic material that acts as a dielectric. Then, a change in pressure is translated as a change in the capacitance of the sensor. A more complete sensor was developed later, in which slip detection and changes in temperature are also detected [61, 62]. Thick-film printing technology was applied to produce this multifunction sensor (see Figure 2-16).

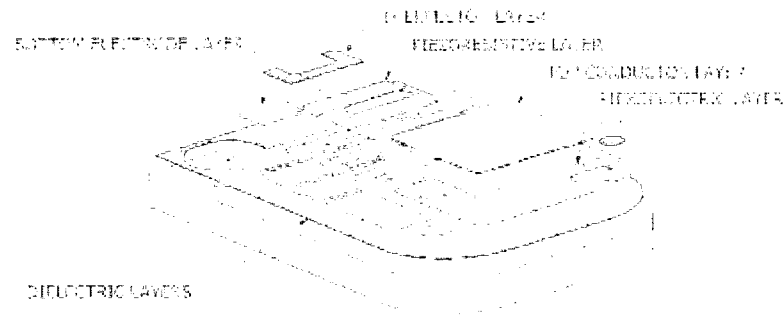


Figure 2-16: Thick-film multifunction sensor (from [62]).

Optical-based sensors are another option for tactile sensors. Four optical sensors [63] were placed in the SmartHand in the intermediate and proximal phalanges of the fingers [39, 49]. Finally, the use of strain gauges for normal and tangential force sensing was also applied [64, 65].

Proprioceptive sensors have been investigated in order to offer feedback from the mechanism itself. The use of a cable tension sensor was reported in [19, 35, 39, 49] for the design of the CyberHand and the SmartHand. It uses strain gauges to measure the stretch of the cable, an indirect measure of the force exerted over the object. In the SmartHand, motor current sensors were also implemented to provide an indirect measurement of the applied force. Another way of measuring cable tension was implemented by Fite et al. [47], which uses load cells between the tendon-cable and the actuator.

Joint position information is also useful information in fine manipulation. Hall effect sensors have been extensively used for this kind of measurement [19, 36, 41, 64, 65]. The main advantage of this type of sensors is the small size and the frictionless characteristics. Finally, motor encoders can be used as proprioceptive sensors in prosthetic hands [19, 36].

2.4 Control Strategies in Advanced Upper-Limb Prosthesis

Different control strategies to drive prosthetic hands have been proposed during the past decades. The four strategies most commonly used are open loop control systems [36, 66-74] (Figure 2-17, a), closed loop systems with feedback to the user [53, 75-79] (Figure 2-17, b), closed loop systems with feedback to the control system [5, 18, 19, 35, 41, 64, 65, 80-83] (Figure 2-17, c), and hybrid closed loop systems with feedback to both the user and the control system [20, 49, 84, 85] (Figure 2-17, d).

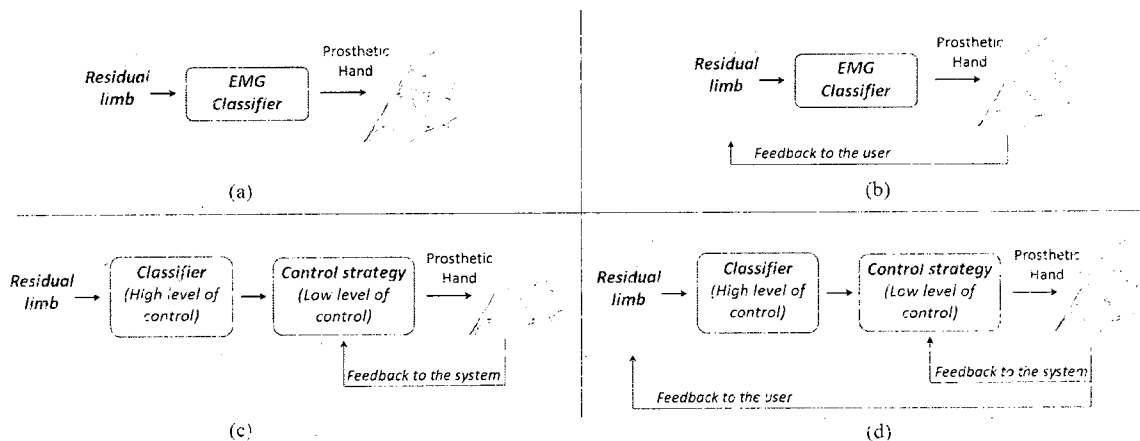


Figure 2-17: Different control strategies of upper-limb prosthetic devices. (a) Open-loop control, (b) Closed-loop feedback to the user, (c) Closed-loop feedback to the device, (d) Closed-loop feedback to both the device and the user.

2.4.1 Open Loop

Prosthetic devices have been controlled with EMG signals, where a classifier is used to decode the muscle contractions. We consider these systems to be open loop because only visual feedback is obtained. One implementation uses the information from the EMG amplitude. Then, the grasping force and joint angle are usually controlled by the amplitude of the EMG signals and the grip configuration is determined by the level of activation of different muscles [66, 70]. Pattern recognition-based classifiers are also

extensively used to discriminate many DoF. These classifiers have reached higher level of accuracy in multifunction prosthesis than conventional muscle activation-based classifiers [69, 71-74]. Specific features containing useful information are first extracted from the raw EMG signal. Then, they are used as inputs to a classifier, which determines which hand motions correspond to the feature set. The output of the classifier is lastly connected directly to the actuators of the hand.

The main drawback of this technique is the possible number of DoFs controllable by these systems, which in general is limited relative to the user necessity. The classification of EMG signals is a complex task when large number of controllable DoFs is demanded (such in the control of prosthetic hand). Hence, the number of separable classes is small and the controllable DoFs are also small. In addition, this type of controller is not easy to operate since the user must learn to differentiate several types of multiple muscle contractions to control the prosthesis, which increases the psychological effort and muscle fatigue [18].

2.4.2 Closed Loop Systems with Feedback to the User

A second group developed exteroceptive and proprioceptive sensory systems in order to bring to the user sensory feedback information. As described in section 2.3.2 and illustrated in Figure 2-13, there are different ways of achieving user stimulation. With these kinds of stimulations the user can obtain information of touch and slippage, which contributes in improving the dexterity of the control of the prosthesis [85] and the comfort of the users.

The most common channel of stimulation is by the skin (non-invasive methods) such as electrical and mechanical stimulation [75, 78, 79]. In general, the stimulation is

produced at some location near to the residual limb. A particular case is presented by Panarese et al. [78], in which grasping force feedback stimulation was delivered to the tip of the participants toes. The idea of giving sensory feedback through the toes seems to overcome common constraints like the limitation in the possible level of feedback discrimination, the problems associated to skin adaptation and to the generation of unpleasant sensations. However, miniaturization of the whole haptic system and improvements in the bandwidth and time delay are necessary before this system can be used by the amputee population [78].

Direct signals from the nervous system are the most natural and promising mode of stimulating a prosthetic device. Dhillon and Horch developed a feedback system by connecting nerves on an amputee stump [77]. The system was successfully fed information about grip force and joint position to the amputee, which improved the control of an artificial arm. Nevertheless, this feedback mode is highly invasive and not yet sufficiently developed for long-term implementation.

2.4.3 Closed Loop Systems with Feedback to the Control System

To reduce the control effort of multifunction prosthetic hands, different closed loop control systems were developed in which the sensory information is fed only to the controller. The user still has the control of the prosthesis, but the control is organized in a hierarchical structure, in which the EMG signals are classified in a functional way. That is, only the intent of the user to open/close the hand (and in some cases a grip pattern selection) are classified. The prosthetic device then takes care of automatically grasping the object by modulating the grasping force to avoid object slippage. The grasp is

implemented by an automatic control system that uses sensory feedback to adapt to the shape of the object and to hold it without producing deformation.

Cipriani et al. developed a closed loop control system for the CyberHand [35] that uses the feedback information in two subsequent stage. The first stage consists of a pre-shape of the hand (depending on the selected grip pattern), in which a position control is used to configure the finger in the desired pattern. The second stage is a grip force control to adjust the grasping force in order to produce a stable grasp around the object.

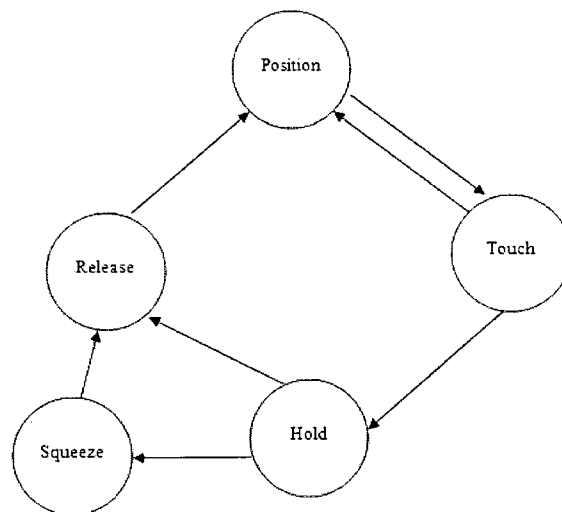


Figure 2-18: Control strategy scheme (from [18]).

In another approach, Light et al. presented a control strategy hierarchical organized to control the multifunction Southampton-REMEDI prosthetic hand [18]. It is also a stage-based control scheme, illustrated in Figure 2-18. At first the hand adopts a grip position controlled by the user. Then, the system switches to a touch state where the hand exerts minimal force over the object. After that, when the user decides to hold the object by a contraction of the muscle, the system switches to a hold state where the hand

adjusts the grasping force to hold the object while avoiding slippage. A squeeze signal from the user makes the hand open and release the object.

Engeberg et al. have used several closed loop control approaches to improve the controllability of the Motion Control hand [64, 65, 81]. Even though in this hand the user controls the grip force directly from the EMG signals, a force control assists in the grasping task. The force-derivative feedback in the force control loop increased the sensibility of the applied force. It increases the damping, which reduces the force overshoot at the beginning of the grasping [65]. In another work, Engeberg et al. presented a hybrid force-velocity-position control implemented also in the Motion Control hand. This system was reported to improve the overshoot problem in initial grasping force regarding to open loop and force control systems [64]. Finally, an adaptive slip prevention system that uses the derivative of the shear force was reported in [81]. The system improved the force control of the Motion Control hand, as demonstrated by quantitative and qualitative results of bench top and human experiments.

Wettels et al. used the biomimetic tactile sensor described in section 2.3.2 (refer to Figure 2-15), to implement a grip control strategy [80] based on the control scheme shown in Figure 2-19. The control system is based on the computation of the normal and tangential force signals from the fluid-based tactile sensor. The algorithm uses this information to detect slippage, and it adjusts the grip force accordingly.

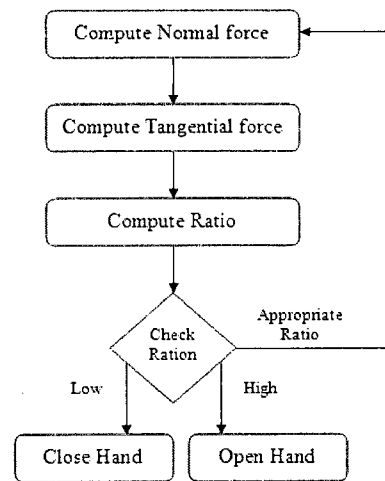


Figure 2-19: Control scheme of a grip control using a biomimetic fluid-based sensor (from [80]).

Although each study presented in this section relies on different control techniques, they all greatly reduce both the amount of concentration required by the user and the handling errors [18].

2.4.4 Hybrid Closed Loop Control Systems

Researchers have been developing hybrid systems that combine the ability of automatic control systems to accomplish tasks such as holding and grasping (section 2.4.3) with the ability of signals fed back to the user to improve user control (section 2.4.2)

Figure 2-20 shows a hybrid control scheme described by Luo et al. [85]. The opening and closing of the hand is controlled by the user by means of EMG signals recorded from the residual limb. Tactile sensory feedback (touch and slippage) is obtained from sensors placed in a 2 DoF prosthetic hand. The sensory information is fed to the user by electric shock stimulation, where one frequency represents touch and

another frequency represents slippage. The tactile feedback is also sent to the controller to automatic avoid slippage. The user has the control of the hand before and after it touches the object, but not during the holding and grasping task.

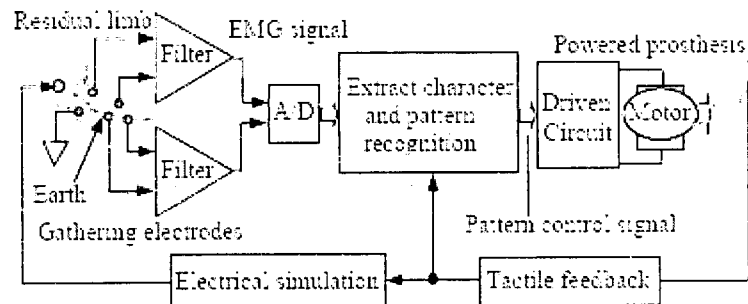


Figure 2-20: Hybrid control system with feedback to both the user and the control system (from [85]).

A similar approach is presented by Cotton et al. [20]. The authors present a scheme similar to the one shown in Figure 2-20, in which the user controls the opening, closing and stopping of the hand and an automatic control system controls the grasping process. Sensory feedback is sent to the user by electro-stimulation in order to offer perceptual information. Finally, a hierarchical structure is presented by Cipriani et al. [84]. In this work, different levels of control are presented to drive an underactuated prosthetic hand, which contain many proprioceptive and exteroceptive sensors. A high level of the structure is used to select grip patterns and also to inform the user about sensory events. The low level is used to automatically adjust the grasping force and to adapt the finger close around the object in order to obtain stable grasping without the supervision of the user.

2.5 Low-Cost Approaches

Although many approaches have been proposed towards the developing of low-cost lower-limb prostheses, only a few upper-limb counterparts have been reported. In the early development, most of the low cost approaches are reduced to body-powered prosthesis. Sitek et al. presented a low-cost body-powered arm made with inexpensive materials with socket fabricated with a simple technique that reduces the need for specialized labor skills and costly equipment [11].

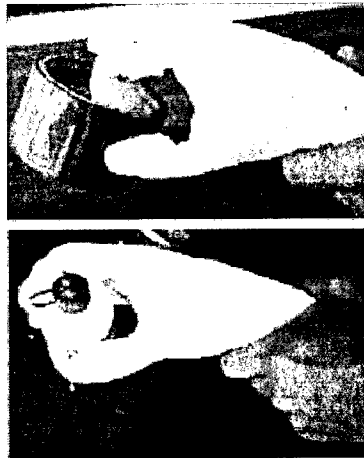


Figure 2-21: Body-powered low-cost prosthetic hand (modified from [86]).

An inexpensive body-powered underactuated hand is proposed with one DoF and made of an elastomeric polymer casting on a mould [86]. Doshi et al. presented a more complex but cost effective body-powered prosthetic hand [87]. It contains 3 joints in each finger and a manually opposable thumb covered with a soft polyurethane foam, offering an adaptive grip that conforms to the shape of the objects [87]. Nevertheless, these hands are limited in dexterity since they are body-powered and allow the user to control only a few DoF.

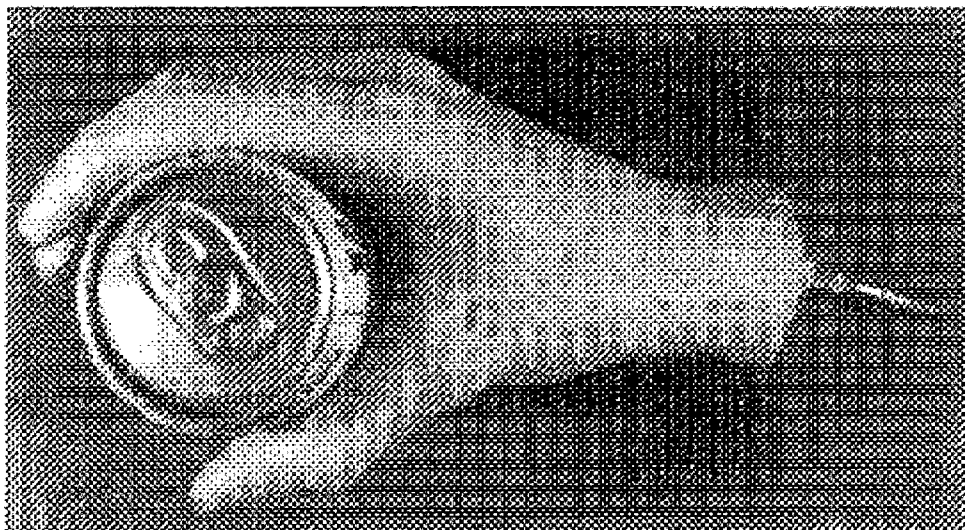


Figure 2-22: Gloveless endoskeletal low-cost prosthetic hand (from [87]).

CHAPTER 3

MECHATRONIC DESIGN OF THE PROTOTYPE

A mechatronic design of a five-finger robotic hand was developed as a flexible platform for implementing and evaluating the proposed control strategy. The design feature criteria are outlined below:

- a) The prototype must contain four underactuated fingers plus an opposable thumb.
- b) The index finger, the middle fingers, and the thumb must move independently.
- c) The prototype must match the human hand in weight and dimensions.
- d) The prototype must contain force and joint position sensory feedback at a cost less than 100 USD.
- e) The prototype construction must be simple, inexpensive and flexible enough to allow modifications.
- f) The prototype must contain enough DoF and grip force to produce most of the ADL.

The mechatronic design was focused in the development of a rapid prototype of the hand. Therefore, issues concerning material selection, efficiency of the mechanical systems (gears, pulleys, etc.) and miniaturization of the electronic boards are outside the scope of this dissertation. We believe that improvements in the mechatronic aspect of the prototype only can improve the performance of the control strategy and not deteriorate it.

This chapter presents a chronological description of the mechatronic design and fabrication of the prototype. The design contained several stages, from the design of a single finger to the development of the second generation prototype. The sensor used and the electronic circuits are also described. Finally, a brief cost analysis of the entire prototype is presented at the end of the chapter.

3.1 Mechanical Design

3.1.1 *Preliminary Finger Design*

As a first step towards the design of the prototype we fabricated the underactuated finger shown in Figure 3-1. A model was implemented in SolidWorks and printed in ABS plastic on a rapid prototyping machine. It contained 3 phalanges and its dimensions were larger than a real finger for testing purposes. The flexion of the finger is obtained by a tendon-cable that runs inside the finger and is attached at one end to the tip of the finger and at the other end to a motor-gear system located at the base (not shown in Figure 3-1). The extension of the finger is achieved by torsion springs located at the joints of the phalanges. The idea behind this system is to mimic the mechanism of a real finger and at the same time to take advantage of the underactuated mechanism. It is considered an underactuated device because the number of actuators used is less than the possible DoF. In this case, the finger has 3 DoF (each DoF refers to a separate joint movement that is not controlled independently) and only one motor.

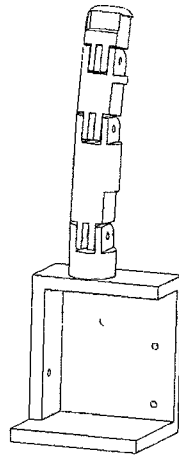


Figure 3-1: Underactuated finger.

Potentiometers were placed at each joint of the finger and a cost effective force sensor resistor (FSR) was placed at the tip. Silicone rubber was attached to the finger tip in order to increase the sensibility of the force sensor. Three modalities were tried and the schematics are shown at the top of Figure 3-2. The last sensor placement configuration is shown at the bottom of Figure 3-2. Modality number two was selected for the sensor placement.

This prototype served as a first platform to test the sensor placement and the overall performance of the system, as well as a decision support towards the development of the whole hand.

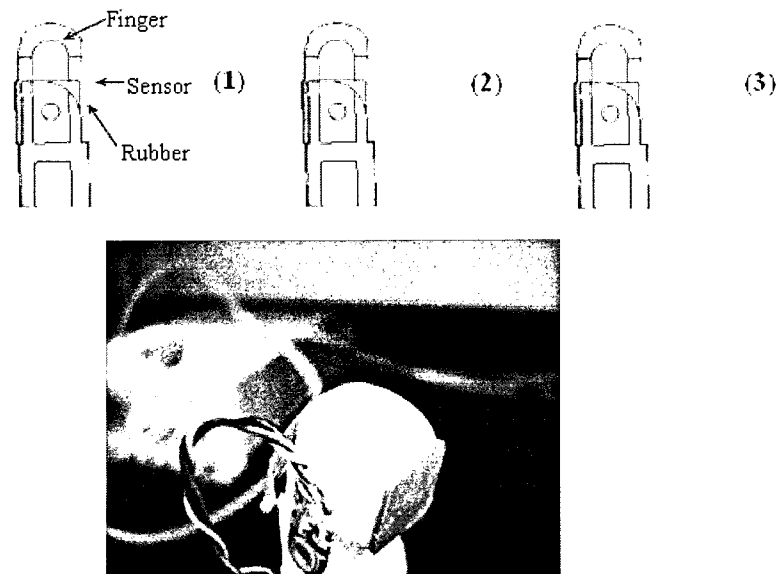


Figure 3-2: Schematics of three different positions for testing the force sensor.

3.1.2 *First Generation Prototype*

Based on the results of the previous finger design, a low-cost five fingered underactuated hand with 10 DoF was constructed (Figure 3-3) as the first generation prototype. Each finger contains two phalanges and the distal phalange has been bended at the tip. It was designed in SolidWorks CAD software and printed in ABS plastic on a rapid prototyping machine. The thumb, index and middle fingers are the active fingers that are driven independently by three low-cost DC gear motors (MS-16024-050 from BaneBots, Loveland, CO). The ring and little fingers are passive and mechanically connected to the middle finger by mean of gears and these three fingers move all together. Note that we are not concerned in making the ring and little fingers move independently, because their major function is to stabilize the grasped object during a cylindrical or spherical grasp. The flexion of each finger is controlled by a flexor tendon-

cable connected to a pulley. The pulley is attached to a worm-gear system driven by the DC motors. This worm gear system allows the level of exerted force to be maintained by each finger even when the DC motor is turned off, working as a locking system and reducing the power consumption. In addition, the extension of the fingers is achieved by springs connected to an extensor tendon-cable. All the actuators and gear systems are housed inside the palm of the hand. The fingers and the palm are covered with soft foam to increase the grip of the hand and to assist in slip detection. The sensory system consisting of inexpensive FSR (Interlink Electronics, Camarillo, CA) and potentiometers is placed at the tip of each active finger and at the proximal and middle joints on the active fingers, respectively.

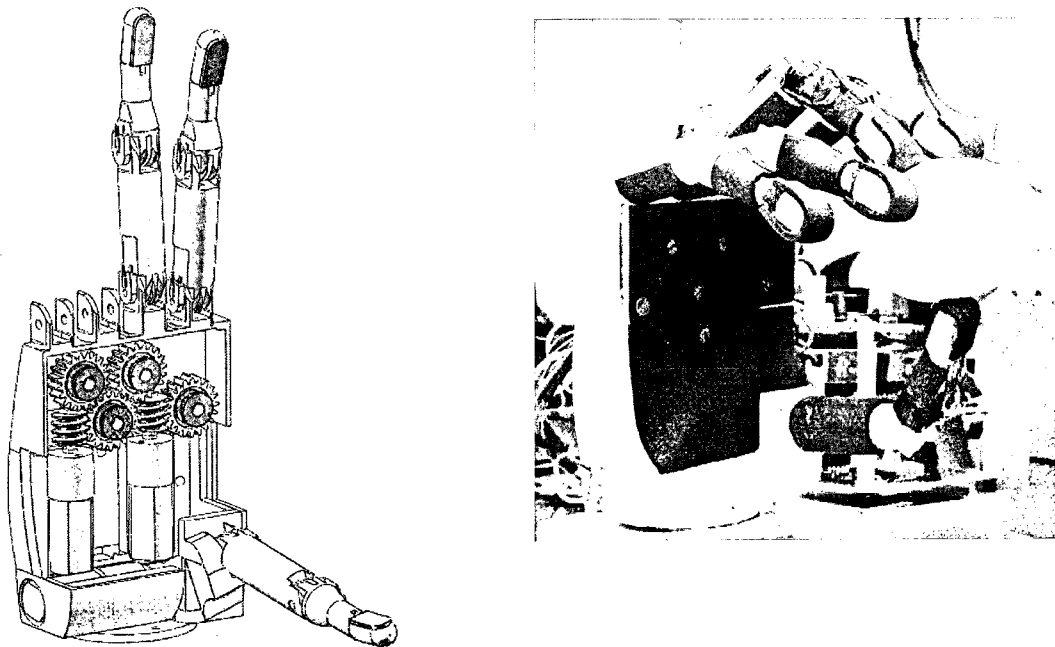


Figure 3-3: First hand generation. CAD model (left). Actual prototype (right).

3.1.3 *Second Generation Prototype*

An improved design of the first generation prototype was fabricated and it is shown in Figure 3-4. Similar to its previous design, it contains five fingers. Each finger consisted of two phalanges and its tip was slightly bent. The thumb, index and middle fingers moved independently, driven by three inexpensive DC gear motors (MS-16024-050 from BaneBots, Loveland, CO) by means of a tendon-cable system. The ring finger and little finger were mechanically connected and were allowed to follow the middle finger. The gear reduction ratio for the motors that drive the index and thumb fingers was 24:1 while for the middle finger was 38:1. The tendon-cable was connected to the DC motors by a worm gear system attached to a pulley (similar to the previous design). The extension of the finger was achieved by a spring fixed across the dorsal part of the palm and at the extensor tendon cable.

One more DoF was added to the thumb in order to produce its opposition. This movement is performed manually by means of a mechanical system that allows fixing the thumb in two positions. This design avoids the addition of a fourth motor to produce the thumb abduction or adduction, reducing the cost and power consumption.

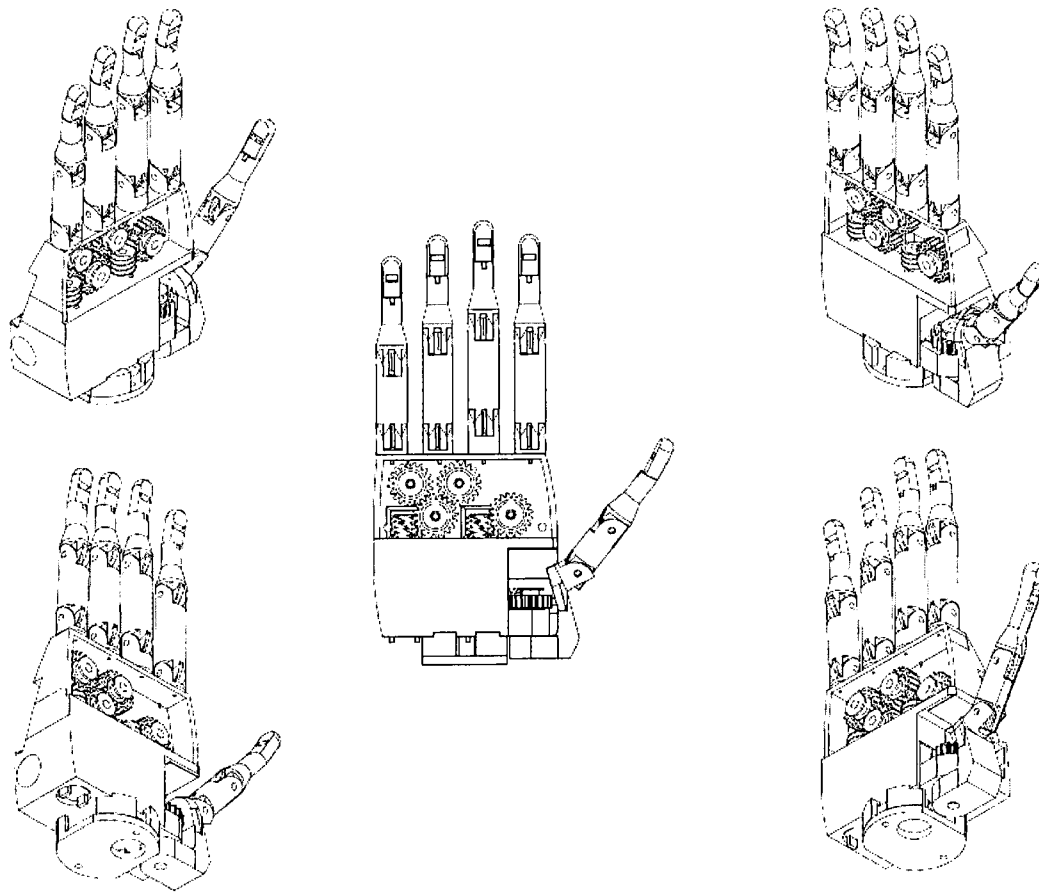


Figure 3-4: CAD model of the second generation prototype.

The whole hand was designed in SolidWorks CAD software and was printed in ABS plastic with a rapid prototype machine. As a result, the robotic hand contains 10 DoF driven passively by the DC motors and one DoF controlled manually, which produces several types of grasp configurations such as cylindrical grasp, pinch grasp, lateral grasp and spherical grasp.



Figure 3-5: Fabrication of the silicone glove.

In order to protect the hand and to increase the grip, a flexible glove was designed. Liquid silicone rubber (Dragon Skin™) was selected as the glove material to provide both flexibility and resistance. This material has been used in other prosthetics [88]. To fabricate the glove, first, a mold of the hand was created and then the silicone rubber was applied to the mold layer by layer until the desired thickness for the glove was obtained (see Figure 3-5). After curing, the glove was peeled off from the mold and used to cover the robotic hand. Figure 3-6 shows the prototype wearing the silicone glove. The glove improved the grip and the cosmetic appearance of the hand.



Figure 3-6: Hand prototype wearing the silicone glove.

3.1.4 *Grasping Patterns*

The mechanical aspect of the prototype was designed to produce several grasping patterns in order to assist the user in performing most of the ADL. For this design the taxonomy presented in [89] was follows. However, some of the grasping patterns shown in [89] were not included in the design since the prototype contains less DoF than a real hand. Figure 3-7 shows the final taxonomy that the prototype was designed to perform.

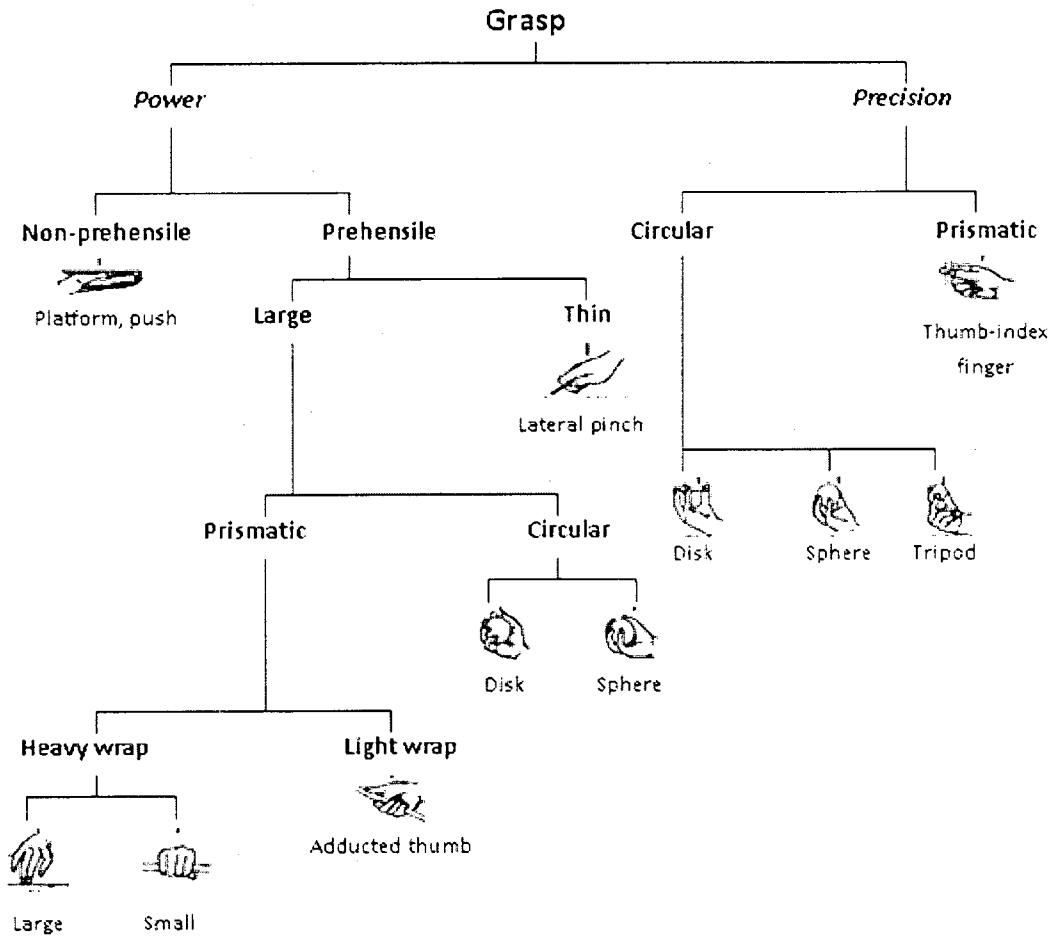


Figure 3-7: Grasping patterns produced by the prototype (modified from [89]).

3.2 Electronic Design

The same electronic circuits were used for the first and second generation prototypes. As it was described before, the contact force and position constitute the sensory system of the prototype. Inexpensive force sensor resistors (FSR) (Interlink Electronics, Camarillo, CA) were used to measure contact force at the tip of each active finger. There is a slight difference in the type of sensors used between the first and second generation prototype; the first included potentiometers at the joints of the active fingers to measure the joint angle, while the second included low-cost resistive flex

sensors (RFS) (Spectra Symbol) at the dorsal part of each active finger to measure the finger angle. With this sensory system it is possible to determine the grasping force and the flexion angle of the fingers at each time, which allows the prosthetic hand to hold different objects without performing any deformation [90].

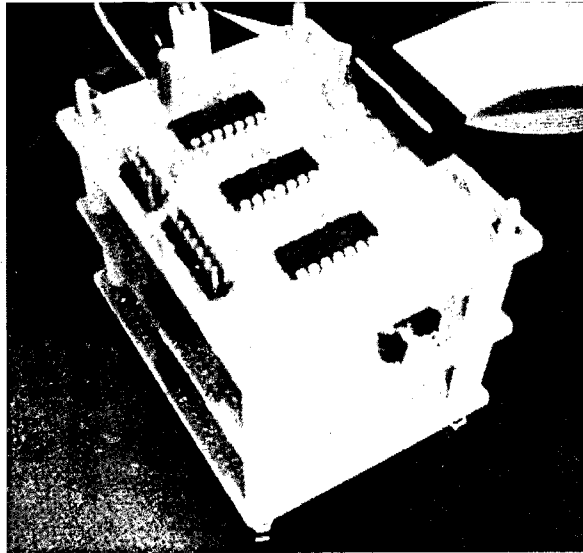


Figure 3-8: Circuit boards.

Three circuit boards (see Figure 3-8) were designed, assembled and used in both generations of prototypes. Two of them are used to drive the three DC motors and the last one is used for conditioning the signals from the force sensors. The signal conditioning system contains three analog filters (one per active finger) and three amplifiers, which are necessary to handle the signals from the FSR. The filters are simple low-pass filters implemented to eliminate high-frequency signal and to avoid electric interference. They are designed with high input impedance in order to avoid loading the sensors. Figure 3-9 shows the schematic of the circuit (the same circuit is repeated 3 times for each of the FSR). It consists on a voltage divider formed by the FSR and a resistor, in order to obtain a voltage proportional to the force exerted over the sensor. Then, the signal is amplified

by a simple non inverting amplifier (with gain 2.2) and filtered with R_3C_1 (cutoff frequency 4.8 Hz).

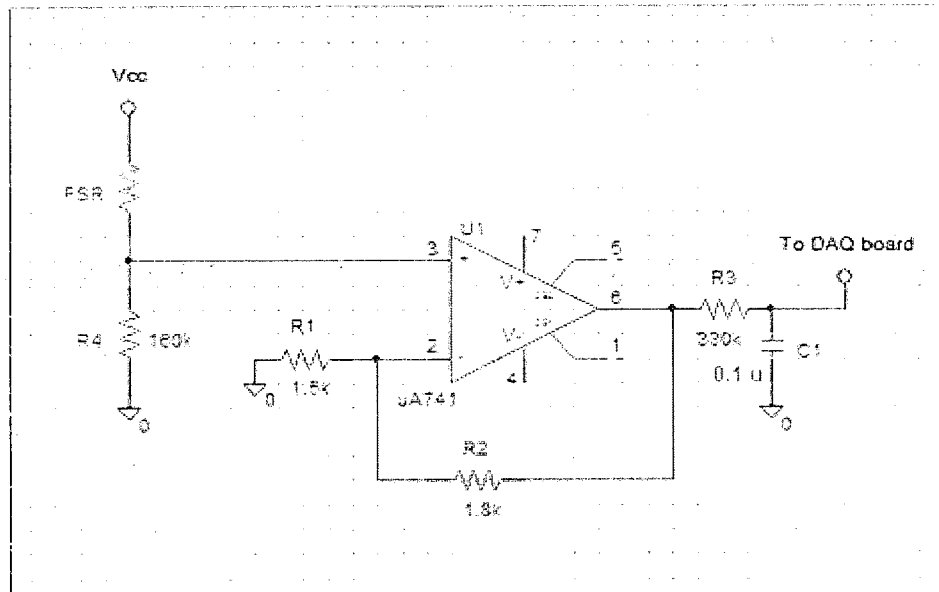


Figure 3-9: Signal conditioning circuit.

The signal conditioning circuit was calibrated using a dual-range force sensor (Vernier DFS-BTA). The calibration setup is shown in Figure 3-10. The force sensor was connected to a small platform through a string. The force sensor was then pulled down in order to apply force over the fingertip while measuring the pulling force. Different force values were applied in order to excite the whole range of the sensor circuit. Using the data from the dual-range force sensor and the FSR circuit output, a 4th polynomial fitting was implemented in Matlab. Figure 3-11 shows the results with the calibration formula for force in Newton.

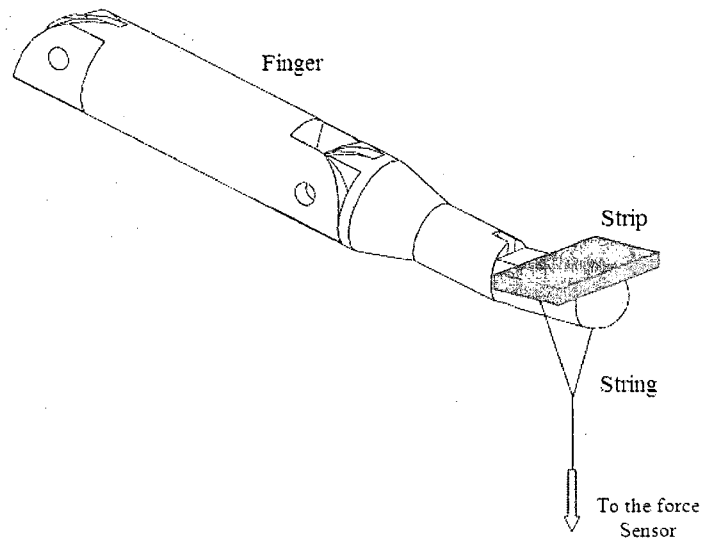


Figure 3-10: Calibration setup.

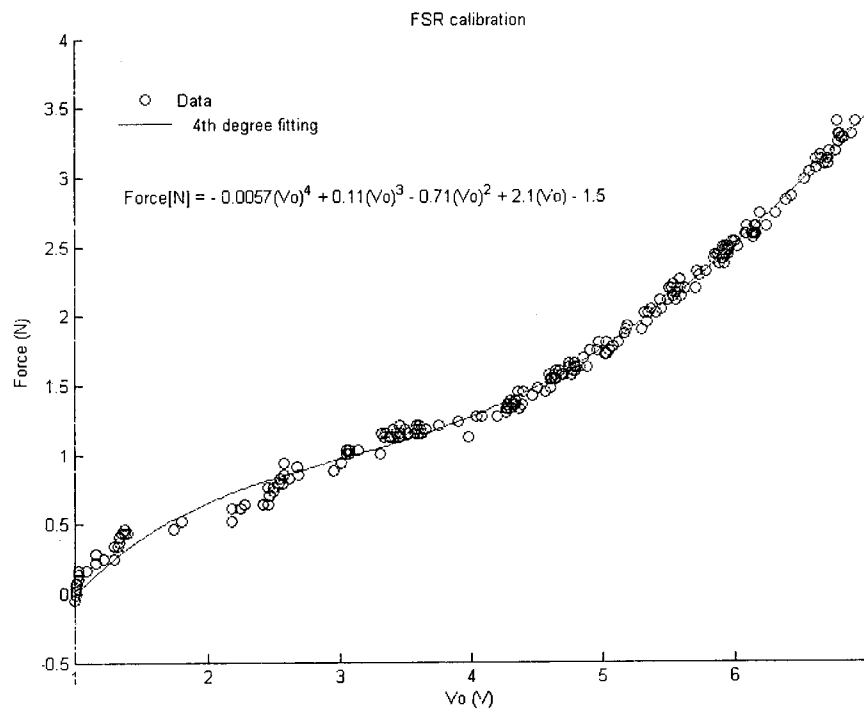


Figure 3-11: 4th polynomial fitting for the calibration of the FSR circuit.

The motor driver circuits consist of two parts. One generates a pulse width modulating (PWM) signal used to control the motor current (Figure 3-12). It is implemented using operational amplifiers and it is basically a triangular signal generator (U1A and U2A) that is compared with respect a threshold (U3A) that can be adjusted from the computer (command digital signal). The other is a switch circuit (Figure 3-13) that uses BJT transistors (Q1 and Q2) to change the direction of rotation. Power operational amplifiers (L2724) are used to drive the current. Therefore, only one PWM signal is used for both directions. By setting S1 and S2 to “0” or “1” the direction of the motor can be selected. A total of three driver circuits were implemented (one per active finger). Finally, NI DAQ boards (NI PXI-6723 and NI PXI-6224 from National Instruments) are used for the data acquisition system.

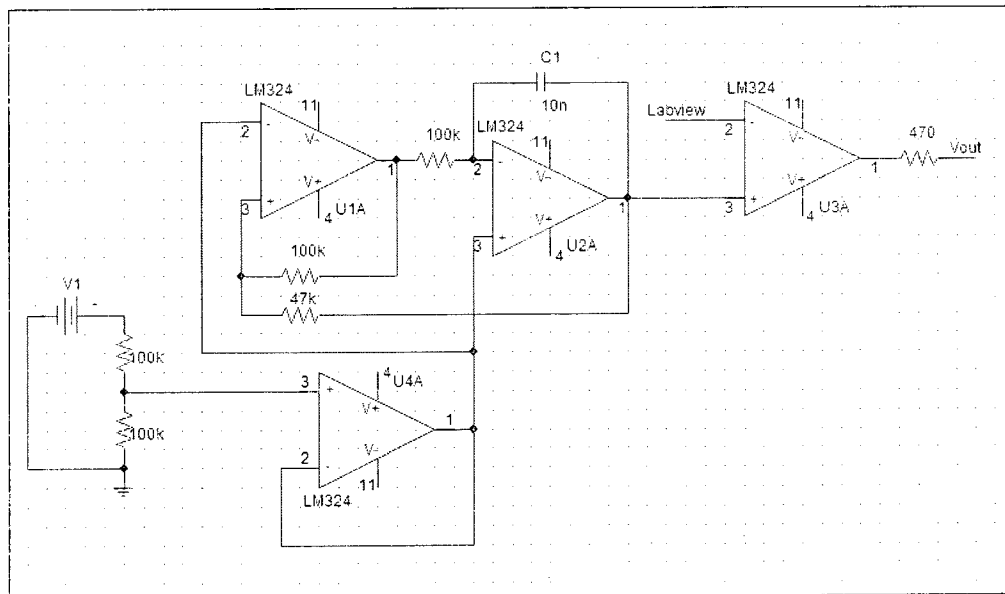


Figure 3-12: PWM circuit.

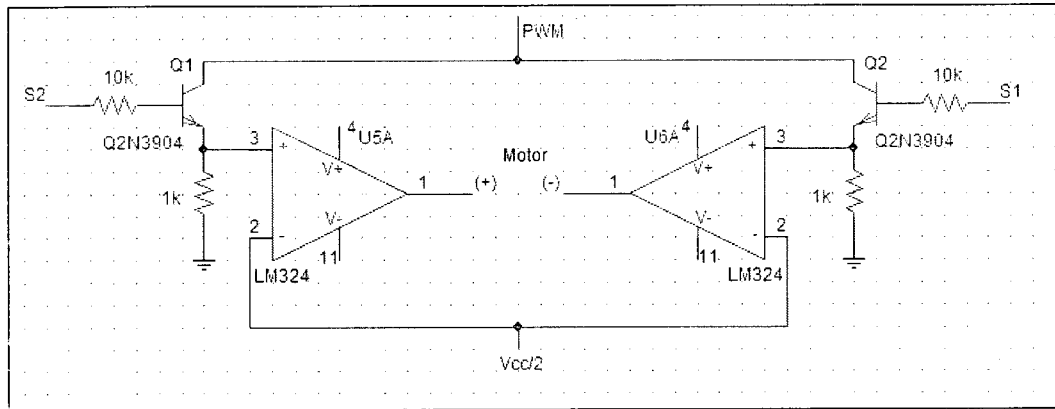


Figure 3-13: Circuit used to switch the direction of rotation of the motors.

3.3 Preliminary Cost Analysis

A preliminary analysis of the cost of the components of the second generation prototype is presented in Table 3-1. The table represents only the cost associated with material used in the fabrication of the prototype but it does not represent other costs related to the development and construction of the hand. However, it gives a general idea of the cost of the prototype and can be used to evaluate its suitability for a cost effective prosthesis.

Table 3-1: Preliminary cost analysis of the prototype.

Item	Number	Cost Per	Total	Vender
½ inch Worm Gear	3	\$1.40	\$4.20	Technobots
¾ inch 20 Tooth Plastic Spur Gear	5	\$0.80	\$4.00	Technobots
¼ inch Plastic Pulley	5	\$0.45	\$2.25	Technobots
Steel Spring 3 Pack	2	\$3.29	\$6.58	True Value
MS-16024-050 DC Motor	3	\$13	\$39.00	Trossen Robotics
Steel cable Pack	1	\$2.50	\$2.50	Wal-Mart
in ³ Prototyping Plastic	19 in ³	\$6-10	\$114.00	Bogard
1.75" X 0.3" Force Sensor	3	\$6	\$18.00	Trossen Robotics
4.5" X 0.2" Flex Sensor	3	\$12.95	\$38.85	Trossen Robotics
TOTAL			\$229.38	

CHAPTER 4

FORCE CONTROL STAGE

The control strategy was briefly described in Chapter 1. One of the principal stages in this control methodology is the force control stage. This stage is activated once the user selects the grasp configuration and the pre-shape stage has been completed, as illustrated in Figure 1-2 and Figure 1-4. Once the force control begins, an initial minimum force reference value, which was empirically determined by an adjusting step, is used as the starting point for the controller. The system will then attempt to maintain this initial force level except when an unintended movement of the object is detected, in which case the reference value is increased. For this reason, the detection stage works in conjunction with the force control stage.

The control of prosthesis is highly nonlinear due to the existence of motor dead bands, friction and large gear ratios [65]. The neural network-based NMPC technique was selected to control the force exerted by the thumb, the index and the middle finger, based on its ability to handle nonlinear systems [91, 92]. This characteristic has led to the use of this technique in different scenarios in a wide range of engineering fields [93-99].

Figure 4-1 shows the block diagram of the force control stage using a neural network-based NMPC scheme. In the figure u is the voltage supplied to the motor, y is

the force measured at the fingertip, θ is the angle of the finger, \hat{y} is the predicted future force and r is the force reference.

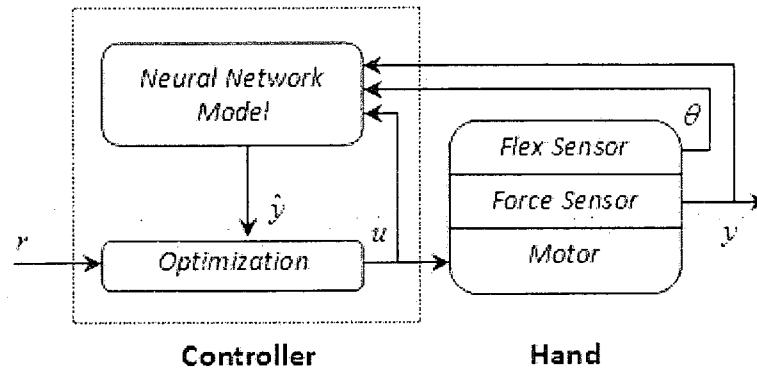


Figure 4-1: Block diagram of the force control system. Here u is the voltage supplied to the motor, y is the force measured at the tip, θ is the angle of the finger, \hat{y} is the predicted future force and r is the force reference.

The idea behind a general NMPC is to create a nonlinear model that estimates the dynamics of the system to predict future system outputs (in this case the contact force \hat{y}) over a defined time horizon. Afterwards, the controller uses this prediction to calculate the optimal input (u), such that the system follows the desired reference force (r) over this horizon [100].

The validity of the controller was first tested through computer simulations of a simple one-finger system, and then on one of the fingers of the actual prototype of the hand. The simulation and experimental results showed promising results in which the system was able to modulate several levels of forces over different objects with small overshoot and short response time.

This chapter is organized as follows. First the control algorithm is explained in details along with the hypothesis; then, simulations results are presented; finally, experiments performed over the prototype are described and the results discussed.

4.1 Hypothesis

The implementation of Nonlinear Model Predicted Control (NMPC) based on Neural Networks as a force control system of an underactuated finger driven by a motor-pulley system produces a rise time below 1 second, an overshoot smaller than 1 N and a steady state error of less than 5% of the reference value, regardless the grasped object stiffness.

4.2 Force Control Design

4.2.1 *Neural Network-Based Modeling*

In our study, the model is implemented by a neural network. Because neural networks are able to approximate any nonlinear function [101], they are usually used in nonlinear modelling. A neural network can be described as a collection of units that are interconnected, forming different layers. Each connection contains a weight and each unit may perform a function. A neural network can be described as a black box that is able to obtain the parameters of a mathematical function by mapping the relationship between the input and output vectors. The neural network are computational tools capable of learning this mapping from observations [100]. This process is usually referred as system identification.

A multilayer perceptron (or feedforward neural network) is a type of neural network topology that contains an input layer, one or more hidden layers and an output layer [102]. Figure 4-2 shows an example of a feedforward topology of a neural network

with an input layer of 4 units, one hidden layer of 15 units, and one output layer with only one unit.

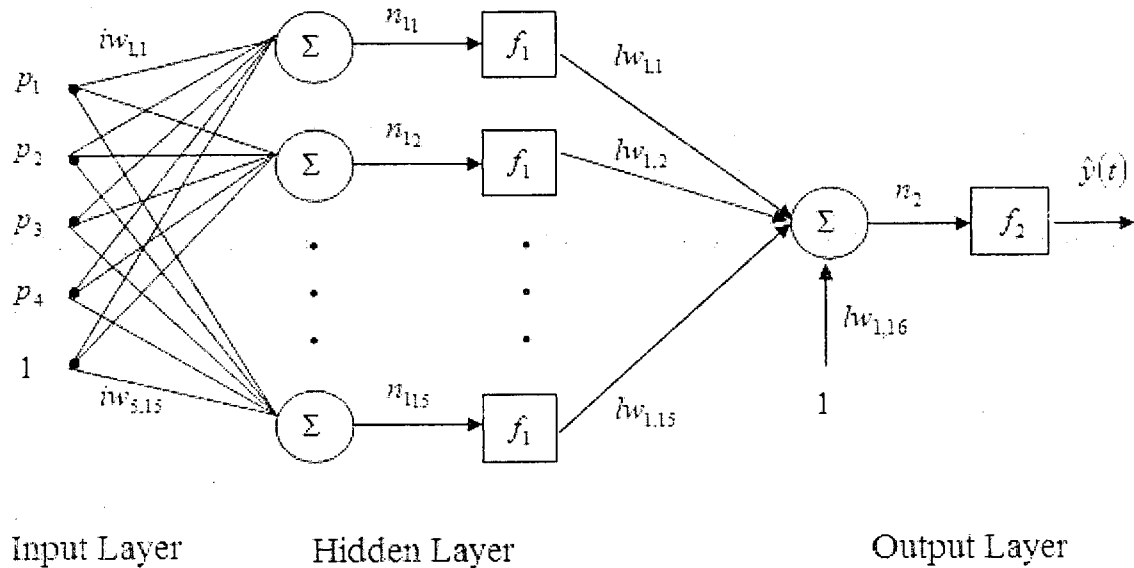


Figure 4-2: Feedforward neural network topology (modified from [103]).

When a given input vector \mathbf{p} is presented to the network, it is multiplied by the input-to-hidden weights ($iw_{i,j}$) and the result is added up at each of the units of the hidden layer. As a result a vector \mathbf{n}_1 is obtained where,

$$n_{1,j} = \sum_j p_j iw_{i,j} \quad (4-1)$$

Then, an activation function f_1 is applied at each of the hidden units and their outputs become the inputs of the next layer. That is,

$$O_j = f_1(n_{1,j}) \quad (4-2)$$

Each O_j is multiplied by the hidden-to-output weights (lw_j) and the result is summed to give,

$$n_2 = \sum_j O_j l w_j \quad (4-3)$$

Finally a second activation function f_2 is applied at the output units. That is,

$$\hat{y}(t) = f_2(n_2 + l w_k) \quad (4-4)$$

The term $l w_k$ in Eq. (4-4) is called the bias term.

In order to map the desired function a set of input data is presented to the network, and its output, $\hat{y}(t)$, is compared to the desired output $y(t)$. If the output of the network does not match the desired output, the weights are adjusted to minimize their difference. This process is called training (or learning) and the set of input and output vectors is called the training set.

The most common metric used to measure the distance between the desired output and the network output is the sum-of-squares cost function. That is, given a training set $\{\mathbf{p}_n, \mathbf{y}_n\}$, the following equation is minimized with respect to the network weights (\mathbf{w})

$$E(\mathbf{w}) = \frac{1}{2N} \sum_{n=1}^N [\hat{y}(\mathbf{x}_n, \mathbf{w}) - y_n]^2 = \frac{1}{2N} \sum_{n=1}^N \varepsilon^2(\mathbf{x}_n, \mathbf{w}) \quad (4-5)$$

$E(\mathbf{w})$ can be approximated by the second-order Taylor expansion around a point \mathbf{w}' :

$$E(\mathbf{w}) \cong E(\mathbf{w}') + (\mathbf{w} - \mathbf{w}')^T \mathbf{G} + \frac{1}{2} (\mathbf{w} - \mathbf{w}')^T \mathbf{H} (\mathbf{w} - \mathbf{w}') \quad (4-6)$$

where,

$$\mathbf{G} \equiv \nabla E|_{\mathbf{w}=\mathbf{w}'} = \frac{1}{N} \sum_{n=1}^N \frac{d\hat{y}(\mathbf{x}_n, \mathbf{w}')}{d\mathbf{w}'} \varepsilon(\mathbf{x}_n, \mathbf{w}') \quad (4-7)$$

is the gradient of the error function, and

$$\mathbf{H} \equiv \nabla \nabla E|_{\mathbf{w}=\mathbf{w}'} = \frac{1}{N} \sum_{n=1}^N \frac{d\hat{y}(\mathbf{x}_n, \mathbf{w}')}{d\mathbf{w}'} \left[\frac{d\hat{y}(\mathbf{x}_n, \mathbf{w}')}{d\mathbf{w}'} \right]^T - \frac{1}{N} \sum_{n=1}^N \frac{d}{d\mathbf{w}'} \left[\frac{d\hat{y}(\mathbf{x}_n, \mathbf{w}')}{d\mathbf{w}'} \right] \varepsilon(\mathbf{x}_n, \mathbf{w}') \quad (4-8)$$

is the Hessian matrix. Given that the cost function is a smooth continuous function of the weight vector [104], its minimum can be found when:

$$\nabla E(\mathbf{w}) = 0 \quad (4-9)$$

This minimum is usually found by an iteration method, which takes the form

$$\mathbf{w}^{(i+1)} = \mathbf{w}^{(i)} + \mu^{(i)} d^{(i)} \quad (4-10)$$

Where $\mathbf{w}^{(i)}$ indicates the current value of the weight vector, $d^{(i)}$ is the search direction and $\mu^{(i)}$ is the step size [100]. An initial guess for $\mathbf{w}^{(i)}$ is necessary to start the iteration process, and it is repeated until $\mathbf{w}^{(i)}$ is sufficiently close to the minimum. A common method used to minimize Eq. (4-5) is the gradient descent method in which the search direction is opposite to the direction of the gradient, that is,

$$d^{(i)} = -\mathbf{G}(\mathbf{w}^{(i)}) \quad (4-11)$$

Even though this method is easy to implement, it converges slowly. Therefore, other methods have been developed to speed up the convergence and hence the training stage. One of these algorithms, the Levenberg-Marquardt method, was selected for this study. This method approximates the error, $\varepsilon = \hat{y}(\mathbf{x}_n, \mathbf{w}) - y_n$, in Eq. (4-5) by its first-order Taylor series expansion around the current weighting values.

$$\varepsilon = \hat{y}(\mathbf{x}_n, \mathbf{w}) - y_n \cong \hat{\varepsilon}(\mathbf{x}_n, \mathbf{w}) = \varepsilon(\mathbf{x}_n, \mathbf{w}^{(i)}) + \left[\frac{d\varepsilon(\mathbf{x}_n, \mathbf{w}^{(i)})}{d\mathbf{w}^{(i)}} \right]^T (\mathbf{w} - \mathbf{w}^{(i)}) \quad (4-12)$$

$$= \varepsilon(\mathbf{x}_n, \mathbf{w}^{(i)}) \left[\frac{d\hat{y}(\mathbf{x}_n, \mathbf{w}^{(i)})}{d\mathbf{w}^{(i)}} \right]^T (\mathbf{w} - \mathbf{w}^{(i)}) \quad (4-13)$$

Then, a new cost function is defined that is analogous to that in Eq. (4-5).

$$L^{(i)}(\mathbf{w}) = \frac{1}{2N} \sum_{n=1}^N \hat{\varepsilon}^2(\mathbf{x}_n, \mathbf{w}) \quad (4-14)$$

With the new cost function in Eq. (4-14), the gradient term of Eq. (4-7) remains the same, but the Hessian term is now approximated as,

$$\hat{\mathbf{H}} \equiv \nabla \nabla L(\mathbf{w}) \Big|_{\mathbf{w}=\mathbf{w}'} = \frac{1}{N} \sum_{n=1}^N \frac{d\hat{y}(\mathbf{x}_n, \mathbf{w}')}{d\mathbf{w}'} \left[\frac{d\hat{y}(\mathbf{x}_n, \mathbf{w}')}{d\mathbf{w}'} \right]^T \quad (4-15)$$

Eq. (4-15) is easier to compute than Eq. (4-8) because it lacks the second derivative term. Moreover, information from the Hessian can be used to speed up the convergence. However, this approximation is useful only in the region of the cost function curve in which a linearization is acceptable. Therefore, the Levenberg-Marquardt method applies the gradient descent technique (minimize Eq. (4-5)) when the linear approximation is not applicable, and minimizes Eq. (4-14) when a linearization is possible [100]. The update rule for this method is,

$$\mathbf{w}^{(i+1)} = \mathbf{w}^{(i)} + d^{(i)} \quad (4-16)$$

The step size ($\mu^{(i)}$) is equal to one. The search direction proposed by this method is calculated by solving the following system,

$$\left[\hat{\mathbf{H}}(\mathbf{w}^{(i)}) + \lambda^{(i)} \mathbf{I} \right] d^{(i)} = -\mathbf{G}(\mathbf{w}^{(i)}) \quad (4-17)$$

Eq. (4-17) shows that when $\lambda \rightarrow \infty$ the method becomes the gradient descent and when $\lambda \rightarrow 0$ a new method (usually called the Gauss-Newton's method) is obtained, in which the information from the approximated Hessian is used to speed up the

convergence. Therefore, when a linear approximation of the cost function is not possible a large λ should be used, and conversely, when the approximation is applicable a small λ should be used [100]. To select an appropriate value of λ at each training step, we can compare the minimization obtained with Eq. (4-5) and the one obtained with the linear approximation (Eq. (4-14)). If the accuracy of the approximation is good enough we can use a small λ . A ratio is proposed to measure how well the linearization approximates the true cost function [100], this is

$$r^{(i)} = \frac{E(\mathbf{w}) - E(\mathbf{w} + d^{(i)})}{E(\mathbf{w}) - L^{(i)}(\mathbf{w} + d^{(i)})} \quad (4-18)$$

If $r^{(i)}$ is close to 1, the approximation is good enough, and λ should be reduced. Conversely, if it is close to zero (or negative) the approximation is not accurate and λ should be increased [100]. Eq. (4-16), Eq. (4-17) and Eq. (4-18) are used iteratively until the desired level of training error is achieved. At that time, the network is considered trained and it should be tested against a testing set, which have to be different from the training set.

The Levenberg-Marquardt method was applied to train the neural network in order to map the desired nonlinear function. This method was used to perform the system identification of the finger dynamics of the proposed prototype.

4.2.2 System Identification

The structure of the model was selected as autoregressive external input (NNARX) (see Figure 4-3). Different lag values were tested in order to find the best possible number of previous values used as inputs to the neural network. They were evaluated based on the testing error, correlation tests between the inputs and the training

error and an autocorrelation test of the training error. These tests were performed using the NNSYSID toolbox for Matlab (The MathWorks) [105]. As a result, for all the three active fingers, 6 inputs are used: 2 previous force values, 2 previous motor current values and 2 previous angle values. The activation function of the hidden layer is the hyperbolic tangent and the output layer is linear. The three network topologies are the same except for the number of hidden neurons used. For the index finger and the thumb, the number of hidden neurons is 10, and for the middle finger it is 15.

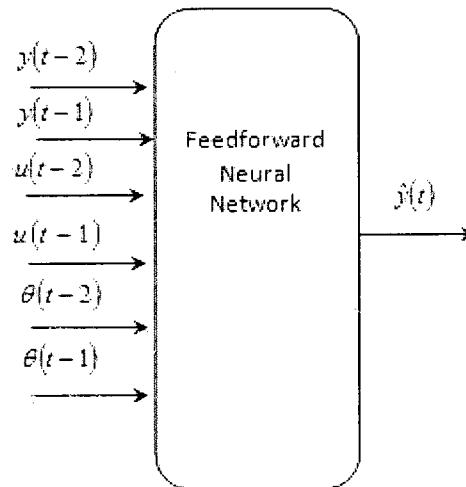


Figure 4-3: Diagram of the Neural Network model.

From the NNARX model, the predictions are obtained by the FFNN output:

$$\hat{y}(t+i) = \mathbf{lw}[\tanh(\mathbf{iw} \mathbf{p} + b_1)] + b_2 \quad (4-19)$$

$$\mathbf{p} = [y(t-2), y(t-1), u(t-2), u(t-1), \theta(t-2), \theta(t-1)] \quad (4-20)$$

Here \mathbf{iw} and \mathbf{lw} are the input-to-hidden and the hidden-to-output weight matrixes respectively. The variables b_1 and b_2 are the bias terms and \mathbf{p} is the input vector. By

shifting \mathbf{p} in time, the predictions in multiple time frames can be obtained. The angle measured by the RFS (θ) is not a controllable variable but it is used to estimate the model of the finger.

Experiments in LabVIEW were conducted to obtain training and testing data to create the model of the finger system (this process is usually referred as system identification). The procedure consisted of closing the finger around different objects while applying an input signal to the motor. The input signal was designed (following [100]) as a chirp signal that is described as follows:

$$u(t) = u_0 + A \sin(\omega_i t) \quad (4-21)$$

$$\omega_i = \omega_{start} + \frac{t}{N} (\omega_{final} - \omega_{start}) \quad (4-22)$$

Different values of u_0 and A along with different values of ω_{start} and ω_{final} were used to excite the whole range of the variables of the system [100]. The force and the angle were measured for each active finger. These experiments were performed on various objects of different shapes and weights (i.e. bottles of different sizes, a carton box, a tennis ball, etc.).

The signal amplitude of the training and testing data sets were scaled to zero-mean and unitary variance using the NNSYSID toolbox for Matlab (The MathWorks) [105]. The synaptic weights of the neural network model were then trained in an iteratively manner based on the Levenberg-Marquardt algorithm using the same toolbox.

After training, the testing error was checked and no pruning of the network size was performed. Sometimes if the sample frequency is too high compared to the dynamics of the system, a low test error would not necessarily translate to a good model [100].

Therefore, a second mode of analysis is required. The correlation tests were performed to validate the accuracy of the model. They are performed since the dynamics of the system has to be modeled such that the error is independent of the inputs and of the error itself.

4.2.3 Optimization Algorithm

To compute the optimum value of the motor current for each finger, the objective function needs to be minimized with respect to the future control inputs:

$$J(t, \mathbf{U}(t)) = \sum_{i=N_1}^{N_2} [r(t+i) - \hat{y}(t+i)]^2 + \rho \sum_{i=1}^{N_u} [\Delta u(t+i-1)]^2 \quad (4-23)$$

$$\mathbf{U}(t) = [u(t) \cdots u(t+N_u-1)]^T \quad (4-24)$$

where N_1 denotes the minimum prediction horizon, N_2 denotes the prediction horizon, N_u the control horizon (after it the control input is considered constant), and ρ is a weighting factor that restricts the changes in the control input [100].

The methodology explained in [92, 100] was used to minimize the objective function. It is performed by using gradient descent technique (presented in section 4.2.1), where the future set of control inputs is determined by the update rule,

$$\mathbf{U}(t+1) = \mathbf{U}(t) - \mu(t) \mathbf{G}[J(t, \mathbf{U}(t))] \quad (4-25)$$

In which $\mathbf{G}[J(t, \mathbf{U}(t))]$ is the gradient of the cost function, defined as:

$$\mathbf{G}[J(t, \mathbf{U}(t))] = \frac{\partial J}{\partial \mathbf{U}(t)} \quad (4-26)$$

Then, replacing Eq. (4-26) into Eq. (4-25), we get,

$$\mathbf{U}(t+1) = \mathbf{U}(t) - \eta(t) \frac{\partial J}{\partial \mathbf{U}(t)} \quad (4-27)$$

where $\eta(t)$ is an adaptive learning rate of the following form:

$$\eta(t) = \eta_0 e^{[\alpha(r(t)-y(t))]} \quad (4-28)$$

And α is a constant determined empirically. Then, if we express

$$J(t, \mathbf{U}(t)) = \mathbf{E}(t)^T \mathbf{E}(t) + \rho \Delta \mathbf{U}(t)^T \Delta \mathbf{U}(t) \quad (4-29)$$

we can expand the term $\frac{\partial J}{\partial \mathbf{U}(t)}$:

$$\frac{\partial J}{\partial \mathbf{U}(t)} = 2\mathbf{E}(t) \frac{\partial \hat{\mathbf{Y}}(t)}{\partial \mathbf{U}(t)} + 2\rho \Delta \mathbf{U}(t) \frac{\partial \Delta \mathbf{U}(t)}{\partial \mathbf{U}(t)} \quad (4-30)$$

where:

$$\mathbf{E}(t) = [e(t+1), \dots, e(t+N_2)]^T \quad (4-31)$$

$$e(t+i) = r(t+i) - \hat{y}(t+i); \text{ for } i = 1, \dots, N_2 \quad (4-32)$$

$$\hat{\mathbf{Y}}(t) = [\hat{y}(t+1), \dots, \hat{y}(t+N_2)]^T \quad (4-33)$$

$$\Delta \mathbf{U}(t) = [\Delta u(t), \dots, \Delta u(t+N_u-1)]^T \quad (4-34)$$

In addition, we have that

$$\frac{\partial \Delta \mathbf{U}(t)}{\partial \mathbf{U}(t)} = \begin{bmatrix} 1 & 0 & 0 & \dots & 0 \\ -1 & 1 & 0 & \ddots & 0 \\ 0 & \ddots & \ddots & \ddots & \vdots \\ \vdots & \ddots & -1 & 1 & 0 \\ 0 & \dots & 0 & -1 & 1 \end{bmatrix} \quad (4-35)$$

is a $N_u \times N_u$ matrix and

$$\frac{\partial \hat{\mathbf{Y}}(t)}{\partial \mathbf{U}(t)} = \begin{bmatrix} \frac{\partial \hat{y}(t+1)}{\partial u(t)} & 0 & \dots & 0 \\ \frac{\partial \hat{y}(t+2)}{\partial u(t)} & \frac{\partial \hat{y}(t+2)}{\partial u(t+1)} & \dots & 0 \\ \vdots & \vdots & \ddots & \vdots \\ \frac{\partial \hat{y}(t+N_2)}{\partial u(t)} & \frac{\partial \hat{y}(t+N_2)}{\partial u(t+1)} & \dots & \frac{\partial \hat{y}(t+N_2)}{\partial u(t+N_u-1)} \end{bmatrix} \quad (4-36)$$

To calculate each element in Eq. (4-36), a recursive algorithm presented by Noriega and Wang is used [92], where each of the elements is computed by the following formula,

$$\frac{\partial \hat{y}(t+n)}{\partial u(t+m-1)} = \frac{\partial \hat{y}(t+n-1)}{\partial u(t+m-1)} \left[1 + \frac{\partial \hat{f}(\mathbf{p})}{\partial \hat{y}(t+n-1)} \right], \quad (4-37)$$

where $n = 1, \dots, N_2$ and $m = 1, \dots, N_2$. The two derivative terms of Eq. (4-37) are calculated as follow,

$$\frac{\partial \hat{y}(t+n-1)}{\partial u(t+m-1)} = \mathbf{Iw} \left[\sec h^2(\mathbf{iw} \mathbf{p} + b_1) \right] \mathbf{iw} \frac{\mathbf{dp}}{\mathbf{du}} \quad (4-38)$$

$$\frac{\partial \hat{f}(p)}{\partial \hat{y}(t+n-1)} = \mathbf{Iw} \left[\sec h^2(\mathbf{iw} \mathbf{p} + b_1) \right] \mathbf{iw} \frac{\mathbf{dp}}{\mathbf{d\hat{y}}} \quad (4-39)$$

where,

$$\frac{\mathbf{dp}}{\mathbf{du}} = [0, 0, 0, \dots, 1, 0, \dots, 0]^T \quad (4-40)$$

$$\frac{\mathbf{dp}}{\mathbf{d\hat{y}}} = [1, 0, \dots, 0, 0, \dots, 0]^T \quad (4-41)$$

Then, at each sample point, $u(t)$ is supplied to the motor of each finger. Moreover, the voltage supplied to the DC motors is constrained to a specific range in order to assist in the convergence of the optimization algorithm, as determined during the tuning of the control system. Also, when the system reaches a tolerance range (generally $\pm 5\%$ of the

reference value) the motor is turned off to reduce power consumption and possible oscillations.

4.3 Preliminary Simulation

4.3.1 Methodology

Before implementing the proposed force control system in the prototype, computer simulations were performed on an analytical solution from a simple physical model of an underactuated finger in order to evaluate the suitability of implementing the control system for this application. The physical model, shown in Figure 4-3 allows a derivation of the relationship between the contact force and the motor current. To simplify the model, only two phalanges were taken into account, ignoring any friction force either in the joint or in the motor-pulley system.

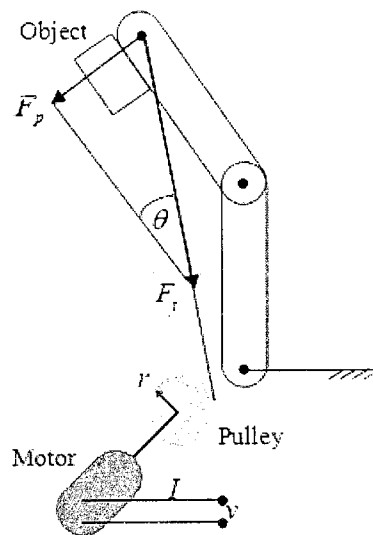


Figure 4-4: Physical model of underactuated finger and the motor-pulley system.

From the model described in Figure 4-4 the equation that relates the contact force with the current applied to the motor is:

$$F_p = \frac{Ki}{r} \sin \theta \quad (4-42)$$

Eq. (4-42) was used as the equation of the system (or plant) to be controlled. K is a motor constant, which was selected from the datasheet of a generic DC motor as $K = 0.0014 \frac{\text{oz. in}}{\text{mA}}$. The pulley radius was selected as $r = 0.01$ in. Although the system depends on two variables, the motor current i and the angle θ , only i can be controlled.

For this project the input vector for the model training purpose was:

$$\mathbf{p} = [y(t-1), y(t-2), \theta(t), u(t-1), u(t-2)]^T, \quad (4-43)$$

where $y(t-1)$, $y(t-2)$ are the system outputs (contact force) at the past two states, $\theta(t)$ is the angle at the present state, and $u(t-1)$, $u(t-2)$ are the motor current at the past two states. In order to train the FFNN, various training sets were used. First, random values were used to train the FFNN with several numbers of samples, but the control system behaved unstable. Then, more smooth signals were used for both inputs, resulting in a final training set of 700 samples generated for the motor current and the joint angle. The FFNN was trained with Levenberg-Marquardt method, using the Neural Network toolbox of Matlab (The MathWorks) [103].

4.3.2 Results

After the FFNN was trained, the control system algorithm was implemented. Figure 4-5 shows the response of the control system to a step function for different joint angles, using a fixed $\eta = 0.2$ and $T = 2$.

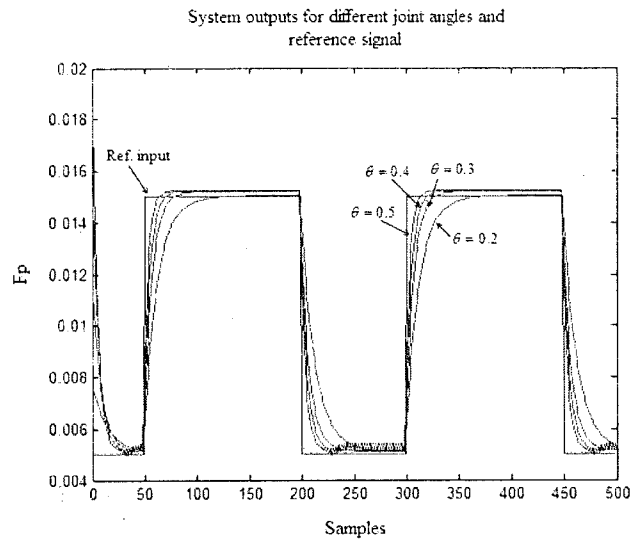


Figure 4-5: Control system outputs (red line) for different joint angles (θ in radians) and reference signal (blue line).

In addition the capacity of dealing with disturbance was checked by adding a constant disturbance to the output at the 100th sample after the steady state was reached.

Figure 4-6 shows the results.

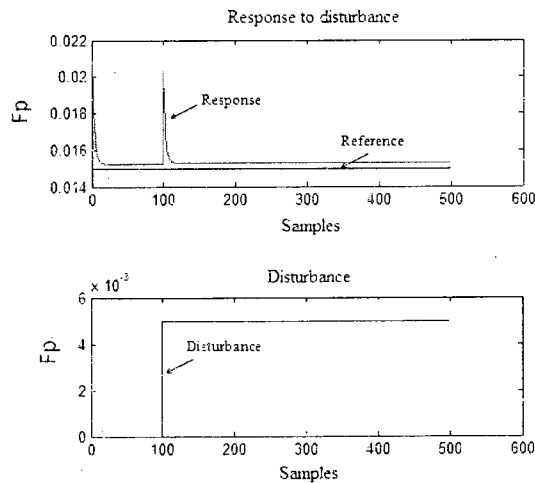


Figure 4-6: Response to a disturbance.

The overall performance of this predictive control system depends significantly on the training of the neural network. Therefore, the system identification stage arises as the main stage in order to obtain a good performance. An acceptable rise time was obtained (transient response) for all the tested joint angles. Moreover, the average steady state error for all the tested joint angles was 2.58% (relative error), which makes it suitable for maintaining constant force during a long period of time. Beside the dependence of the training stage, the system requires low number of calculation, which makes it suitable to be performed in real time. Finally, the simulation results showed that this control system appears to be robust enough to external disturbance.

4.4 Evaluation over the Prototype

4.4.1 *Methodology*

After running the simulation, with the aim of evaluating the performance of the force control system on a real prototype, we conducted a set of experiments on the second generation prototype, in which the step response of the system was tested. In these experiments the finger automatically closed around four objects with different densities while a step signal was applied as the force reference of the control system. Five trials per object were recorded and each trial contained five different steps. The interval for each step was approximately 20 seconds. A diagram of the experimental setup is shown in Figure 4-7.

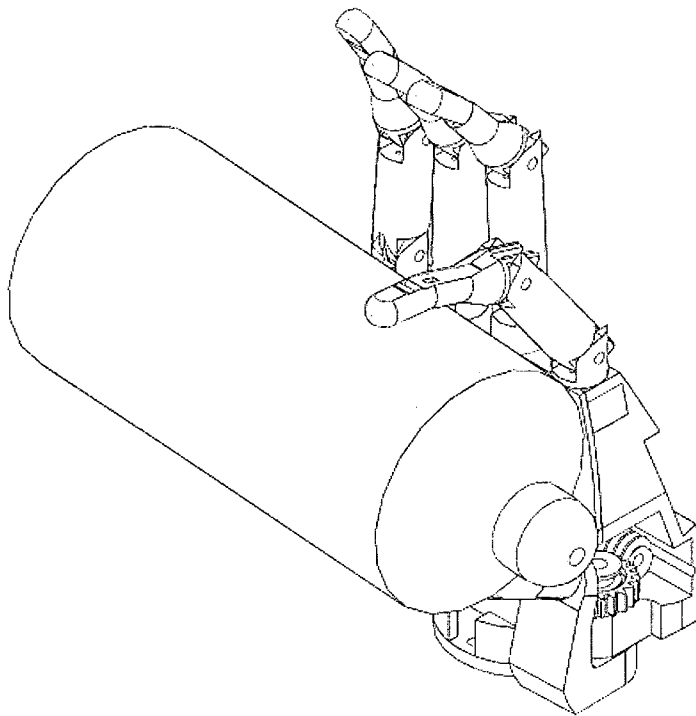


Figure 4-7: Experiment setup.

An extra trial per object was recorded in which the force reference was maintained constant during 2 minutes in order to analyze the performance of the control system during long-term steady-state conditions. Table 4-1 shows the objects used in these experiments.

Table 4-1: Objects used in the experiments.

Object	Diameter	Weight
Small plastic bottle	6.5 cm	15 g
Big plastic bottle	8.5 cm	40 g
Styrofoam cup	7 cm	2 g
Aluminum cylinder	7.3 cm	110 g

The performance metrics were the average closing time, the average overshoot, the average rise time and the average steady state error (SSE). Metrics were calculated for each of the reference steps. In addition, the power consumption of the finger was obtained from the signal supplied to the motor driver. An example is shown in Figure 4-8, which illustrates the definition of these metrics for the step response of a second order system controlled in a closed loop fashion. The rise time is defined as the time in which the system reaches 85% of the reference value. SSE is the average of the error between the system and the reference (absolute value) after overcoming the transient stage. We define the transient part of the response as the time in which the peak value of the oscillations of the system differ more than 15% from the reference (see Figure 4-8). The whole methodology was implemented using the NI DAQ boards (NI PXI-6723 and NI PXI-6224 from National Instruments) and LabVIEW 8.2.

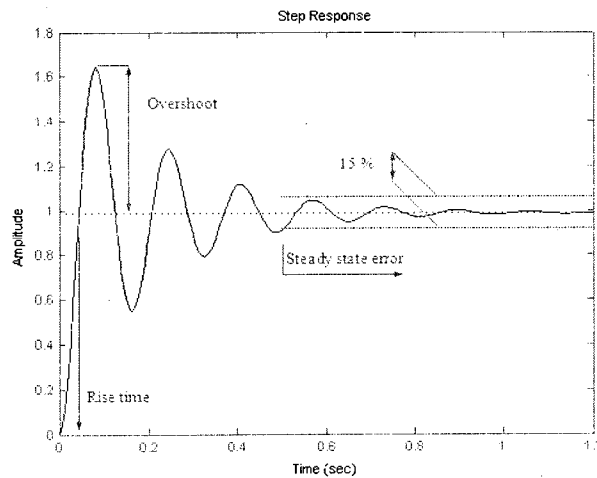


Figure 4-8: Typical step response of a second order system.

4.4.2 Results

The control system was able to follow the force reference for each step size with low rise time, small overshoot and small steady state error. Figure 4-9 shows a sample of the signals recorded during the experiments. The top graph shows the reference steps (red line) and the system output (blue line). The bottom graph shows the voltage signal supplied to the DC motor.

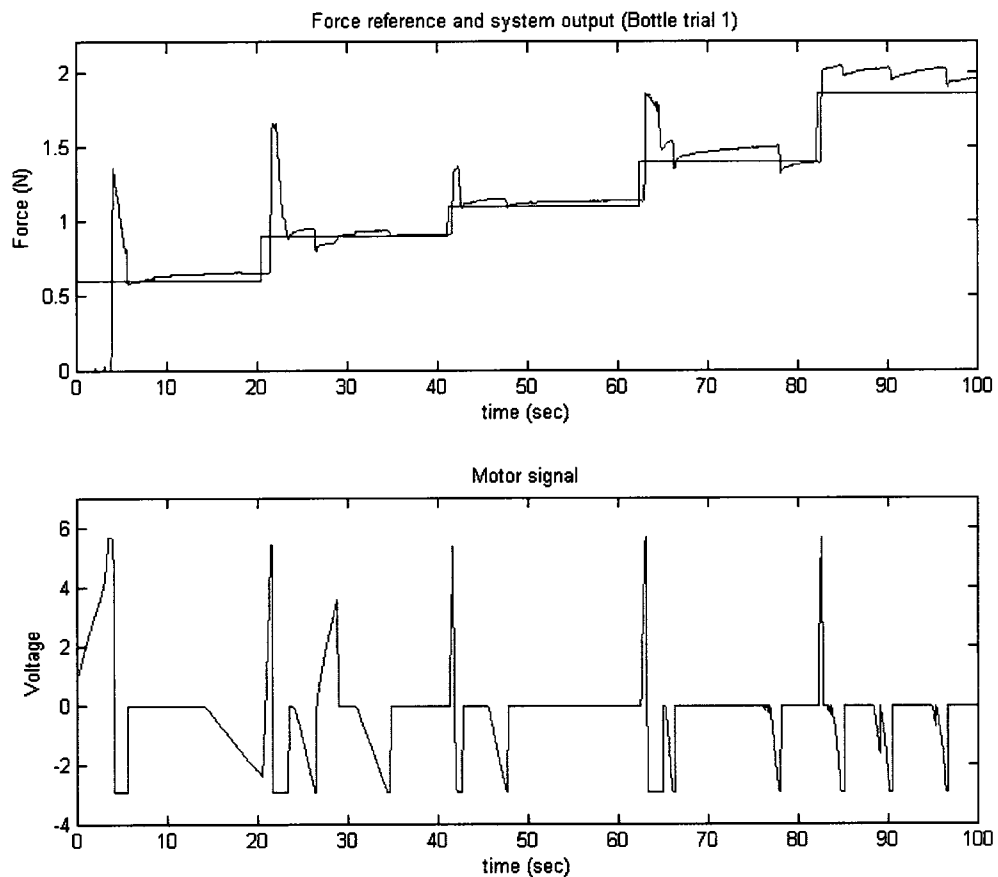


Figure 4-9: Sample of the signals recorded during the experiments. Top: reference step signal (red line) and the system output (blue line). Bottom: the voltage signal supplied to the motor.

The results for the average closing time and rise time (Figure 4-10) indicate that the control system responds in a reasonable period of time. The maximum average closing time was 3.36 seconds. The average rising time for each step was less than 1 second (around 0.5 seconds) for all objects except cylinder, for which it was 1.22 seconds. There were no significant differences between objects except for the 0.89 N step, in which there was a marginal statistical difference (P value = 0.0458) between the Styrofoam cup and the cylinder. These results show that the time response of the control system is fast enough after the finger close around the object; however there is a significant delay before the finger makes contact with the object.

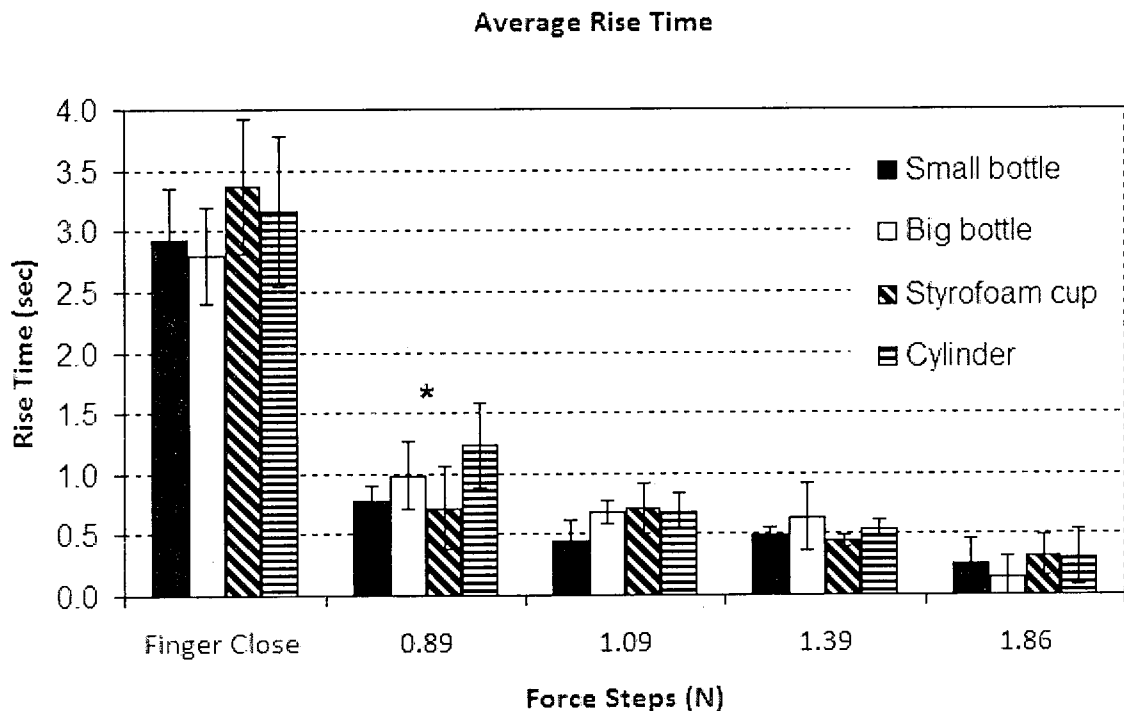


Figure 4-10: Average closing and rise time for each object.

Overshoot was found for all step sizes. The maximum overshoot was produced when the finger made contact with the object. However, the overshoot values were

relatively small and no significant deformation of the object was noted. Figure 4-11 shows the results for the average overshoot for each object. Note that for objects with rigid surfaces, like the aluminum cylinder, the overshoot was smaller than for softer surfaces like the small plastic bottle. For the initial overshoot (finger close) the difference was statistically significant ($P < 0.01$) between all the objects except the small bottle and the cylinder. For the “0.89 N” step the difference was statistically significant ($P < 0.001$) between the small bottle, the Styrofoam cup and the cylinder. No statistical difference was found for the other steps. Moreover, the overshoot tended to decrease with as the force reference value increased.

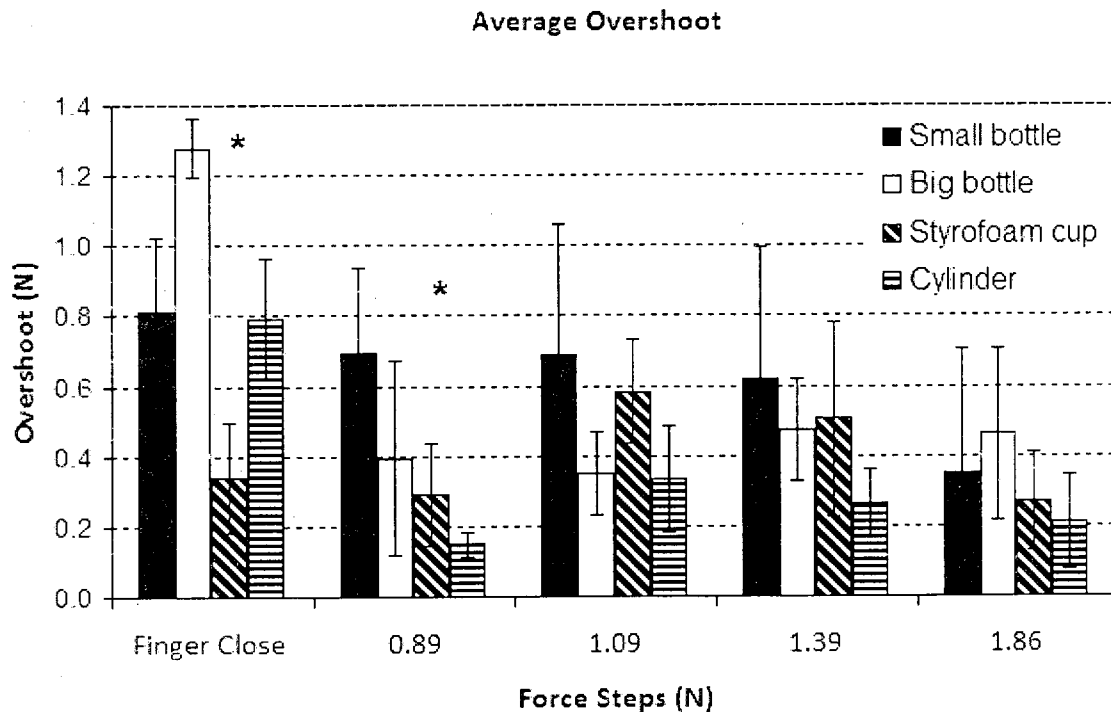


Figure 4-11: Average overshoot results for each object.

Small average SSE was found for all the step sizes. The results of the average SSE are shown in Figure 4-12. The SSE tended to increase with the force reference value,

but the increase occurred because the control system was designed to turn off the motor when the signal is within 5% of the reference value. Thus, as the force reference increased, the tolerance increased. No significant difference was found among the objects.

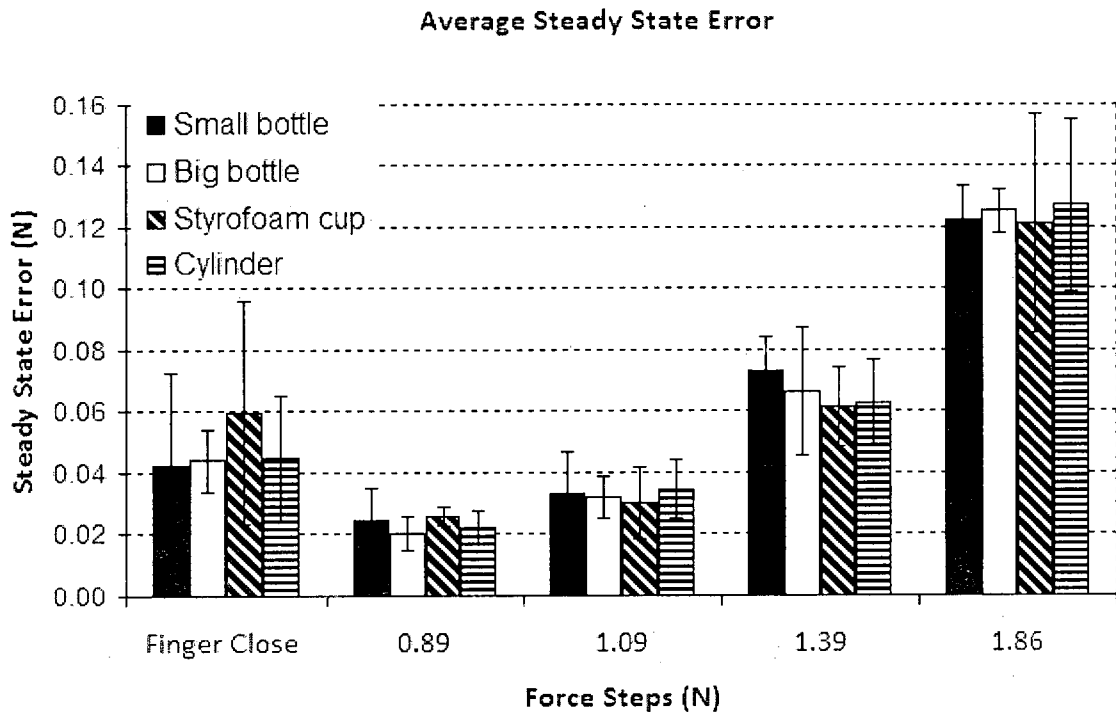


Figure 4-12: Average steady state error for each object.

In all of the performed experiments, the motor was turned on less than a half of the experiment duration. Figure 4-13 shows the results for the average percentage of time that the motor was on during the experiments for each object. No significant difference was found among the objects. The results should be approximately 40% of the motor usage. This shows that the system can save power consumption, which may lead to longer battery life.

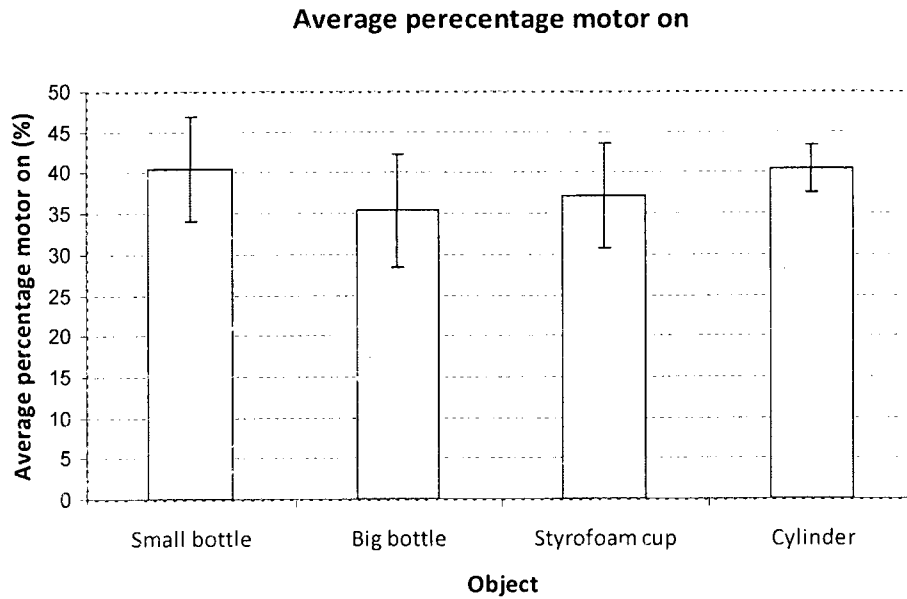


Figure 4-13: Average percentage of time in which the motor was on for each object.

Finally, during the long-term steady-state experiments, the system remains stable with low SSE. An example of signals recorded during these experiments is shown in Figure 4-14. The motor is turned on only during the first 15 seconds. The average SSE for each object is shown in Figure 4-15. The average SSE is small, which indicates that the system is stable over long periods of time.

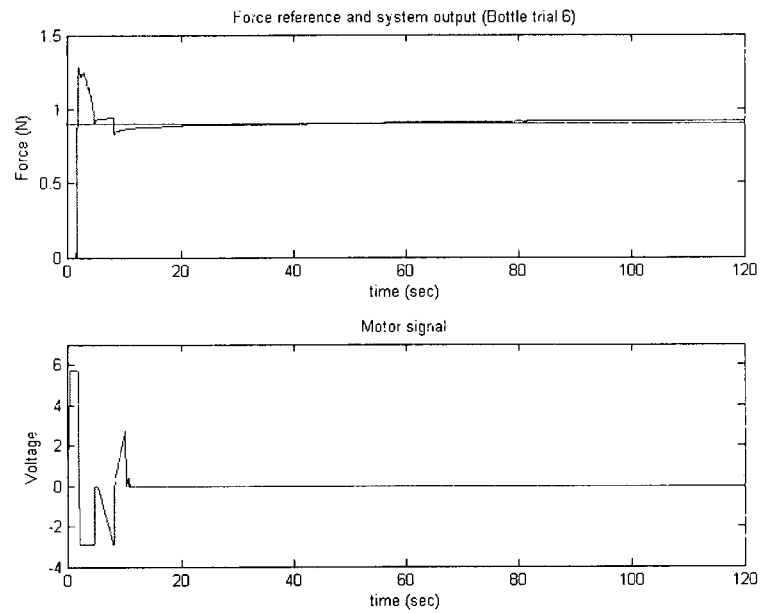


Figure 4-14: Sample of the 2 minutes experiment

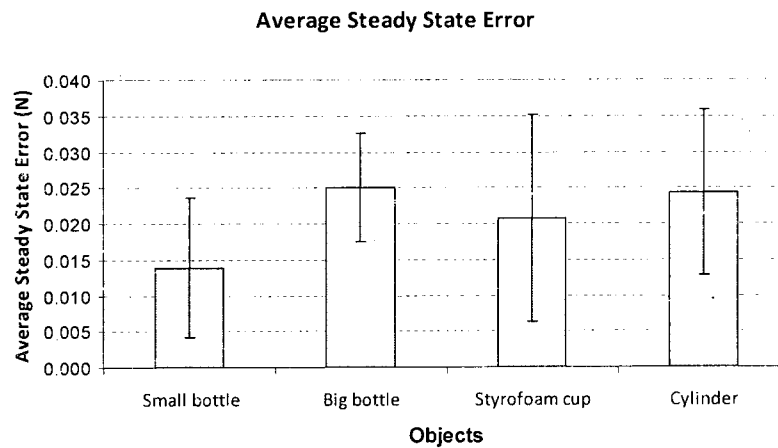


Figure 4-15: Results for the two minutes trial.

4.5 Discussion

The experimental results obtained from the simulations and the prototype experiments suggest that the force control system can adequately control the force

exerted by the fingers. The rise time is within the specifications (around 500 ms) and the overshoot does not cause significant deformation. Moreover, the small SSE ensures that the fingers are able to exert the same force during a long period of time.

Low power consumption is an important criterion in prosthetic devices since it may allow small batteries or longer battery lifetime. The controller design reduces the period of time in which the DC motor is turned on to less than 50% of the whole experiment duration. This is due mainly to the gear locking system and the design of the control system itself, which might assist in reducing the power consumption of the device.

The closing time of the finger is relatively large (around 3 seconds). However this time might be reduced by adding a closing stage between the pre-shape stage and the force control stage. During the closing stage the finger should close at a constant velocity until it reaches the object. The system should then switch to the force control stage. This methodology was not implemented when the whole control strategy was implemented on the second generation prototype and it will be discussed in Chapter 6.

The results suggest that the control system is independent of the grasped object since similar results were found in almost all the experiments. In this study, only cylindrical objects were used because it would be difficult to surround other geometries with only one finger. A study using more objects was performed and will be explained in Chapter 6. However, the results indicate that the system performance is within the design specification.

CHAPTER 5

DETECTION STAGE

After the system uses the force control stage, explained in Chapter 4, to obtain a stable grasp, it switches to the detection stage, where any unintended movement of the object is monitored. The grasp was considered to be stable when the fingers remained in a fixed position, as determined from the rate of change of the angle measured by the RFS.

Since slip sensors are not commercially available for prosthetic applications, researchers have developed their own sensors to incorporate an estimation of slippage into prosthetic devices [59, 62, 106, 107]. However, the cost of fabricating prostheses that use this kind of sensor may be drastically increased. Consequently, we present here a potential strategy to detect slippage without using specialized sensors. The strategy uses fluctuations that sliding causes in the force signal from the fingertip. These fluctuations are quantized by calculating the derivative of the force signal, which is then compared against a threshold to determine whether slippage is produced.

Experiments in which slippage was induced over different objects were conducted to evaluate the detection delay and to determine a possible optimum threshold value. The proposed technique maintained detection delays of less than 200 ms.

This chapter is organized as follows. First the hypothesis is described and the detection algorithm is presented. Then, experiments are described that were used to

evaluate the hypothesis and hence the algorithm performance. The results are then presented and, finally, discussed.

5.1 Hypothesis

The information from the rate of change of the force measured by the FSR and the information from the rate of change of the finger angle measured by the RFS can be used to detect unintended movements of the object (i.e. slippage) with respect to the hand.

5.2 Slippage Detection Algorithm

The FSR measures the normal force exerted by the prosthetic device. We propose that the onset of unintended movements of the object from the hand, defined here as slippage, can be detected from the fluctuations in the FSR signal. This approach was suggested by the rapid changes in the FSR output that were observed during slippage. Once the hand has reached a stable grasping position, (when the fingers are no longer moving), the slippage detection algorithm is activated. The absolute value of the derivative of the normal force at each sample point is a measure of the rate of change of the force. The force signal is differentiated numerically at each sample point by the following five-point formula [108]:

$$f'(x_0) = \frac{1}{12} [f(x_0 - 2) - 8f(x_0 - 1) + 8f(x_0 + 1) - f(x_0 + 2)] \quad (5-1)$$

Here, we are not concerned with is the rate of sliding, but rather with the onset of this activity, which is what we want to avoid. We are also not concerned about the sign of the change since sliding can occur in multiple directions, depending on the position of the hand in the space. Therefore, we compute the absolute value of the rate of change of the force signal. Then, if the rate of change exceeds a threshold, empirically determined by a

trade-off between the signal noise level and delay (described in section 5.4), an unintended movement of the object is expected. When this happens, the reference force of the control system is increased to compensate. A similar methodology was reported by Birglen and Gosselin for a robotic finger [90].

5.3 Preliminary Evaluation

5.3.1 Methodology

To evaluate the algorithm, ten objects, with different shapes and weights (Table 5-1), were grasped with different grasping patterns (Figure 5-1) by the first-generation prototype. Slippage was initially induced manually, where a person pulled the object in the direction perpendicular to the grasping force applied by the prototype. The NI DAQ cards (NI USB6009 National Instruments) were used to sample force at a frequency of 40 Hz, and the algorithm was implemented in LabVIEW 8.2 (National Instruments).

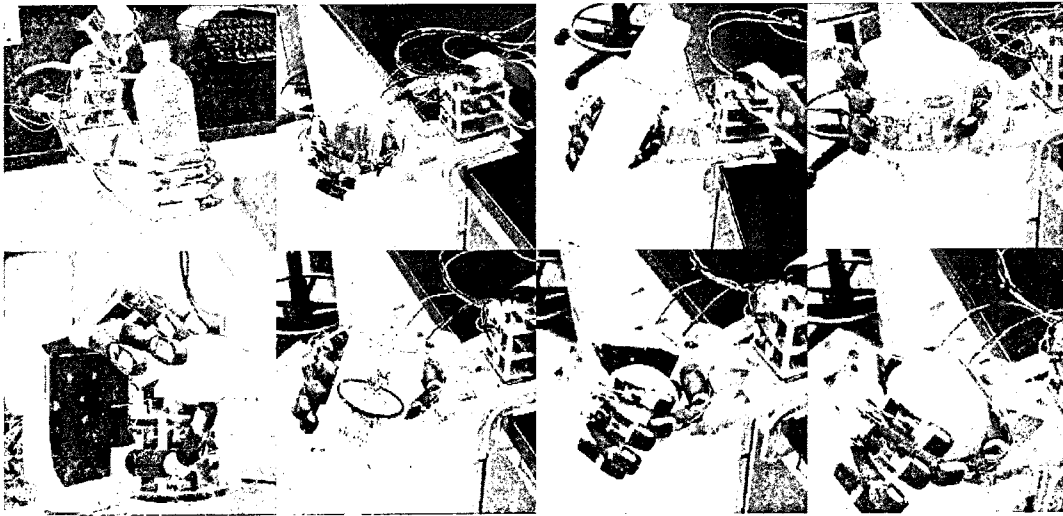


Figure 5-1: Different grasping patterns for the slippage experiments.

Table 5-1: Objects used in the preliminary slip experiments.

Object	Dimension (cm)	Weight (g)
Small plastic bottle	d = 6.5	15
Plastic cup	d = 6	100
Tennis ball	d = 6	55
Big carton box	17 x 24.5 x 5	80
Small carton box	7 x 10 x 7	30
Egg	d = 5	70
Cup	d = 9	150
Round sponge	d = 9	30
Tape	d = 10	40
Thermo	d = 9.5	150

5.3.2 Results

The rate of change of the force measured by the FSR during stable grasping is notably different from when slippage is induced. Similar results were obtained for all the objects used in these experiments. An example of the result is illustrated in Figure 5-2, corresponding to the signals recorded from the index finger while the hand was holding the small plastic bottle. We observe a significant change in the normal force when slippage is induced. This change is produced by force redistribution at the tip of the finger. These fluctuations are represented in the force slope signal. A threshold value can be identified because this force slope differs greatly between the stable grasping state and the sliding state. Only the first non-zero value in the slip signal is important given that it represents the onset of the sliding.

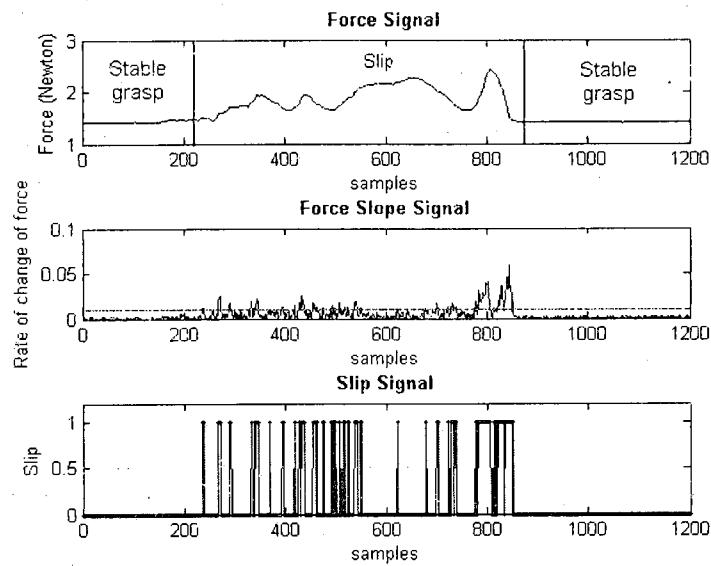


Figure 5-2: Force signal obtained from the index finger while holding a small bottle. Derivative of the force and setting of the threshold.

The top graph in Figure 5-2 shows the force signal recorded during the experiment while holding a small bottle. First, stable grasp is reached, and then slippage is induced after 5 seconds and stopped after 20 seconds such that a stable grasp is produced again. The middle graph shows the absolute value of the derivative of the force signal. This graph also shows that the threshold was set arbitrarily to 0.01 N/s, which was determined empirically. Finally, the bottom graph presents the slip signal resulting from the comparison between the slope of the force and the threshold. Similar results were obtained for other grasping configurations. Figure 5-2 shows that some minimum force must be exerted over the object for the system to detect slippage. However, this level of force is small enough to avoid causing any deformation to the object.

5.4 Quantitative Evaluation

5.4.1 *Methodology*

The experiments showed that the detection algorithm is suitable for detecting unintended movements of different objects; however these preliminary experiments did not address the delay in the detection. Therefore, in order to evaluate more quantitatively the efficacy of the Detection stage and also to find a possible threshold value, experiments were conducted on the second generation prototype to compute the delay between the onset of the movement and its detection.

In these experiments slippage was induced over different objects by a DC motor connected to a gear-pulley system, as illustrated in the diagram of Figure 5-3. The hand is first closed around the object until it makes contact with it. The object have attached at one end a cable connected to the motor-pulley system. This system pulls on the object for 2 seconds thereby inducing slippage. The DC motor is connected to a standard PC by the NI DAQ boards (NI PXI-6723 and NI PXI-6224 from National Instruments) and it is controlled by a LabVIEW program (LabVIEW 8.2). Consequently, the exact onset time for slippage is known, and we can calculate the delay in the detection. In offline analysis, we set different threshold values and compared them to the detection delay.

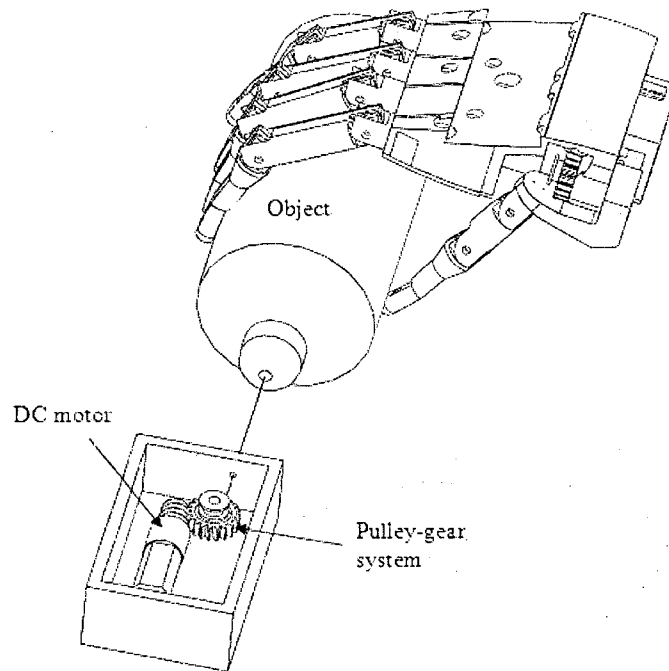


Figure 5-3: Setup of the slip detection experiments.

Nine objects with different shapes and friction coefficients were used to evaluate the Detection algorithm in different scenarios and to find a possible threshold value. The objects, along with their dimensions and weights, are listed in Table 5-2.

Table 5-2: Objects used in the quantitative slip experiments.

Object	Geometry	Weight
Big can	d = 6.5 cm	330 g
Medium can	d = 5 cm	150 g
Small can	d = 4.5 cm	60 g
Card	5.5 x 8.5 cm	5 g
Plastic cup	d = 6 cm	100 g
Small carton box	7 x 10 x 7 cm	30 g
Mug	d = 7.5 cm	320 g
Big wood block	7 x 11.5 cm	120 g
Small wood block	7 x 5 cm	60 g

A total of 5 trials per object were performed and the signals from the force sensors of the index and middle fingers, and the thumb were recorded along with their respective derivative values. The derivative of the force signals was then compared offline against 13 threshold values ranging from 0.01 to 0.07 N/s (with step of 0.005 N/s).

The difference between the onset of the slippage and the detection time for each threshold value was recorded for further analysis. Although the three active fingers make contact with the object in these experiments, not all of the force sensors touch the surface of the object. Detection was calculated only for the sensors that contacted the object.

5.4.2 Results

The detection algorithm is able to detect unintended movements of different objects, and the detection delay depends on the selected threshold value. Figure 5-4 shows a signal recorded from the force, along with the force slope and the post-processed slip signal during the grasping of a wood block. Slippage was induced at 2 seconds and

was stopped at 4 seconds. As it was illustrated in Figure 5-2, the second graph in Figure 5-4 shows the slippage information that lies within the derivative of the normal force (slope signal). Two well-defined states are determined in the slope signal, which allows slippage to be detected.

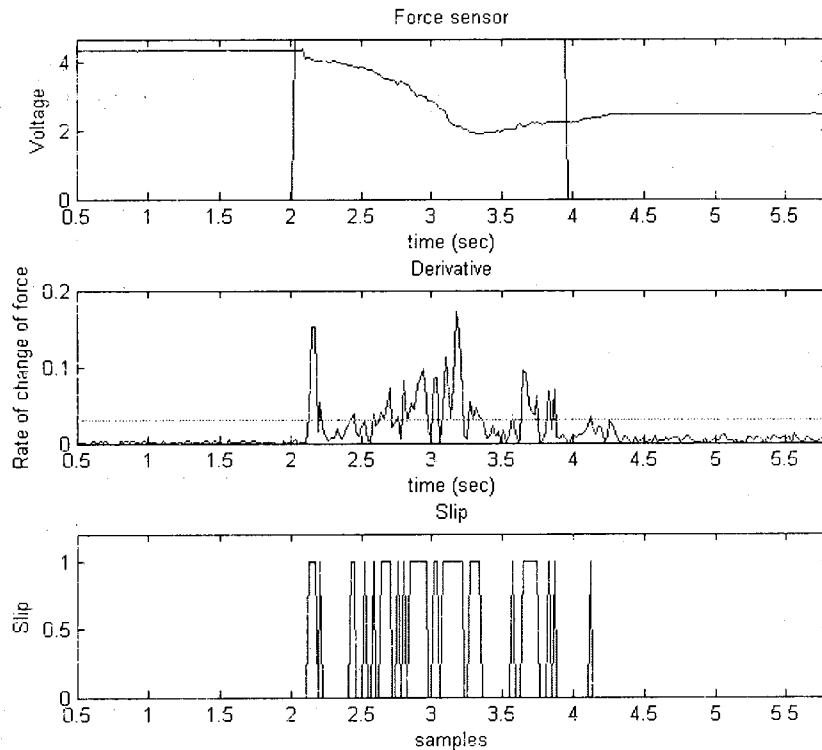


Figure 5-4: Example of the results obtained during the slippage detection experiments.

The detection delay was calculated offline for the 13 proposed threshold values and for all the experiments (a total of 45 trials). The cumulative probability function of the detection delay,

$$F(x) = P(X \leq x) \quad (5-2)$$

was then empirically computed for each threshold value using the Statistic toolbox of Matlab. $F(x)$ gives the probability that an observed value X takes a value less than or

equal to x . In this case, x represents the detection delay and therefore the cumulative probability curve shows the probability of obtaining a detection delay equal to or less than x . Figure 5-5 shows the cumulative probability curves for each threshold value. Threshold values that produce non-zero cumulative probability at negative time delays imply false positive detection, mainly influenced by noise.

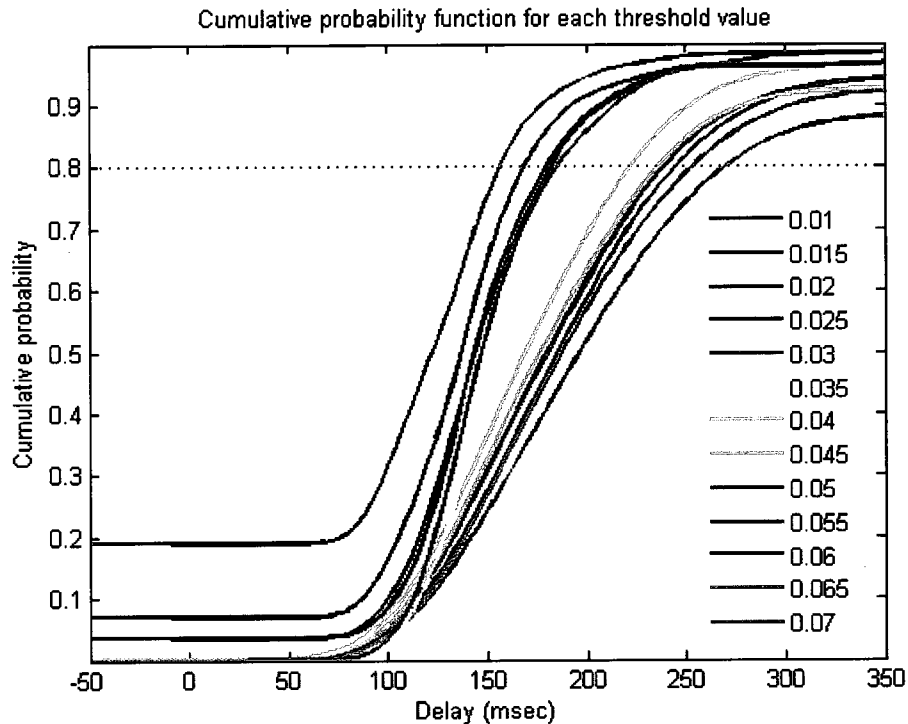


Figure 5-5: Cumulative probability function as a function of the detection delay values, parameterized with respect to each threshold value.

The detection delay for a cumulative probability of 0.8 (80%) for each threshold value is shown in Figure 5-6. A trade-off between false positive classification and small delay must be performed in order to find a possible optimum threshold value. In Figure 5-5 and Figure 5-6 the threshold value of 0.03 N/s appears to be most favorable since it leads to a small delay with low probability of having false positive detections. The

average delay for the threshold value of 0.03 N/s was 157 ms (± 46 ms) and the delay for 80% of the experiments was 180 msec.

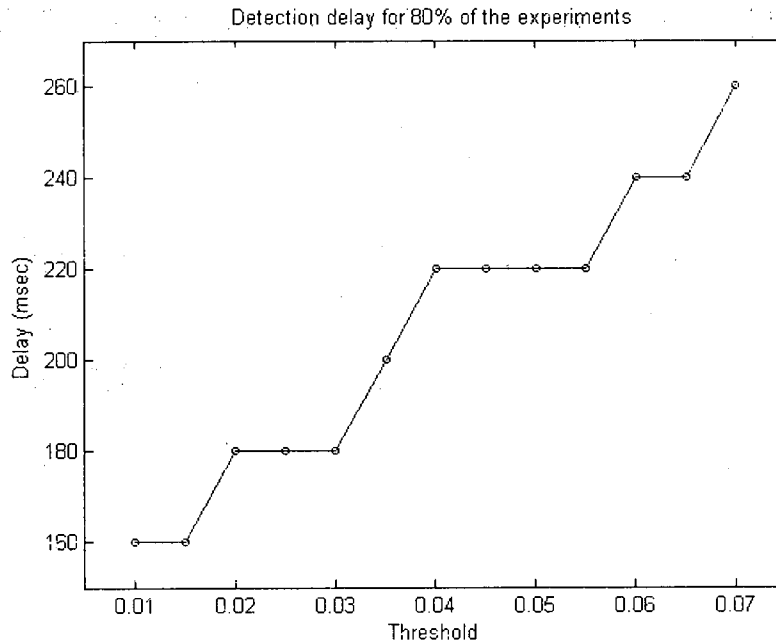


Figure 5-6: Detection delay for 80% of the experiments.

5.5 Discussion

The Detection algorithm identifies slip, but a manual calibration step is necessary to adjust the threshold. The experiments suggest that a threshold value of 0.03 N/s should be used for the second generation prototype since it leads to detection delays less than 200 ms with a low probability of false positive.

Although the detection delay is larger than the typical 74 ± 9 ms response of the human hand [109], it is not possible to make a direct comparison since the control mechanism of the human hand differs from the control strategy proposed here. The motor control of the human hand is based mostly on prediction by means of parametric models of the objects previously grasped and lifted [29]. Moreover, the human hand contains far

more sensors than the prototype used in this study. However, studies reported in Chapter 6 show that a delay of 200 ms is sufficiently small to prevent the object from dropping from the hand.

The slope of the normal force is not necessarily a unique indicator of slippage. It may also depend on a rearrangement of the forces during the grasping process or on deformation of the object. However, since the fingers remain in a fixed position during the experiments these fluctuations in the normal force are most likely to be caused by slippage. Therefore, it is necessary to ensure a stable grasping condition before attempting to detect slippage with this methodology.

The silicone glove that covers the hand influences slip detection since the object drags it when the load is applied to the object. Glove displacement increases the fluctuation measured by the force sensor, and hence increases the sensibility to slippage. However, if the force sensor does not adequately contact the surface of the object, the methodology is not effective. A possible solution to this problem is to add more sensors to each finger and the palm in order to increase the sensory information.

The experimental results suggest that the detection stage ensures secure grasping. The algorithm was tested using objects with different geometries and surface, which are found commonly in most of the ADL. In addition, the system is manually calibrated by a straightforward adjustment of the threshold value. Finally, the algorithm uses inexpensive force sensors only, which may reduce the final cost of the prosthesis. Therefore, these results encourage the implementation of this methodology in the proposed control strategy to assist in the control of a low-cost prosthetic hand.

CHAPTER 6

EVALUATION AND ADJUSTMENT

Different metrics have been described to assess the performance of underactuated robotic hands with respect to their ability to grasp and hold different objects [110]. Even though these metrics are related mainly to the evaluation of the mechanical aspects of underactuated hands, some of them may be used to evaluate the performance of the control strategy as well. From the metrics presented in the literature, we tested the performance of our hand (and consequently the control strategy) using the *equilibrium between fingers and objects* metric. This metric corresponds to the situation when an object is solely supported by the hand. It tests the ability of the hand to maintain the object in equilibrium [110]. We also tested the algorithm using the *force disturbance* metric. This metric corresponds to the ability of the hand to resist external forces and moments on grasped objects [110].

Experimental designs have been reported [110] on the response of prosthetic hands to sudden, gradual and torsional external forces [40, 80, 81, 111, 112]. Here we tested the ability of the hand to adapt to different objects encountered in ADL. Consequently, we tested the response of the hand to induced gradual and sudden movements by measuring the vertical displacement. The vertical displacement measurement encompassed many aspect of a successfully grasping and holding task, such

as time response of the hand, adjustment of the grasping force and slip detection delay. We believe that it is a good measure of the overall effectiveness of the device.

This chapter will address three focus areas. First, the *equilibrium between fingers and objects* metric is presented in section 6.2. Second, in section 6.3 an adjustment stage is presented to determine the best possible initial force and step increment. These two parameters were empirically found to drastically improve the performance of the hand. Selecting the correct hand configuration and strength can affect the success of the grasping process, while the force increment can influence the holding stage. Finally, a modified test of the *force disturbance* metric is discussed in section 6.4. Instead of the maximum external force that the hand can resist, the displacement of the object was measured when different external forces were applied.

6.1 Hypothesis

By combining and adjusting the pre-shape stage, the force control stage and the detection stage to drive a cost effective prosthetic hand, it is possible to assist the user in most of the ADL.

6.2 Evaluation of the Equilibrium between Fingers and Objects

6.2.1 Methodology

We performed experiments using the second generation prototype to determine the ability of the prototype to grasp objects of different weights and shapes. In these experiments, the hand grasps and lifts a determined object from a table and returns it to its initial location. Table 6-1 lists the grasped objects, their weights and their dimensions. Nineteen objects were selected based on the grip patterns approximately used in 70% of

the ADL (Table 1-1). The success rate for five trials was calculated for each pre-shape category.

Table 6-1: Different objects that were used for the grasping experiments and their approximate weights and dimensions. Most of the object were selected following Cipriani et al. [35].

Object	Dimensions	Weight
Plastic cup	d = 6 cm	100 g
Styrofoam cup	d = 7 cm	2 g
Big plastic bottle	d = 9.5 cm	40 g
Small plastic bottle	d = 6.5 cm	15 g
Mug	d = 7.5 cm	320 g
Round sponge	d = 9 cm	30 g
Tennis ball	d = 6 cm	57 g
Wood block	7 x 5.3 cm	120 g
Egg	d = 5 cm	70 g
Lamp bulb	d = 6 cm	20 g
Potato chip	d = 5 cm	1 g
Small plastic cup	d = 5 cm	2.7 g
Coin	d = 2.5 cm	5.5 g
Screw	d = 0.5 cm	5 g
Card	5.5 x 8.5 cm	5 g
Key	2.5 x 5 cm	11 g
CD	d = 12 cm	16 g
Big carton box	17 x 24.5	80 g
Tomato	d = 8 cm	260 g

A support device was designed and fabricated to allow easy manipulation of the device. Figure 6-1 shows the prototype attached to the support device. Four push-button

switches were placed at the handle of the device in order to simulate the signals from the EMG classifier. Therefore, the user can handle the robotic hand and simulate the output from the EMG signal classification in order to control it. The methodology was implemented using the NI DAQ boards (NI PXI-6723 and NI PXI-6224 from National Instruments) and LabVIEW 8.2 (National Instruments).

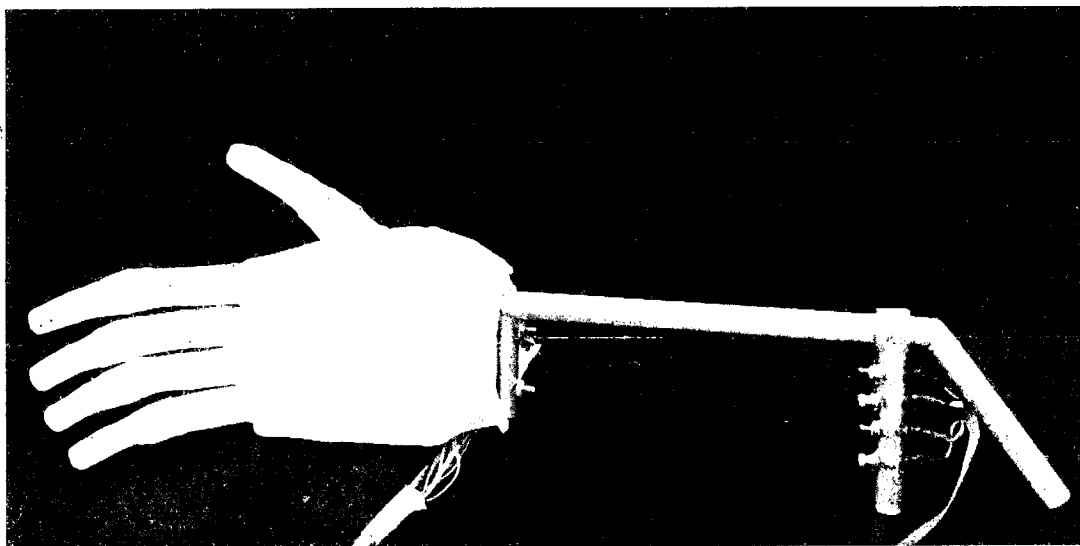


Figure 6-1: Support device designed to assist during the different tests. It contains 4 buttons that simulate the four possible outputs from the EMG classifier.

6.2.2 Results

The different objects detailed in Table 6-1 were securely grasped and lifted without producing any significant deformation. The ability of the device to grasp without slippage depended strongly on the grasping type. Figure 6-2 shows some of the objects while they were lifted by the hand.

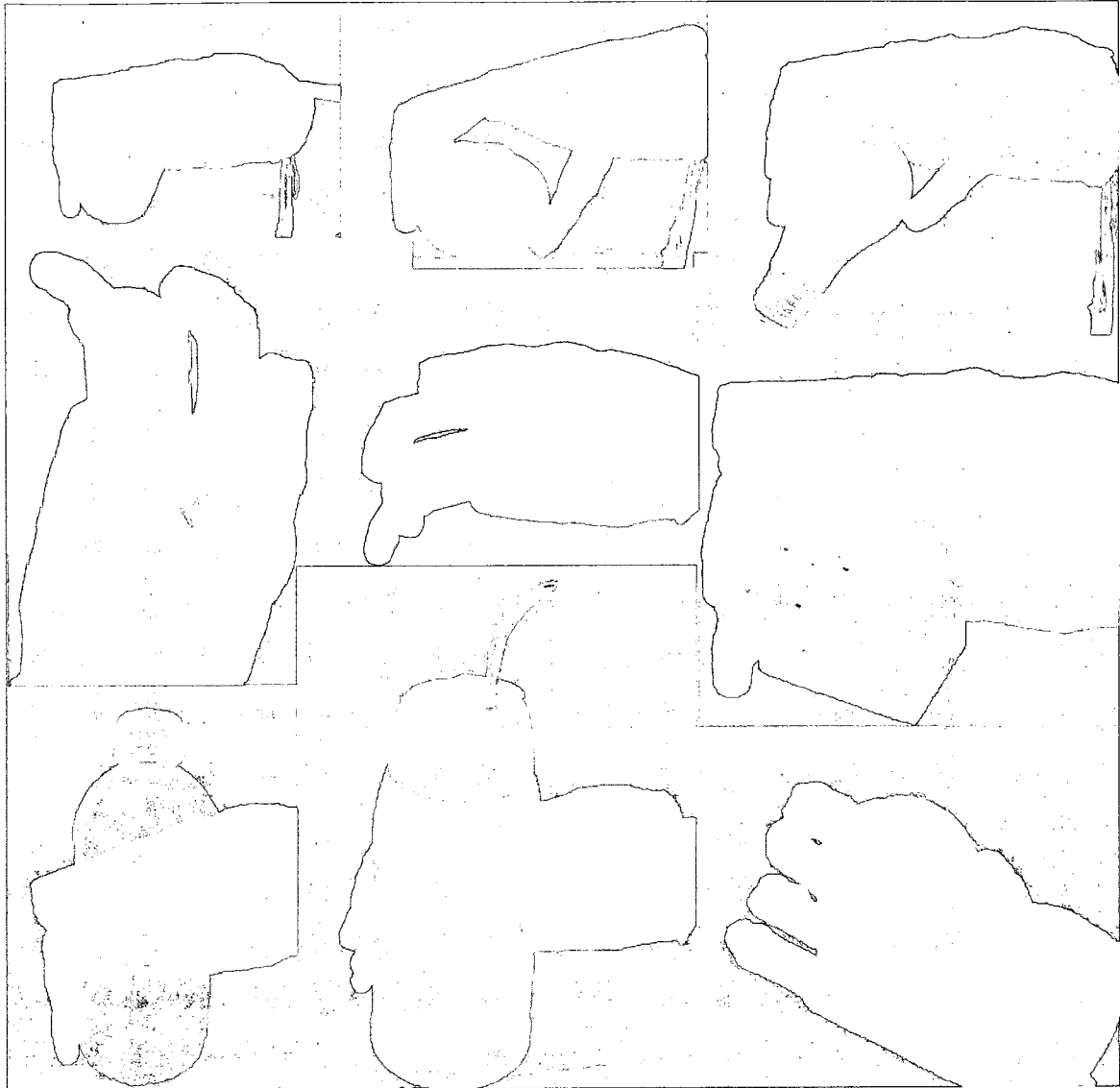


Figure 6-2: Some of the objects used in the static experiments.

The prototype securely held the objects with over 90% success rate for five trials. Table 6-2 shows the results. The failures were caused because the object was not securely grasped, but any of the objects were crushed by the hand. The success rate may be affected by the approach angle and the configuration with respect to the geometry of the object.

Table 6-2: Result from the grasping experiments.

Grasp Type	Object	Object	Grasp type	Global
		Success rate	Success rate	Success rate
Cylindrical and spherical	Plastic cup	5/5	36/40 (90%)	86/95 (90.5%)
	Styrofoam glass	5/5		
	Mug	5/5		
	Small plastic bottle	5/5		
	Big plastic bottle	5/5		
	Egg	3/5		
	Round sponge	4/5		
	Tomato	4/5		
Tripod	Tennis ball	5/5	13/15 (86.6%)	
	Wood block	5/5		
	Lamp bulb	3/5		
Tip	Potato chip	4/5	17/20 (85%)	
	Small cup	5/5		
	Coin	4/5		
	Screw	4/5		
Lateral	Postcard	5/5	15/15 (100%)	
	Key	5/5		
	CD	5/5		
Extension	Big carton box	5/5	5/5 (100%)	

6.3 Adjusting of the Control Strategy

The experiments conducted on the prototype demonstrated that the success of the grasping task strongly depends on the chosen grip pattern and the initial force with which the hand grasps the object. This dependency is also found in human beings, since we use internal parametric models of the objects that are updated with sensory information, to predict the outcomes of different approaches and choose an appropriate grip force [29]. In the prototype, we are not able to create and use such models of the objects to adjust the initial grip force; however visual information may assist the user in the grip pattern

choice and an adjusted value for the initial grip force may be sufficient to securely grasp the objects used in most of the ADL. We found also that the ability to hold different objects (to resist external forces) is affected by the amount of force incremented when slippage is detected. Therefore, there is a need to adjust the initial grip force and the force increment when slippage is detected to improve the performance of the hand.

Sitek et al. compared the grasping forces in human hands and different prostheses during the holding of a small bottle (5.7 cm in diameter and 522 grams in mass) [113]. The average contact force, measured at 20 different locations (in the fingers and the palm), was 0.8 ± 0.7 N for the human hand, 1.3 ± 0.4 N for an adaptive prosthesis (15 DoF) and 2.6 ± 2.7 N, and 3.9 ± 4.6 N for two non-adaptive prostheses (System-electro-handTM and Sensor-handTM, respectively). The maximum grip force for the human hand was 3.8 N (at the proximal phalange of the index finger) and the highest average forces (2 N) were found at the distal phalange of the middle and ring fingers, and the thumb. Higher average contact forces were found for the adaptive and non-adaptive prostheses, with average contact force up to 6.5 times larger compared with the human hand.

Based on this information, we decided to test the hand response (and consequently the control strategy) using a range from 0.7 N to 1 N for the initial force parameter and a range from 0.25 N to 0.45 N for the step size parameter. We conducted an experimental design in order to find the most favorable values of the initial force and the force increment step size, which would lead to improve the performance of the control strategy. The response variable to be minimized is the vertical displacement of the object from the hand while external forces are applied.

Before the control strategy was adjusted, slight modifications were included to improve the performance of the overall system. These modifications are presented next.

6.3.1 *Modifications*

Significant delay in the closing time of the hand was found in the previous work. In order to reduce this delay, a closing stage was added between the pre-shape stage and the force control stage, in which the active fingers move at a constant velocity until contact is made with the object. In order to know when this occurs, the derivative of the RFS (finger velocity) is computed. If the derivative is close to zero (less than 0.05) it is considered that the finger has made contact with the object. The force control stage was then commenced where the force exerted over the object can be modulated.

In addition, slight modifications were introduced to the detection stage and the force control stage. During the detection stage, instead of computing the derivative of the normal force at each time instance, the average derivative over a time window of 5 samples was used. By averaging the derivatives, the noise introduced by differentiation was reduced, resulting in a smoother and more stable grasping motion. The second modification was introduced to the force control stage. For the cylindrical/spherical grip configuration, the learning rate and the voltage supplied to the DC motors were reduced to slow down the dynamic response and prevent overshoot and oscillation.

6.3.2 *Methodology*

The experiment consisted of grasping an aluminum cylinder (diameter 7.4 cm, weight 100 g) that is attached to a mass hanger through a dual-range force sensor (Vernier DFS-BTA).

Figure 6-3 shows the experiment setup. The combined weight of the cylinder, the force sensor and the hanger is 280 g. This experiment contained two steps: The cylinder is first grasped during approximately 20 seconds, and then 700 grams are added to the hanger for the next 20 seconds. A motion sensor (Vernier MD-BTD) is used to record the displacement of the object.

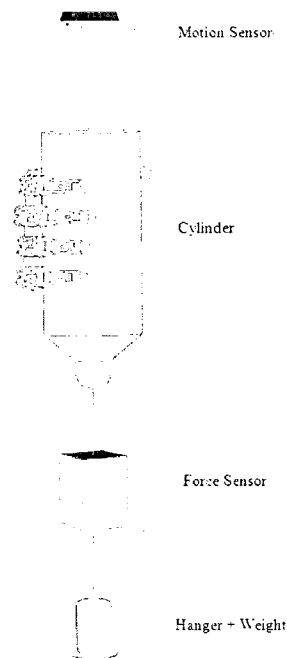


Figure 6-3: Cylindrical experiments setup. The hand grasps an aluminum cylinder that has attached a hanger through a force sensor. Different weights are added to the hanger to produce vertical disturbances. The displacement of the object from the hand is measured by a motion sensor placed at the top.

For these experiments, a two-factor (initial force and step size) factorial design was implemented as a decision support technique. It is difficult to resolve forces less than 0.1 N; therefore we divided the initial force factor in 3 levels, and the step size in 2 levels, as shown in Table 6-3. Three replicates were used for each level combination.

Table 6-3: Factors and levels of the factorial design.

Initial Force		Step Size	
Level	Range (N)	Level	Range (N)
Low	[0.7-0.8)	Low	[0.25-0.35)
Medium	[0.8-0.9]	High	[0.35-0.45]
High	(0.9-1.0]		

There is a significant difference in the displacement if the force reference is changed before the weight is added to the hanger. In order to control this source of variability, experiments were carefully selected to prevent the reference of the index and middle finger from changing before any changes in mass.

6.3.3 Results

Minimum displacement can be achieved at the high level of initial force, corresponding to the range (0.9-1.0] N, and the high level of step size, corresponding to the range [0.35-0.45] N. With this combination, some soft objects became deformed, which suggested that further increments in both the initial force and the step size should be avoided. Figure 6-4 shows the box plot of the results obtained for the displacement experiment: The left plot suggests that minimum displacement is obtained with the *high* step size since the median for the high level is notably lower than for the low level. By looking at the initial force parameter (right plot), and following the same criteria, the *high* option seems to be the most favorable. Figure 6-5 gives more information about the iteration between the two factors. The plot shows that some small iteration exists since the three lines do not have the same slope. For all the levels of initial force the high level

of step size gives the smallest displacement. Moreover, the high level of initial force gives the smallest displacement for all the levels of step size.

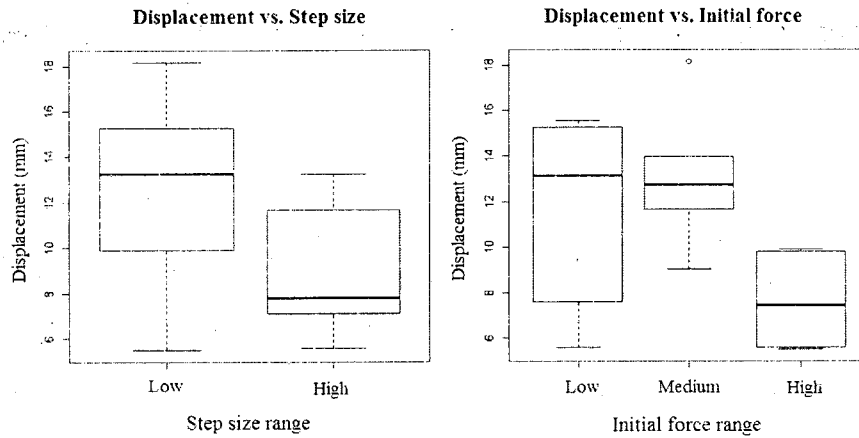


Figure 6-4: Box plot of the displacement vs. step size and initial force.

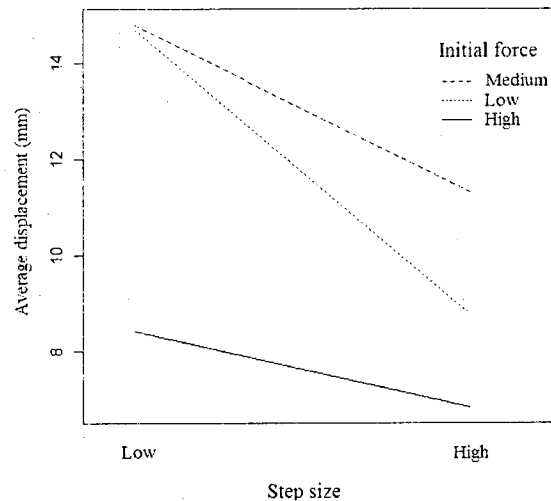


Figure 6-5: Iteration plot for the displacement results. The plot acts as a decision support to find the most favorable parameters of the force control system.

A two-way ANOVA was performed to test if the influence of the two factors is significant. Both step size and initial force significantly influenced the displacement ($P < 0.01$ for both cases). However, no significant interaction between the two parameters was

reported in the ANOVA test, suggesting that varying the levels of one factor does not affect the other. Therefore, the best combination is to use *high* initial force and *high* step size. This strategy is logical since a stronger initial force and a larger increment should prevent objects from sliding.

6.4 Evaluation of the response to force disturbance

6.4.1 Methodology

After determining the parameters of the control strategy, we tested the response of the adjusted algorithm by inducing slippage in different objects. Three sets of experiments were designed based on the testing methodology presented in [40, 80, 81, 111, 112] to evaluate the control strategy. These experiments were performed to simulate real situations likely encountered in ADL, but in a bench top environment. The cylindrical and tip configurations were used to test vertical displacements. The ability to resist torsional forces was evaluated using the torque experiments.

Cylindrical experiment: The response of the hand was tested on two experimental conditions simulating sudden or gradual changes in mass. For the case of inducing sudden changes, the procedure was identical to that described in section 6.3 using five different weights (200, 400, 550, 650 and 750g). It was repeated 7 times for each weight. To induce gradual changes, the prosthetic device was instructed to hold an empty thin plastic cup with water being poured at approximately 30 ml/sec, or approximately 0.3 N/sec. This procedure was also repeated 7 times.

Tip experiment: Experiments similar to the cylindrical one were performed to test the tip grip configuration, as it is illustrated in Figure 6-6. The experiments consisted of grasping a piece of thin plastic (2.5cm x 2cm x 1.5mm) with the tip configuration. The

object was attached to a mass hanger (without the force sensor since it is beyond the capability of this grip configuration). First, the piece with the hanger was grasped for approximately 20 seconds and then a predetermined weight was added for another 20 seconds. The whole procedure was repeated 7 times for each weight (20, 50, 100 and 150g). The Vernier motion sensor was used to record the displacement of the plastic piece from the fingers.

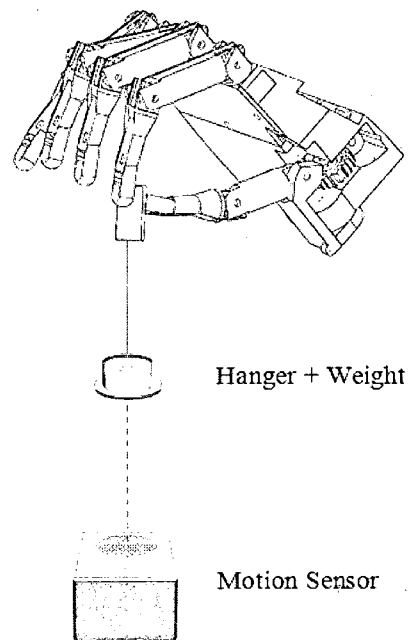


Figure 6-6: Tip experiments setup. The hand grasps a piece of plastic attached a hanger. Different weights are added to produce vertical disturbances. The displacement is measured from the bottom.

Torque experiment: Experiments were performed to evaluate the ability to modulate the force when a rotational force is applied, as illustrated in Figure 6-7. The experiments consisted of grasping a plastic lid (diameter 6.5 cm) that was attached to a string-pulley system connected to a mass hanger through the force sensor. The lid was first grasped with the cylindrical grip configuration for approximately 20 seconds and

then a predetermined torque was applied to the pulley for another 20 seconds. Four different torques (4.4, 6.6, 8.8 and 11 N.cm) were induced 7 times. The motion sensor was used to record the displacement of the hanger which gives an indirect measure of the rotational displacement of the lid in terms of angular displacement. The force sensor was used to measure the induced torque.

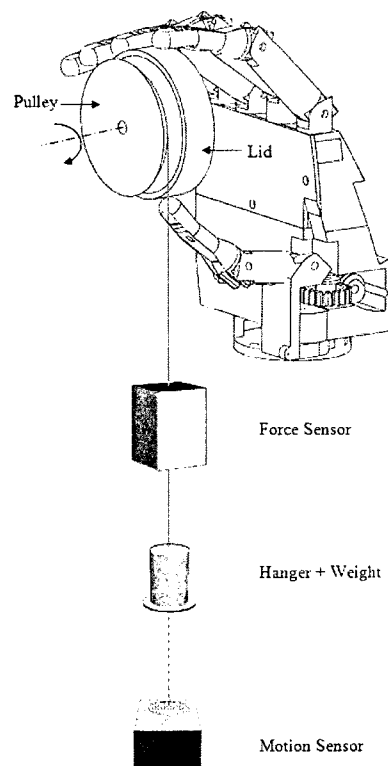


Figure 6-7: Torque experiment setup. The hand grasps a plastic lid that is attached to a pulley. The pulley is connected to a hanger through a force sensor. Different weights are added to the hanger to produce rotational movements. The displacement the mass is measured from the bottom as an indirect measurement of the angular displacement.

6.4.2 Results

The control strategy performed well while adjusting the grasping force to minimize the displacement of the object. The signal from the motion sensor was smoothed using a low pass filter to calculate displacement, computed as the difference

between the distance measured before (average of 5 seconds after the cylinder was grasped) and after (average of the last 2.5 seconds of the experiment) applying the disturbance. An example of one trial of cylindrical grasping is shown in Figure 6-8.

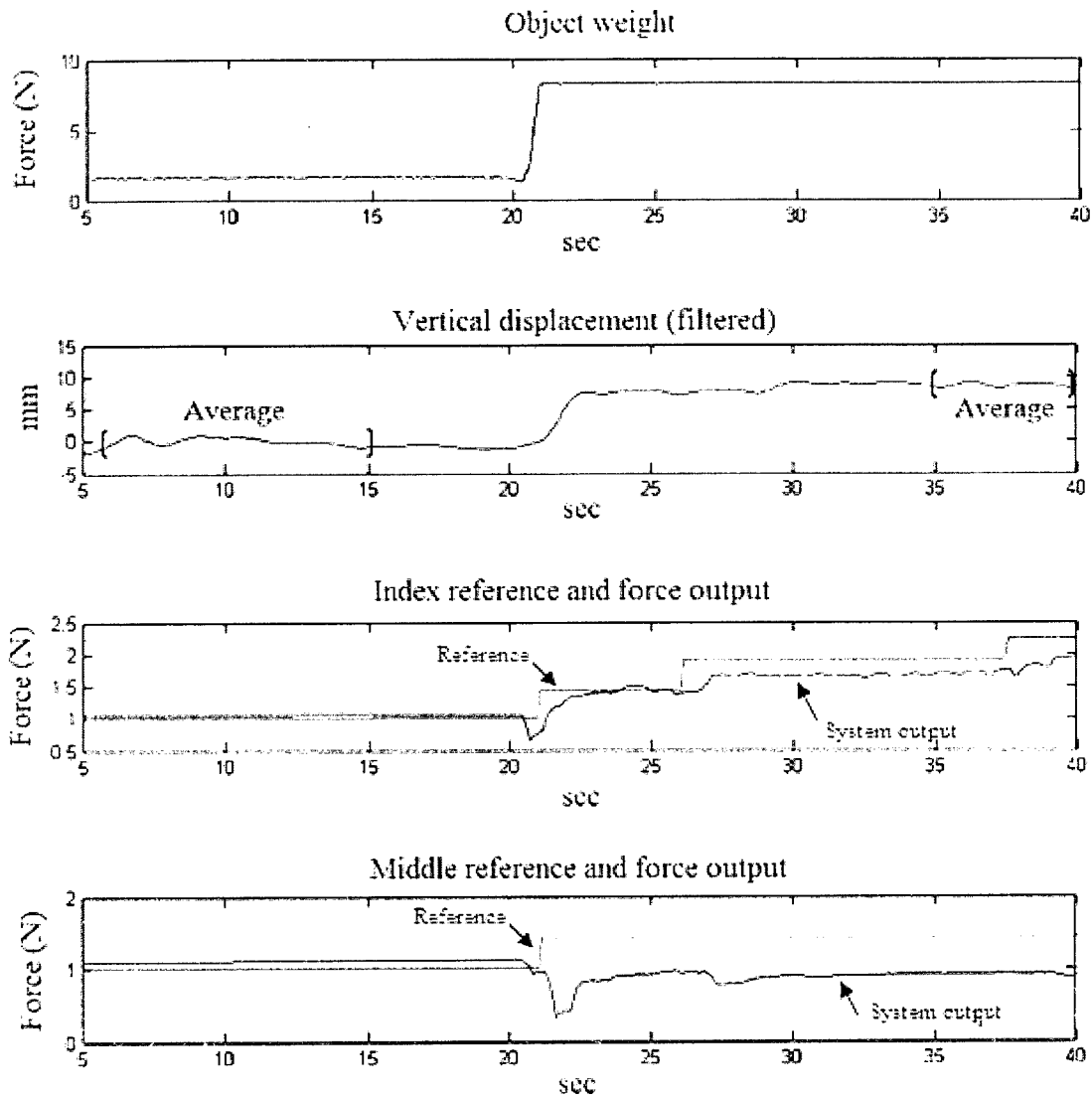


Figure 6-8: Top: The force sensor output, indicating that 750 grams were added to the hanger at approximately 20 second. Second: The motion sensor, showing the vertical displacement of the object. Bottom two: The reference and force control signals for the index and middle finger, respectively. When the mass is added at 20 seconds, the force reference of the index and middle finger increases in response to the external disturbance. However, the control system for the middle finger was unable to follow the reference in this case since the force sensor lost contact with the object.

During the cylindrical, tip and torque experiments, the hand was able to adjust the grasping force fast enough to avoid the dropping of the objects in all the trials. The maximum average displacement for the cylindrical experiments (7.6 mm) was recorded

(Figure 6-9). The variability of these results was within the accuracy of the motion sensor (± 2 mm). Moreover, the displacements of light weight objects were within the resolution of the motion sensor at 2 mm.

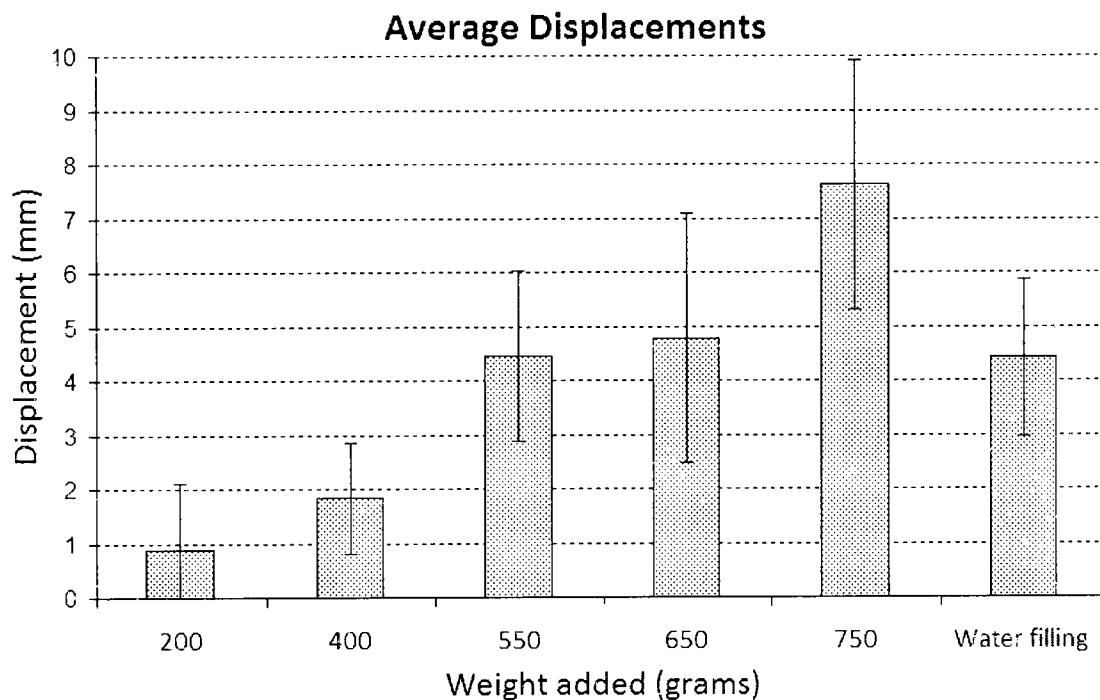


Figure 6-9: Seven displacements were obtained for each experiment. They were averaged to obtain the average displacement of the corresponding experiments (200 grams, 400 grams, etc). Good performance was found for this grip configuration.

For the tip configuration, the observed displacement was small, with a maximum average displacement of 3.05 mm (Figure 6-10). In addition, when small amount of weights were introduced suddenly, the average displacement was less than the precision of the sensor. The variability for the tip experiments was also within the accuracy of the motion sensor, which is less than 2 mm.

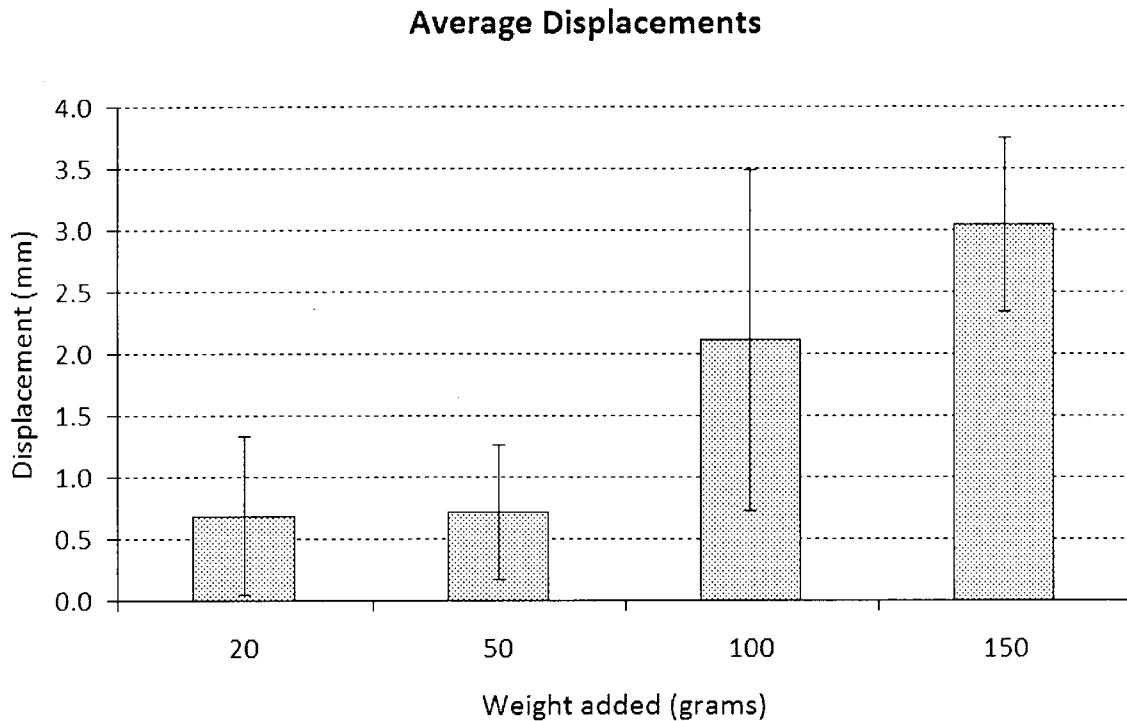


Figure 6-10: Average displacements over 7 trials. The measurements show good performance of the hand in this configuration.

During the torque experiments, the control strategy was able to modulate the grasping force when different torque was applied without showing significant angular sliding. The average displacements are shown in Figure 6-11. The vertical displacement measurements were translated to angular displacement of the lid in degrees. This was achieved using the radius of the pulley (2.25cm) attached to the object from $d = r\theta$, where d is the displacement, r is the radius of the pulley, and θ is the angle of rotation in radians. The maximum average angle displacement was 10.7 degrees when 11 N.cm were applied (equivalent to adding 500 g to the hanger). The variability of all the average rotational displacements fell within the accuracy of the motion sensor.

Average Angle Displacements

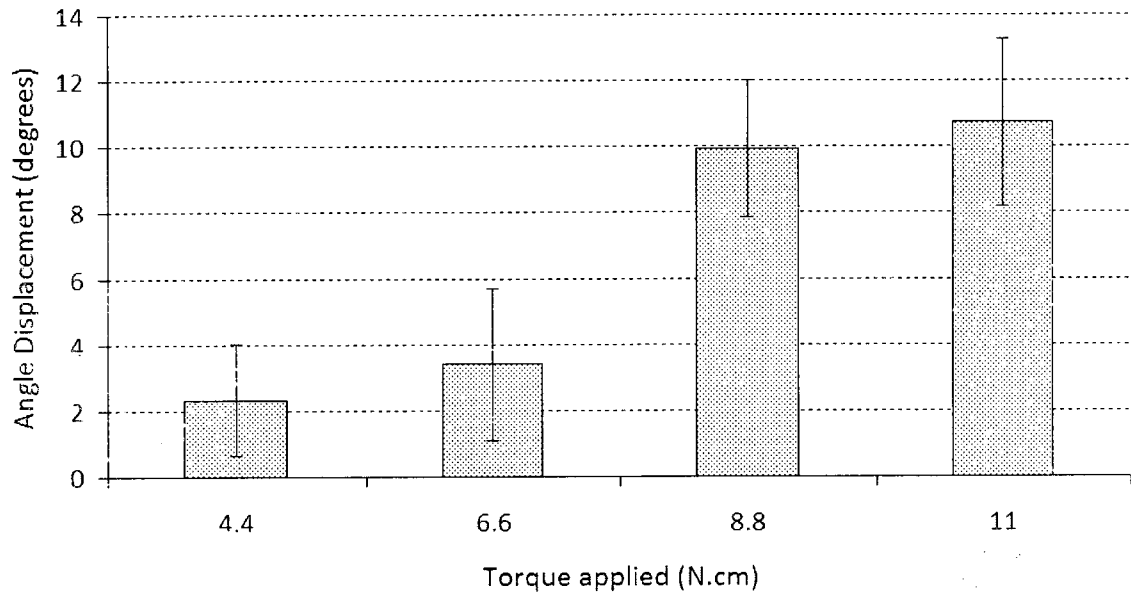


Figure 6-11: Similar results were found from the average of the 7 displacement measured for each torque experiments. This results shows that the hand is also able to handle rotational disturbances.

6.5 Discussion

The objective of the proposed control strategy is to produce stable grasping while minimizing the chances of the object slipping out from the prosthetic device, by modulating the grasping force in an adaptive fashion.

The adjusting stage, where the initial force and step size were defined, influenced the results considerably. The range of applied forces selected for this study is consistent with the range in a human hand for similar procedure [113]. However, the displacement result is difficult to compare with the literature since the testing outcome [40, 81, 112] and the range of the disturbance force are different [111]. However, the results obtained during the cylindrical, tip and torque experiments using the adjusted control strategy

showed that the device handled different grasping tasks with relatively small displacements. Slippage is a function of multiple factors, including friction coefficients, time response of the hand, adequate adjusting of the grasping force, and slip detection time. By reducing the object slippage to an acceptable range, we inherently have accounted for all these factors. Consequently, the results suggested that the device was able to adjust the grasping force to securely grasp and hold different objects, and it can potentially assist the users in the ADL.

During the adjusting stage in the cylindrical experiments, the object was intentionally grasped with the tips of the fingers in order to attain full contact with the force sensors. The drawback of this procedure is that the force distribution characteristic of the underactuated fingers is not used if the hand grasps the object just with the tips of the fingers. However, the results showed that even while grasping a relatively heavy object (around 1 kg) the vertical displacement was relative small (7.6 mm). This small displacement suggests that even smaller displacement can be achieved if the whole hand is used to grasp the object.

The values of displacement may be exaggerated by slight movements produced at the joint of the links (phalanges) of the fingers since the joints are not rigid. The combined vertical displacement of the finger together with the object may be measured. In addition, when grasping force is adjusted while the hand is grasping an object, the reference can sometimes change as the thumb and the index finger both try to exert force on the object at opposite direction. This change in reference influences the displacement of the object. Another factor that may influence the displacement result is that the sensor

sometimes loses contact with the object when the external perturbation is applied (as demonstrated in the middle finger in Figure 6-8).

The experiments were performed using only rigid objects (aluminum cylinder, a piece of hard plastic and a plastic lid). However, if the hand has to grasp a softer object, like a Styrofoam cup, it may be more complicated to reach the initial force. In this case, a modification in the force control stage is being investigated. When the force measured at the tips remains constant but lower than the preset initial force and the fingers continue to close, the initial force has to be set as the force measured at the tip of the fingers. This initialization would avoid continued closing of the finger that could deform the object.

The control strategy is being tested in a proof-of-concept prototype; therefore the mechanical problems of the prototype were not taken into account here. Our aim is to evaluate the feasibility of applying the proposed control algorithm to adjust the grasping force. A future direction to this work is to improve the mechanical strength of the prototype. Clearly, the tip configuration must hold masses heavier than 150 g.

The results also showed that the control strategy was able to handle sudden and gradual external forces and that it could handle the nonlinearities associated with the use of low-cost sensor and actuator systems as well as a simple mechanical design. Moreover, the control strategy was tested using objects usually encountered in common daily activities, which require the selection of different grip patterns. The results suggest, based on the grip pattern used in the experiments, that the proposed strategy can assist the user in most of ADL.

CHAPTER 7

CONCLUSIONS AND FUTURE WORK

7.1 Conclusions

The human hand is one of the most important parts of the human body and its loss drastically reduces functionality and social interaction. Moreover, the high cost of replacement limbs may limit their use by the low-income population. We hypothesized that by using advanced EMG signal processing and control algorithms, we can replace the use of expensive, specialized actuators and sensors, hence reducing the cost.

The aim of this dissertation was to present the design of a control strategy for a low-cost robotic hand for prosthetic applications. The main objective of this work is to bridge the translational gap between the technology and commercialization to bring a possible solution for reducing the cost of prosthesis.

A low-cost mechatronic system for a five-fingered prosthetic hand was presented. The objective of this prototype was to serve as a testing platform to evaluate the proposed control strategy. Anthropomorphic size and weigh along with cost effective sensor and actuators were the constraints of it design. Although the present version of the prototype is far from it final version, it can be considered as a starting point for future developments.

A possible control strategy that can be used to drive a low-cost prosthetic hand was designed and evaluated. It is divided in three principal stages: a pre-shape stage, a force control stage and a detection stage. These stages were designed and evaluated separately in order to test its feasibility for the control of the prosthetic hand. The results suggest that the force control stage can modulate the force exerted by the fingers with rise times below 1 second, overshoots smaller than 1 N and a steady state error of less than 5%. Moreover, the detection algorithm was able to detect unintended object movements with a delay of less than 200 ms.

After the different stages were separately evaluated, the control strategy was modified slightly and tested in different scenarios simulating ADL. Once the best values were found for the initial grasping force and the force increment, the results of the displacement experiments showed object displacements less than 10 mm for the worst-case scenario, which encourages the authors to continue working in this direction. The control strategy overcame the limitations of inexpensive sensors and actuators and securely manipulated the prosthetic device. It maintained a stable grasp during dynamic tasks, demonstrating its ability to automatically modulate the grasping force to compensate for vertical and torsional perturbations. Although more effort is needed to improve the performance of the overall system, we believe that the work presented here is a major step towards the development of a cost effective myoelectric hand.

7.2 Ongoing and Future Work

7.2.1 *Ongoing Improvements on the Prototype*

The efficiency and durability of the prototype need to be improved before it can be used in clinical trials. It will be important to: (1) enable an electrically driven saddle joint movement in the thumb; (2) eliminate skipping and stripping of gears; (3) improve force detection to enable a wider range of detectable grips; and (4) reduce friction of moving parts to increase battery life and durability.

A new prototype is being developed to address the above issues (Figure 7-1). In an effort to improve the second generation prototype, the new design contains a better alignment of the motors and gears and an active DoF was added to the thumb to produce its opposition. The routing of the sensors inside the finger was improved and torsion springs were added to the joints of the fingers.

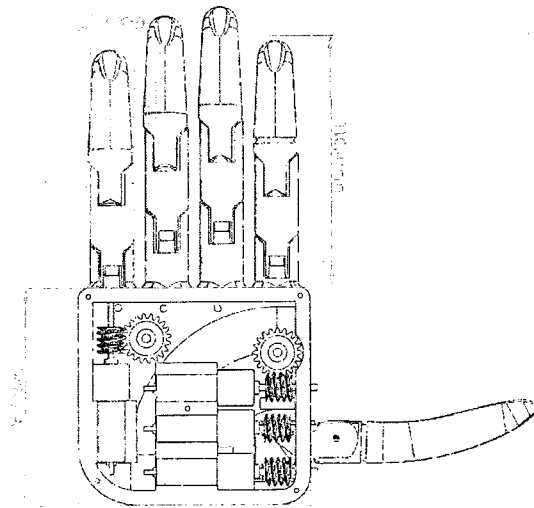


Figure 7-1: New improved prototype.

Although this new prototype improves on the previous version, further changes are needed to enable clinical trials. The tendon cable used is not resistant enough to friction; therefore a more robust tendon-cable system is needed. The new prototype is slightly larger than a natural hand, which increases the difficulty of manipulation tasks. In addition, an extra DoF in the thumb is necessary to create a distal phalanx. With this addition, the thumb will be able to adapt better to the shape of the object. Finally, the glove that covers the hand must be improved to increase its durability and improve the hand grip.

Finally, the small contact surface of the FSR sometimes causes the control strategy to lose control of objects. Additional force sensors in others parts of the hand might overcome this limitation. The work of Kargov et al. [113] suggests that more FSR sensors in the second phalanges of the thumb and index finger, and in the distal part of the second metacarpal, would be beneficial.

7.2.2 Future Improvements on the Control Strategy

Some issues must be addressed in order to improve the performance of the system. At this moment, each finger is been controlled in a predictive fashion, based on a static model. However, it is important to make the model to approach asymptotically to the real system in order to better represent the system dynamics [92]. This added precision will result in better performance of the control system. Consequently, the incorporation of an adaptive algorithm such that the model can be dynamically modified in real time is being considered as a next step of the controller design.

The system identification stage uses a feedforward neural network. The implementation of others topologies, such as recurrent neural networks, may improve the

model accuracy, which is a key element in the performance of the force controller. Moreover, other pattern recognition and machine learning techniques, such as Support Vector Machines or Kalman Filters, might be other options for system identification.

Currently, the control system uses the information from the gradient of the objective function to compute the control signal. It is well known that this method is slow compared with any Hessian-based algorithms for nonlinear optimization. Therefore, the implementation of an optimization algorithm based on the second derivative of the objective function should be addressed. The Levenberg-Marquardt method described in section 4.2.1 may be a good choice for the optimization stage of the force control system.

In the Detection stage, only the information from the derivative of the normal force is used. Inclusion of the frequency/time-frequency information of the normal force could improve the slip detection algorithm, leading to a more robust system.

Finally, the inclusion of a position control system for the finger configuration might be useful in the Pre-shape stage. An accurate tracking of the finger angle position by means of a control system before grasping the object can produce a more stable grasping.

7.2.3 Future Implementation of the Control Strategy on Microcontrollers

While the abovementioned aspects of the prototype and control algorithms are being improved, the whole control system should be embedded inside the hand in order to allow a clinical evaluation of the prototype.

With this objective, a custom board should be designed that contains the sensors, signal processing circuits, the motor drivers and a microcontroller, which would replace the PC-based setup described in this work. The circuits described here are simple and do

not need extensive room to be implemented. A possible choice for the microcontroller is the Arduino platform (Figure 7-2) [114]. It is an open-source electronic platform that integrates analog and digital ports, PWM motor drivers and the ATmega1280 microcontroller. The open-source characteristics make it a suitable platform for a low-cost system. In addition, a huge flexibility is obtained, since it can be customized to match the different design specifications.

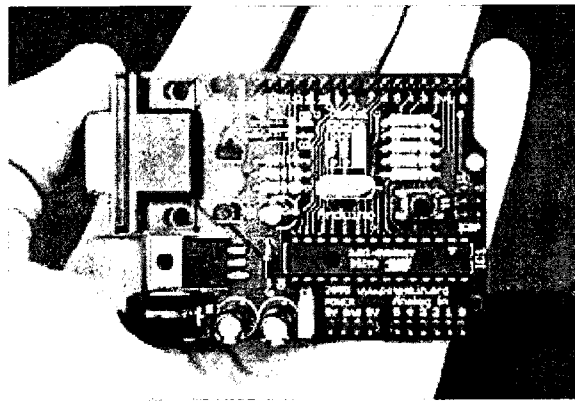


Figure 7-2: Arduino platform (from [114]).

APPENDIX A

IMPLEMENTATION OF THE CONTROL STRATEGY IN

LABVIEW

In this section the online implementation of the control strategy is presented. The different stages of the control algorithm are represented by the different sequences in the “Stacked Sequence Structure” of the main LabVIEW program. The main program is presented first and then its sub programs are shown. If there is a Matlab Script in one of the section of the program, it is detailed following the diagram to which it belongs.

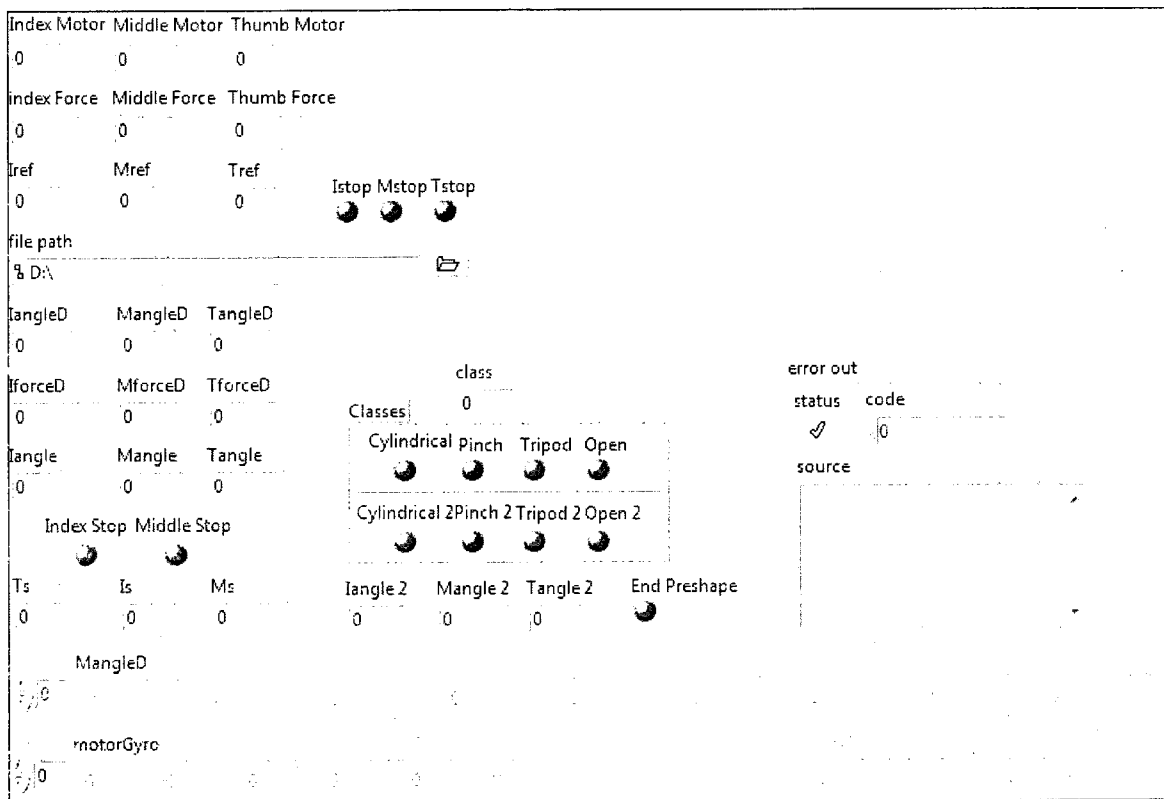


Figure A-1: Front panel of the control strategy.

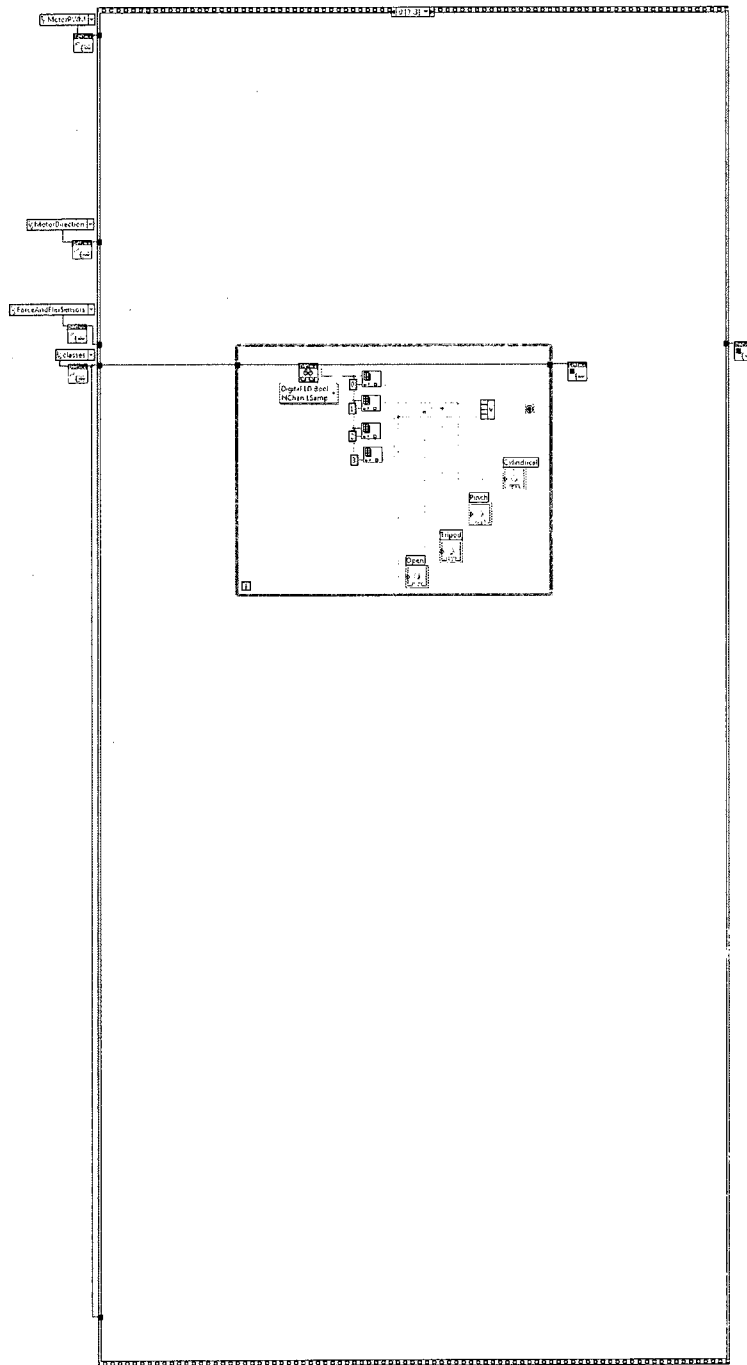


Figure A-2: Block diagram: Grasping type selection.

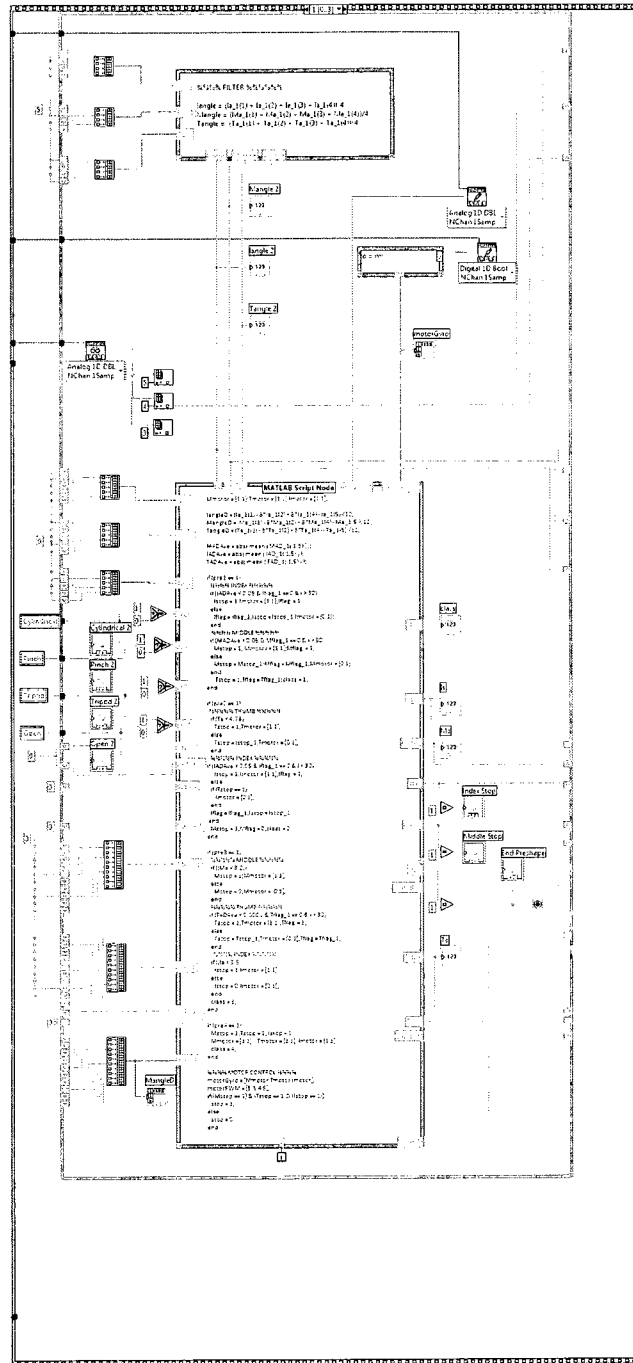


Figure A-3: Block diagram: Whole Pre-shape stage.

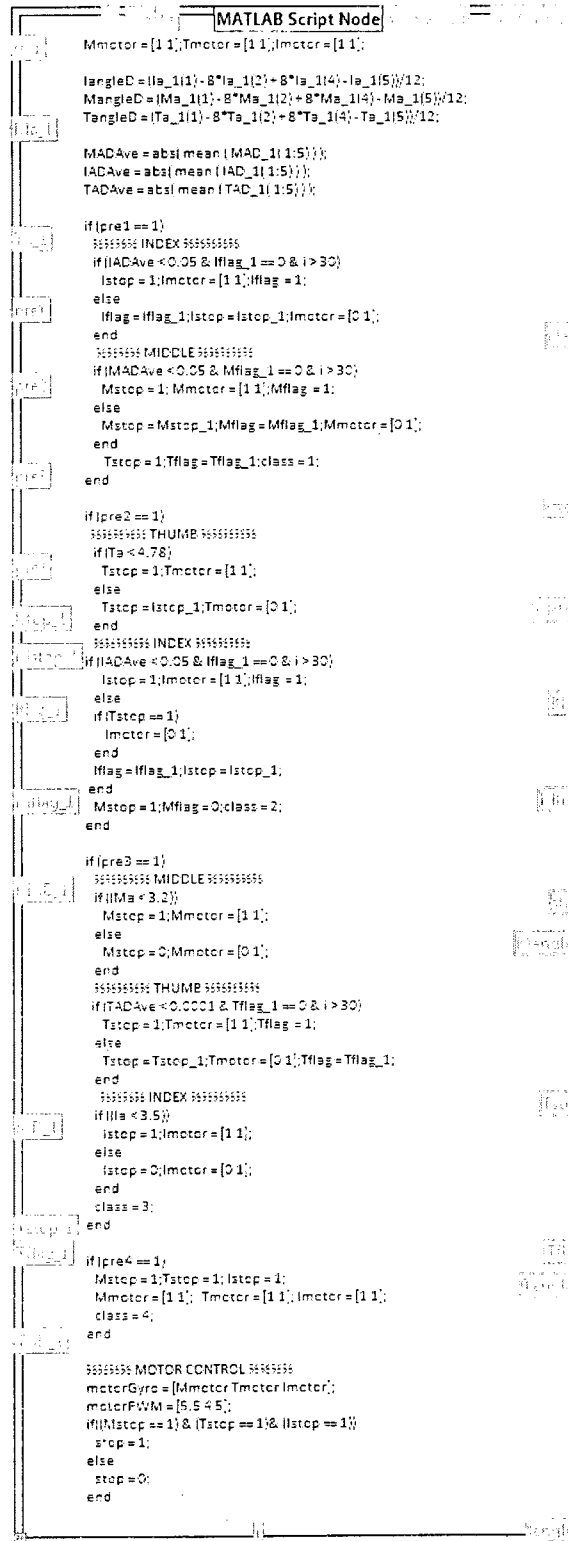


Figure A-4: Block diagram: Detail of Pre-shape stage

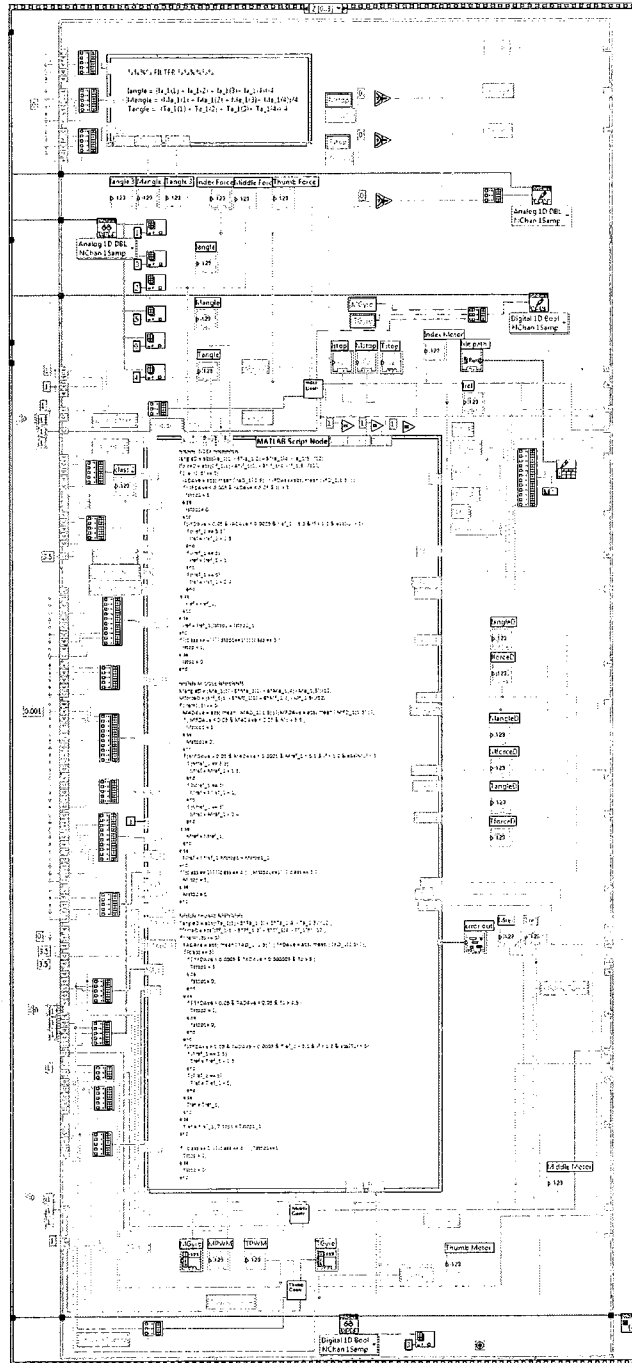


Figure A-5: Block diagram: Whole Force Control and Detection stage.

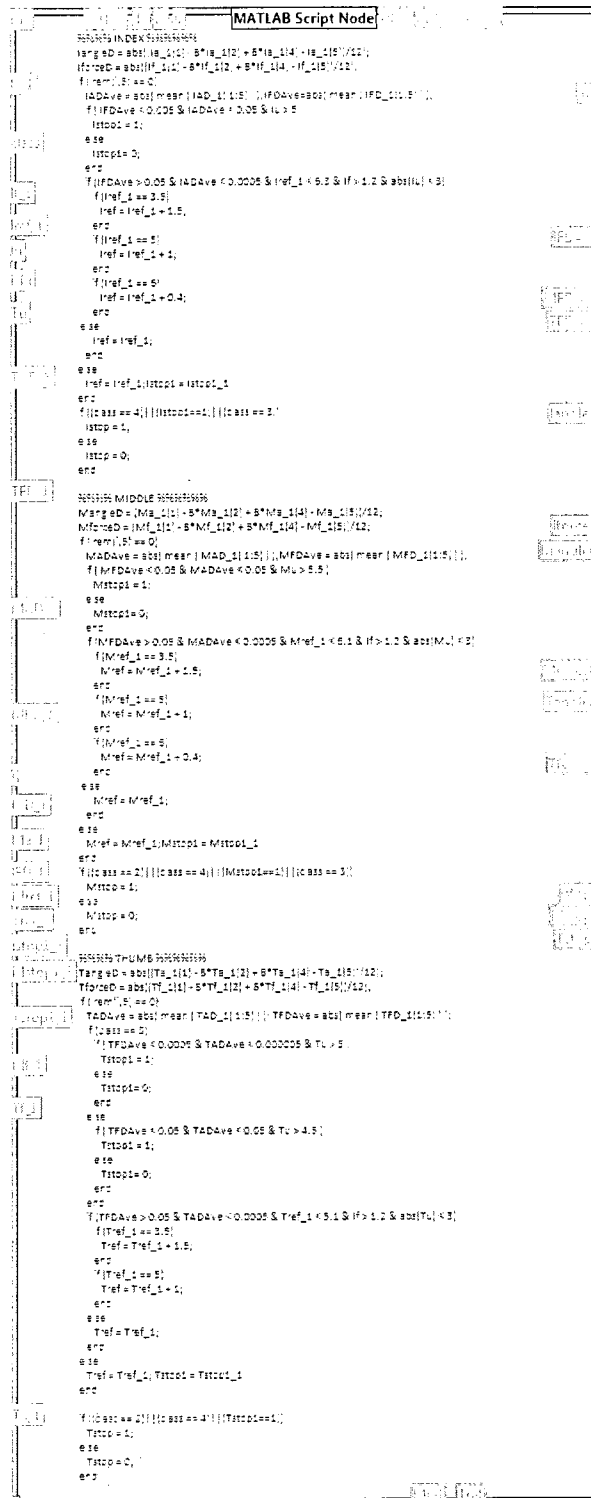


Figure A-6: Block diagram: Detail of the Force Control and Detection stage.


```

MATLAB Script Node
%%%%%%%%%%%%%%%%%%%%%%%%%%%%%%%%%%%%%%%%%%%%%%%%%%%%%%%%%%%%%%%%%%%%%%%%%%%%%% INDEX %%%%%%%%%%%%%%%%%%%%%%%%%%%%%%%%%%%%%%%%%%%%%%%%%%%%%%%%%%%%%%%%%%%%%%%%%%%%%%%
Id = abs(|Ip(1) - 8*Ip(2) - 8*Ip(4) - Ip(5)|/12);

if (|Ia| > 5.2)
    Istop = true;
    Imotor = [1 1];
else
    Istop = false;
    Imotor = [1 0];
end

%%%%%%%%%%%%%%%%%%%%%%%%%%%%%%%%%%%%%%%%%%%%%%%%%%%%%%%%%%%%%%%%%%%%%%%%%%%%%% MIDDLE %%%%%%%%%%%%%%%%%%%%%%%%%%%%%%%%%%%%%%%%%%%%%%%%%%%%%%%%%%%%%%%%%%%%%%%%%%%%%%%
Md = abs(|Mp(1) - 8*Mp(2) - 8*Mp(4) - Mp(5)|/12);

if (|Ma| > 4.25)
    Mstop = true;
    Mmotor = [1 1];
else
    Mstop = false;
    Mmotor = [1 0];
end

%%%%%%%%%%%%%%%%%%%%%%%%%%%%%%%%%%%%%%%%%%%%%%%%%%%%%%%%%%%%%%%%%%%%%%%%%%%%%% THUMB %%%%%%%%%%%%%%%%%%%%%%%%%%%%%%%%%%%%%%%%%%%%%%%%%%%%%%%%%%%%%%%%%%%%%%%%%%%%%%%
Td = abs(|Tp(1) - 8*Tp(2) + 8*Tp(4) - Tp(5)|/12);

if (|Ta| > 4.6) & (|Tf| < 0.3)
    Tstop = true;
    Tmotor = [1 1];
else
    Tstop = false;
    Tmotor = [1 0];
end

%%%%%%%%%%%%%%%%%%%%%%%%%%%%%%%%%%%%%%%%%%%%%%%%%%%%%%%%%%%%%%%%%%%%%%%%%%%%%% MOTOR CONTROL %%%%%%%%%%%%%%%%%%%%%%%%%%%%%%%%%%%%%%%%%%%%%%%%%%%%%%%%%%%%%%%%%%%%%%%%%%%%%%%
motorGyro = [Mmotor Tmotor Imotor];
motorPWM = [5.2 4.5 5];

if (Istop == true) & (Mstop == true) & (Tstop == true)
    stop = 1;
else
    stop = 0;
end

```

Figure A-8: Block diagram: Detail of the Release stage.

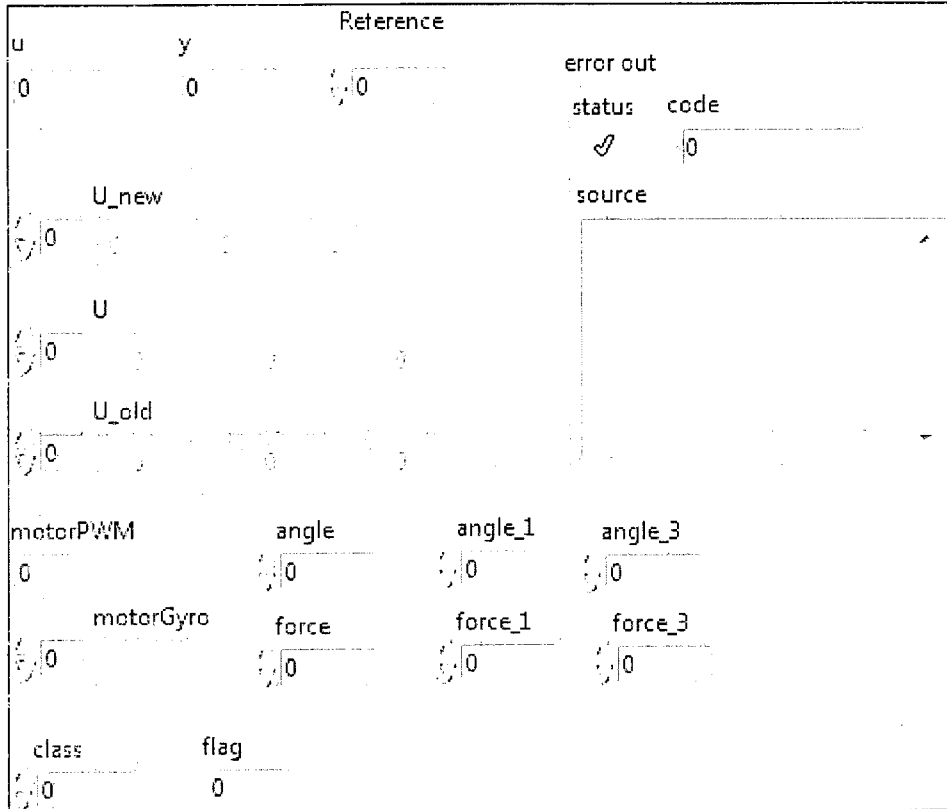


Figure A-9: Front Panel of the Force Control stage of the index finger.

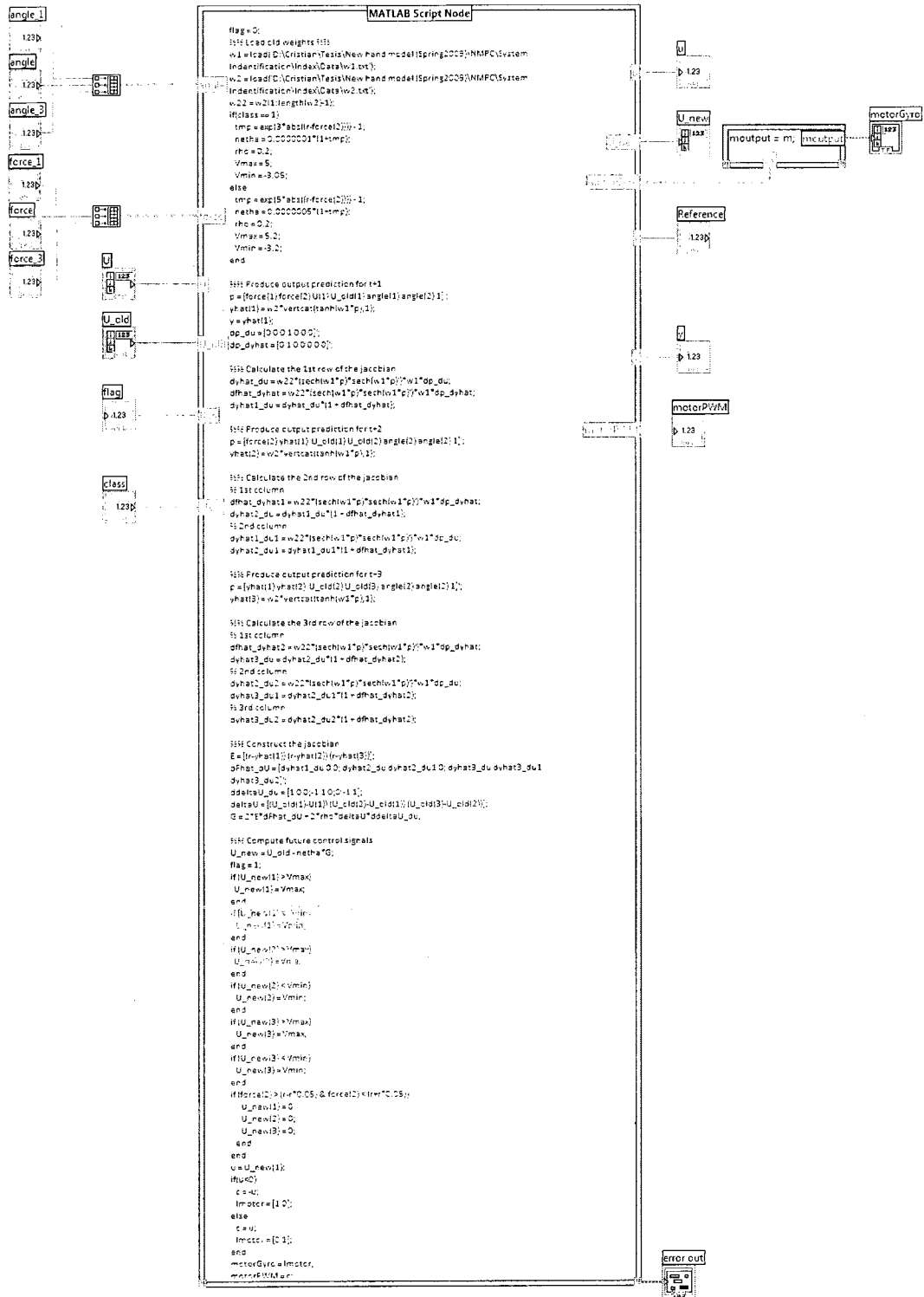


Figure A-10: Block Diagram of the Force Control stage of the index finger.

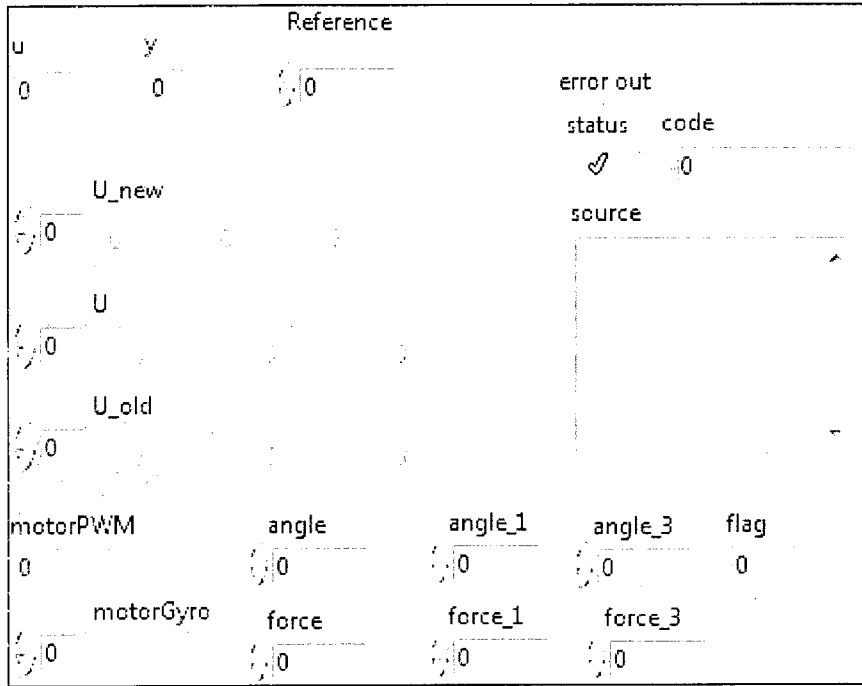


Figure A-11: Front Panel of the Force Control stage of the middle finger.

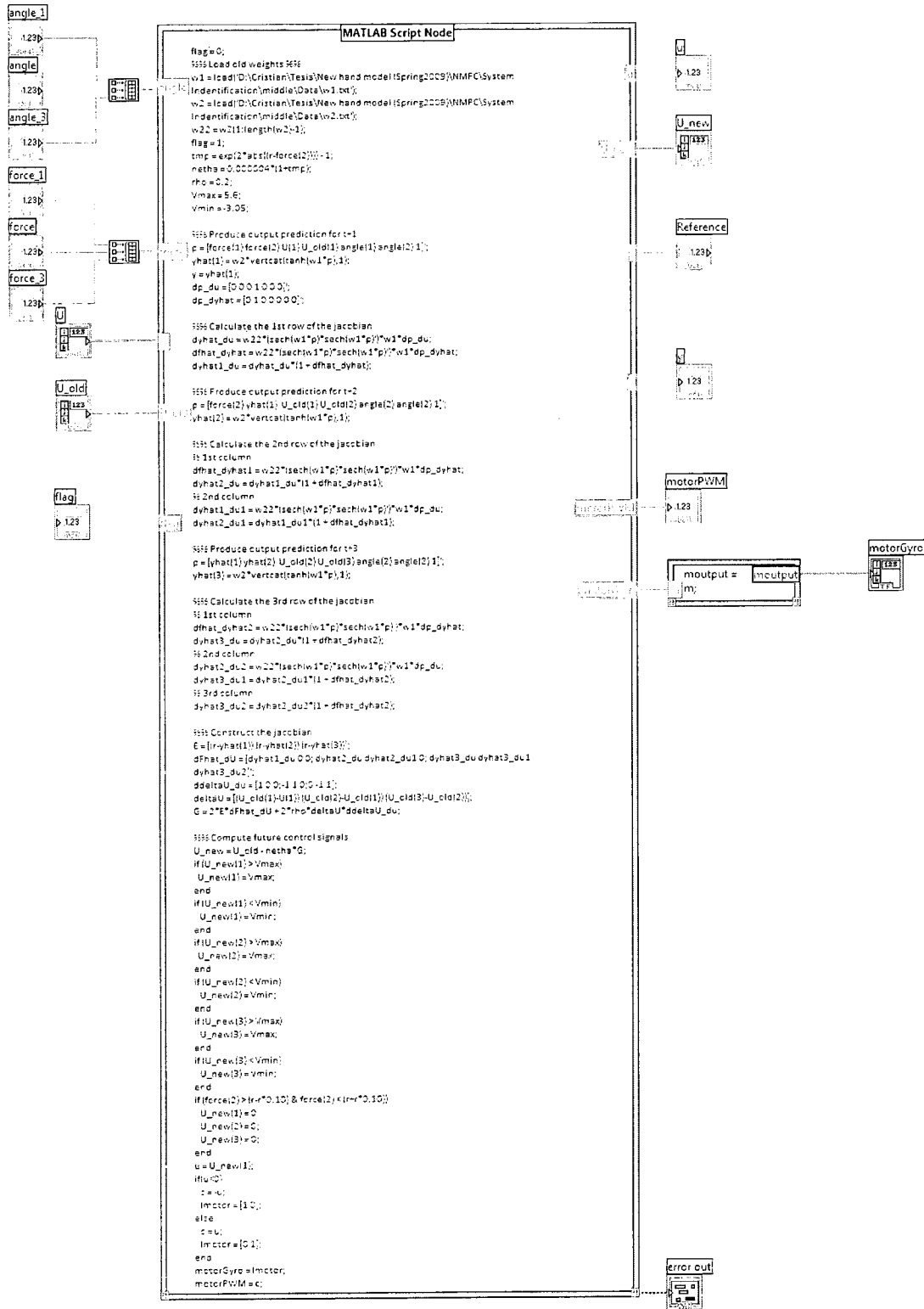


Figure A-12: Block Diagram of the Force Control stage of the middle finger.

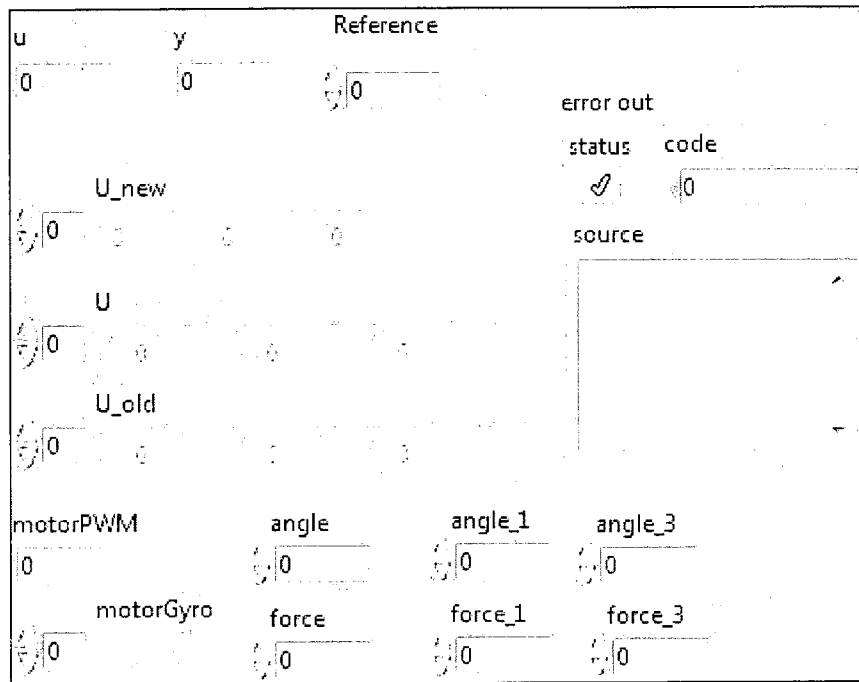


Figure A-13: Front Panel of the Force Control stage of the thumb.

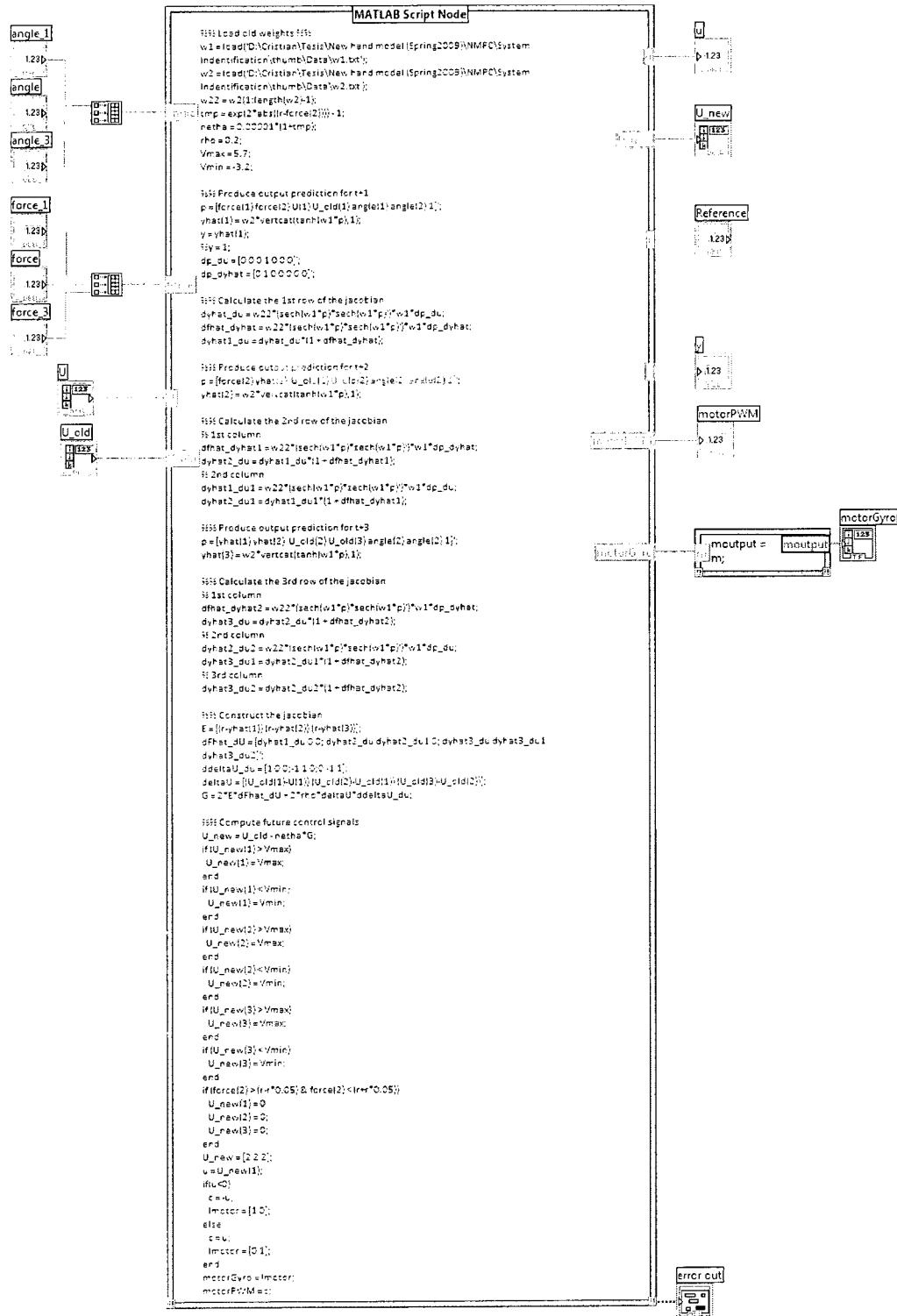


Figure A-14: Block Diagram of the Force Control stage of the thumb.

APPENDIX B

OFF-LINE SYSTEM IDENTIFICATION IMPLEMENTED IN

MATLAB

```

%%%%%%%%%%%%%%%%%%%%%%%%%%%%%%%%%%%%%%%%%%%%%%%%%%%%%%%%%%%%%%%%%%%%%%%%
%                               System Identification                               %
%
% Description: Modeling of the                                               %
% dynamics of the index finger using                                       %
% a feedforward neural network                                           %
% (using NNSYSID toolbox for Matlab.                                       %
%
%
% Author: Cristian Pasluosta                                             %
%%%%%%%%%%%%%%%%%%%%%%%%%%%%%%%%%%%%%%%%%%%%%%%%%%%%%%%%%%%%%%%%%%%%%%%%

```

```

clear all;
clc;

```

```

%%%%%%%%%%%%%%%%%%%%%%%%%%%%%%%%%%%%%%%%%%%%%%%%%%%%%%%%%%%%%%%%%%%%%%%%
%                               Signal Preparation                               %
%%%%%%%%%%%%%%%%%%%%%%%%%%%%%%%%%%%%%%%%%%%%%%%%%%%%%%%%%%%%%%%%%%%%%%%%

```

```

% Loading the files %%
% Object1
s1 = load('Object1_01.txt');
s2 = load('Object1_02.txt');
s3 = load('Object1_03.txt');
s4 = load('Object1_04.txt');
s5 = load('Object1_05.txt');
% Object2
s6 = load('Object2_01.txt');
s7 = load('Object2_02.txt');
s8 = load('Object2_03.txt');
s9 = load('Object2_04.txt');
s10 = load('Object2_05.txt');
% Object3
s11 = load('Object3_01.txt');
s12 = load('Object3_02.txt');
s13 = load('Object3_03.txt');
s14 = load('Object3_04.txt');
s15 = load('Object3_05.txt');
% Object4
s16 = load('Object4_01.txt');
s17 = load('Object4_02.txt');
s18 = load('Object4_03.txt');
s19 = load('Object4_04.txt');
s20 = load('Object4_05.txt');
% Object5
s21 = load('Object5_01.txt');
s22 = load('Object5_02.txt');

```

```

s24 = load('Object5_04.txt');
s25 = load('Object5_05.txt');
% Testing
s26 = load('Object1_06.txt');
s27 = load('Object2_06.txt');
s28 = load('Object3_06.txt');
s29 = load('Object4_06.txt');
s30 = load('Object5_06.txt');

% Concatenating the signals %%
% Training signals
currentTr =
vertcat(s1(:,1),s2(:,1),s3(:,1),s4(:,1),s5(:,1),s6(:,1),
s7(:,1),s8(:,1),s9(:,1),s10(:,1),s11(:,1),s12(:,1),s13(:,
1),s14(:,1),s15(:,1),s16(:,1),s17(:,1),s18(:,1),s19(:,1)
),s20(:,1),s21(:,1),s22(:,1),s24(:,1),s25(:,1));
forceTr =
vertcat(s1(:,2),s2(:,2),s3(:,2),s4(:,2),s5(:,2),s6(:,2),
s7(:,2),s8(:,2),s9(:,2),s10(:,2),s11(:,2),s12(:,2),s13(:,
2),s14(:,2),s15(:,2),s16(:,2),s17(:,2),s18(:,2),s19(:,2)
),s20(:,2),s21(:,2),s22(:,2),s24(:,2),s25(:,2));
thetaTr =
vertcat(s1(:,3),s2(:,3),s3(:,3),s4(:,3),s5(:,3),s6(:,3),
s7(:,3),s8(:,3),s9(:,3),s10(:,3),s11(:,3),s12(:,3),s13(:,
3),s14(:,3),s15(:,3),s16(:,3),s17(:,3),s18(:,3),s19(:,3)
),s20(:,3),s21(:,3),s22(:,3),s24(:,3),s25(:,3));
% Testing signals
currentTs =
vertcat(s26(:,1),s27(:,1),s28(:,1),s29(:,1),s30(:,1));
forceTs =
vertcat(s26(:,2),s27(:,2),s28(:,2),s29(:,2),s30(:,2));
thetaTs =
vertcat(s26(:,3),s27(:,3),s28(:,3),s29(:,3),s30(:,3));
currentTs = currentTs';
thetaTs = thetaTs';
forceTs = forceTs';

% Scaling the signals to zero mean and variance one %%
% Training signals
U1 = [currentTr thetaTr];
U1 = U1';
Y1 = forceTr';
[US1,uscales] = dscale(U1);
[YS1,yscales] = dscale(Y1);
% Testing signals
U2 = [currentTs; thetaTs];
Y2 = forceTs;

```

```

US2 = dscale(U2,uscales);
YS2 = dscale(Y2,yscales);

%%%%%%%%%%%%%%%%%%%%%%%%%%%%%%%%%%%%%%%%%%%%%%%%%%%%%%%%%%%%%%%%%%%%%%%%
%                               Nonlinear Model                               %
%%%%%%%%%%%%%%%%%%%%%%%%%%%%%%%%%%%%%%%%%%%%%%%%%%%%%%%%%%%%%%%%%%%%%%%%
%%% Defining the structure of the NN %%
NetDef = ['HHHHHHHHHHH';'L-----'];%10 hidden units,
tan h and linear activation fuctions.
NN = [2 2 2 1 1];% 1 past outputs, 1 past inputs and 1
time delay.
%%% Defining training parameters %%
trparms = settrain;%set training parameters to default.
trparms = settrain(trparms,'maxiter',500,'critmin',1e-
3,'paramterm',1e-3);%Setting the training parameters
%%% Training the NN %%
[W1,W2,critvec,iteration,lambda]=nnarx(NetDef,NN,[],[],t
rparms,YS1,US1);%Training a NNARX model.
[w1,w2]=wrescale('nnarx',W1,W2,uscales,yscales,NN);%Resc
aling
%%% Testing %%
[yhat,NSSE] = nnvalid('nnarx',NetDef,NN,w1,w2,Y2,U2);
%%% Pruning if necessary %%
prparms = [50 0];
[thd,trv,fpev,tev,deff,pv] =
nnprune('nnarx',NetDef,W1,W2,US1,YS1,NN,trparms,prparms,
US2,YS2);
[mintev,index]=min(tev(pv));
index=pv(index);
[W1,W2]=netstruc(NetDef,thd,index);
%%% Retraining after pruning %%
trparms = settrain(trparms,'D',0);
[W1,W2,critvec,iteration,lambda]=nnarx(NetDef,NN,W1,W2,t
rparms,YS1,US1);%Training a NNARX model.
[w1,w2]=wrescale('nnarx',W1,W2,uscales,yscales,NN);%Resc
aling
[yhat,NSSE] =
nnvalid('nnarx',NetDef,NN,w1,w2,Y2,U2);%Testing

```

REFERENCES

- [1] C. Lake and R. Dodson, "Progressive upper limb prosthetics," *Physical Medicine and Rehabilitation Clinics of North America*, vol. 17, 2006, pp. 49.
- [2] R. F. Baumgartner, "Guest Editorial: Upper extremity amputation and prosthetics," *Journal of Rehabilitation Research and Development*, vol. 38, 2001, pp. vii.
- [3] M. C. Carrozza, G. Cappiello, L. Beccai, F. Zaccone, S. Micera, and P. Dario, "Design methods for innovative hand prostheses," in Proceedings of the Annual International Conference of the IEEE Engineering in Medicine and Biology, 2004, pp. 4345.
- [4] C. Pylatiuk, S. Schulz, and L. Döderlein, "Results of an internet survey of myoelectric prosthetic hand users," *Prosthetics and Orthotics International*, vol. 31, 2007, pp. 362.
- [5] C. Connolly, "Prosthetic hands from Touch Bionics," *Industrial Robot*, vol. 35, 2008, pp. 290.
- [6] C. Cipriani, M. Controzzi, and M. C. Carrozza, "Progress towards the development of the SmartHand transradial prosthesis," in 2009 IEEE International Conference on Rehabilitation Robotics, ICORR 2009, 2009, pp. 682.
- [7] R. Weir, S. Clark, M. Mitchell, G. Puchhammer, K. Kelley, M. Haslinger, N. Kumar, R. Hofbauer, P. Kuschnigg, V. Cornelius, M. Eder, and R. Grausenburger, "New Multifunctional Prosthetic Arm and hand Systems," in 2007 IEEE Engineering in Medicine and Biology Society 29th Annual International Conference, EMBS 2007, 2007, pp. 4359.
- [8] K. Ziegler-Graham, E. J. MacKenzie, P. L. Ephraim, T. G. Trivison, and R. Brookmeyer, "Estimating the Prevalence of Limb Loss in the United States: 2005 to 2050," *Archives of Physical Medicine and Rehabilitation*, vol. 89, 2008, pp. 422.

- [9] P. F. Adams, G. E. Hendershot, and M. A. Marano, "Current estimates from the National Health Interview Survey, 1996," *Vital and health statistics. Series 10, Data from the National Health Survey*, 1999, pp. 1.
- [10] R. Turner, "What is Prosthetic Parity?" Available: <http://www.disabled-world.com/assistivedevices/prostheses/prosthetic-parity.php>, last update: May 30, 2009, accessed on August 16, 2010.
- [11] A. J. Sitek, G. T. Yamaguchi, D. E. Herring, C. J. Willems, D. Boninger, and R. M. Boninger, "Development of an inexpensive upper-extremity prosthesis for use in developing countries," *Journal of Prosthetics and Orthotics*, vol. 16, 2004, pp. 94.
- [12] K. Bhaskaranand, A. K. Bhat, and K. N. Acharya, "Prosthetic rehabilitation in traumatic upper limb amputees (an Indian perspective)," *Archives of Orthopaedic and Trauma Surgery*, vol. 123, 2003, pp. 363.
- [13] S. L. Matsen, "A closer look at amputees in Vietnam: A field survey of Vietnamese using prostheses," *Prosthetics and Orthotics International*, vol. 23, 1999, pp. 93.
- [14] J. M. Fontana and A. W. L. Chiu, "Control of prosthetic device using Support Vector Machine signal classification technique," *American Journal of Biomedical Science*, vol. 1, 2009, pp. 336-343.
- [15] A. M. Okamura, N. Smaby, and M. R. Cutkosky, "An overview of dexterous manipulation," in *Proceedings of the IEEE International Conference on Robotics and Automation, ICRA '00.*, 2000, pp. 255.
- [16] C. Sollerman and A. Ejeskar, "Sollerman hand function test: A standardised method and its use in tetraplegic patients," *Scandinavian Journal of Plastic and Reconstructive Surgery and Hand Surgery*, vol. 29, 1995, pp. 167.
- [17] P. J. Kyberd and P. H. Chappell, "The Southampton hand: An intelligent myoelectric prosthesis," *Journal of Rehabilitation Research and Development*, vol. 31, 1994, pp. 326.
- [18] C. M. Light, P. H. Chappell, B. Hudgins, and K. Engelhart, "Intelligent multifunction myoelectric control of hand prostheses," *Journal of Medical Engineering and Technology*, vol. 26, 2002, pp. 139.

- [19] M. C. Carrozza, G. Cappiello, S. Micera, B. B. Edin, L. Beccai, and C. Cipriani, "Design of a cybernetic hand for perception and action," *Biological Cybernetics*, vol. 95, 2006, pp. 629.
- [20] L. E. Rodriguez-Cheu, D. Gonzalez, and M. Rodriguez, "Result of a perceptual feedback of the grasping forces to prosthetic hand users," in 2008 IEEE RAS & EMBS 2nd International Conference on Biomedical Robotics and Biomechatronics, BioRob 2008, 2008, pp. 901.
- [21] H. Gray, *Anatomy of the Human Body*, 28 ed, 1966.
- [22] I. K. Kuni Sadamoto, *Mechanical hands illustrated. Revised Edition*: Hemisphere Publishing Corporation, 1987.
- [23] C. Changmök, S. Mihye, K. Suncheol, P. Wonil, and K. Jung, "Understanding of hands and task characteristics for development of biomimetic robot hands," in 2008 IEEE-RAS 8th International Conference on Humanoid Robots, Humanoids 2008, 2008, pp. 413.
- [24] I. MacKay Murray, *Human Anatomy Made Simple: A Comprehensive Course for Self-Study and Review*. Garden City, New York: Doubleday & Company, 1969.
- [25] M. R. Cutkosky, *Robotic Grasping and Fine Manipulation*: Kluwer Academic Publishers, 1985.
- [26] M. Vande Weghe, M. Rogers, M. Weissert, and Y. Matsuoka, "The ACT Hand: design of the skeletal structure," in Robotics and Automation, 2004. Proceedings. ICRA '04. 2004 IEEE International Conference on, 2004, pp. 3375.
- [27] R. Balasubramanian and Y. Matsuoka, "The role of small redundant actuators in precise manipulation," in Robotics and Automation, 2009. ICRA '09. IEEE International Conference on, 2009, pp. 4409.
- [28] A. Guyton and J. Hall, *Textbook of medical physiology*, 11th ed. Philadelphia: Elsevier, 2006.
- [29] R. S. Johansson, "Sensory input and control of grip," *Novartis Foundation Symposium*, 1998, pp. 45.

- [30] J. R. Flanagan, M. C. Bowman, and R. S. Johansson, "Control strategies in object manipulation tasks," *Current Opinion in Neurobiology*, vol. 16, 2006, pp. 650.
- [31] J. R. Flanagan, M. K. O. Burstedt, and R. S. Johansson, "Control of fingertip forces in multidigit manipulation," *Journal of Neurophysiology*, vol. 81, 1999, pp. 1706.
- [32] B. M. Kelly, P. H. Pangilinan Jr, G. M. Rodriguez, R. C. Mipro Jr, and V. S. Bodeau, "Upper Limb Prosthetics." Available: <http://emedicine.medscape.com/article/317234-overview>, last update: January 14, 2009, accessed on July 12, 2010.
- [33] L. Birglen and C. M. Gosselin, "Kinetostatic analysis of underactuated fingers," *IEEE Transactions on Robotics and Automation*, vol. 20, 2004, pp. 211.
- [34] M. C. Carrozza, C. Suppo, F. Sebastiani, B. Massa, F. Vecchi, R. Lazzarini, M. R. Cutkosky, and P. Dario, "The SPRING Hand: Development of a Self-Adaptive Prosthesis for Restoring Natural Grasping," *Autonomous Robots*, vol. 16, 2004, pp. 125.
- [35] C. Cipriani, F. Zaccone, G. Stellin, L. Beccai, G. Cappiello, M. C. Carrozza, and P. Dario, "Closed-loop controller for a bio-inspired multi-fingered underactuated prosthesis," in Proceedings of the 2006 IEEE International Conference on Robotics and Automation, 2006, pp. 2111.
- [36] S. A. Dalley, T. E. Wiste, T. J. Withrow, and M. Goldfarb, "Design of a Multifunctional Anthropomorphic Prosthetic Hand With Extrinsic Actuation," *IEEE/ASME Transactions on Mechatronics*, vol. 14, 2009, pp. 699.
- [37] K. Andrianesis and A. Tzes, "Design of an anthropomorphic prosthetic hand driven by shape memory alloy actuators," in Proceedings of the 2nd Biennial IEEE/RAS-EMBS International Conference on Biomedical Robotics and Biomechatronics, BioRob 2008, 2008, pp. 517.
- [38] S. Y. Jung, S. K. Kang, and I. Moon, "Design of biomimetic hand prosthesis with tendon-driven five fingers," in Proceedings of the 2nd Biennial IEEE/RAS-EMBS International Conference on Biomedical Robotics and Biomechatronics, BioRob 2008, 2008, pp. 895.

- [39] M. Contrözzi, C. Cipriani, and M. C. Carrozza, "Mechatronic design of a transradial cybernetic hand," in IEEE International Conference on Intelligent Robots and Systems, 2008, pp.
- [40] Y. Kamikawa and T. Maeno, "Underactuated five-finger prosthetic hand inspired by grasping force distribution of humans," in 2008 IEEE/RSJ International Conference on Intelligent Robots and Systems, IROS 2008, 2008, pp. 717.
- [41] D. W. Zhao, L. Jiang, H. Huang, M. H. Jin, H. G. Cai, and H. Liu, "Development of a multi-DOF anthropomorphic prosthetic hand," in 2006 IEEE International Conference on Robotics and Biomimetics, ROBIO 2006, 2006, pp. 878.
- [42] H. Huang, L. Jiang, Y. Liu, L. Hou, H. Cai, and H. Liu, "The mechanical design and experiments of HIT/DLR prosthetic hand," in 2006 IEEE International Conference on Robotics and Biomimetics, ROBIO 2006, 2006, pp. 896.
- [43] M. C. Carrozza, G. Cappiello, E. Cavallaro, S. Micera, F. Vecchl, and P. Dario, "Design and control of an underactuated cybernetic artificial hand," in Proceedings of the Sixth Biannual World Automation Congress, WAC, 2004, pp. 111.
- [44] M. C. Carozza, G. Cappiello, G. Stellin, F. Zacccone, F. Vecchi, S. Micera, and P. Dario, "On the development of a novel adaptive prosthetic hand with compliant joints: experimental platform and EMG control," in Intelligent Robots and Systems, 2005. (IROS 2005). 2005 IEEE/RSJ International Conference on, 2005, pp. 1271.
- [45] J. Sung-yoon and M. Inhyuk, "Grip force modeling of a tendon-driven prosthetic hand," in Control, Automation and Systems, 2008. ICCAS 2008. International Conference on, 2008, pp. 2006.
- [46] H. Takeda, N. Tsujiuchi, T. Koizumi, H. Kan, M. Hirano, and Y. Nakamura, "Development of prosthetic arm with pneumatic prosthetic hand and tendon-driven wrist," in Engineering in Medicine and Biology Society, 2009. EMBC 2009. Annual International Conference of the IEEE, 2009, pp. 5048.
- [47] K. B. Fite, T. J. Withrow, S. Xiangrong, K. W. Wait, J. E. Mitchell, and M. Goldfarb, "A Gas-Actuated Anthropomorphic Prosthesis for Transhumeral Amputees," *Robotics, IEEE Transactions on*, vol. 24, 2008, pp. 159.

- [48] B. B. Edin, L. Beccai, L. Ascari, S. Roccella, J. J. Cabibihan, and M. C. Carrozza, "A bio-inspired approach for the design and characterization of a tactile sensory system for a cybernetic prosthetic hand," in Proceedings of the 2006 IEEE International Conference on Robotics and Automation, 2006, pp. 1354.
- [49] C. Cipriani, M. Controzzi, F. Vecchi, and M. C. Carrozza, "Embedded hardware architecture based on microcontrollers for the action and perception of a transradial prosthesis," in Proceedings of the 2nd Biennial IEEE/RAS-EMBS International Conference on Biomedical Robotics and Biomechatronics, BioRob 2008, 2008, pp. 848.
- [50] D. P. J. Cotton, A. Cranny, P. M. Chappell, N. M. White, and S. P. Beeby, "Control strategies for a multiple degree of freedom prosthetic hand," *Measurement and Control*, vol. 40, 2007, pp. 24.
- [51] "SensorHand, Otto Bock Healthcare, Minneapolis, MN." Available: www.ottobockus.com, last update: 2010, accessed on July 19, 2010.
- [52] S. Adey, "The revolution will be prosthetized," *Spectrum, IEEE*, vol. 46, 2009, pp. 44.
- [53] G. Lundborg and B. Rosén, "Sensory substitution in prosthetics," *Hand Clinics*, vol. 17, 2001, pp. 481.
- [54] D. Goger, N. Gorges, and H. Worn, "Tactile sensing for an anthropomorphic robotic hand: Hardware and signal processing," in Robotics and Automation, 2009. ICRA '09. IEEE International Conference on, 2009, pp. 895.
- [55] J. Carpaneto, S. Micera, F. Zaccone, F. Vecchi, and P. Dario, "A Sensorized Thumb for Force Closed-Loop Control of Hand Neuroprostheses," *IEEE Transactions on Neural Systems and Rehabilitation Engineering*, vol. 11, 2003, pp. 346.
- [56] B. B. Edin, L. Ascari, L. Beccai, S. Roccella, J. J. Cabibihan, and M. C. Carrozza, "Bio-inspired sensorization of a biomechatronic robot hand for the grasp-and-lift task," *Brain Research Bulletin*, vol. 75, 2008, pp. 785.
- [57] N. Wettels, V. J. Santos, R. S. Johansson, and G. E. Loeb, "Biomimetic tactile sensor array," *Advanced Robotics*, vol. 22, 2008, pp. 829.

- [58] J. A. Fishel, V. J. Santos, and G. E. Loeb, "A robust micro-vibration sensor for biomimetic fingertips," in *Biomedical Robotics and Biomechanics*, 2008. BioRob 2008. 2nd IEEE RAS & EMBS International Conference on, 2008, pp. 659.
- [59] L. Beccai, S. Roccella, L. Ascari, P. Valdastri, A. Sieber, M. C. Carrozza, and P. Dario, "Development and experimental analysis of a soft compliant tactile microsensor for anthropomorphic artificial hand," *IEEE/ASME Transactions on Mechatronics*, vol. 13, 2008, pp. 158.
- [60] P. H. Chappell and J. A. Elliott, "Contact force sensor for artificial hands with a digital interface for a controller," *Measurement Science and Technology*, vol. 14, 2003, pp. 1275.
- [61] A. Cranny, D. P. J. Cotton, P. H. Chappell, S. P. Beeby, and N. M. White, "Thick-film force, slip and temperature sensors for a prosthetic hand," *Measurement Science and Technology*, vol. 16, 2005, pp. 931.
- [62] D. P. J. Cotton, P. H. Chappell, A. Cranny, N. M. White, and S. P. Beeby, "A novel thick-film piezoelectric slip sensor for a prosthetic hand," *IEEE Sensors Journal*, vol. 7, 2007, pp. 752.
- [63] A. Persichetti, F. Vecchi, and M. C. Carrozza, "Optoelectronic-Based Flexible Contact Sensor for Prosthetic Hand Application," in *Rehabilitation Robotics*, 2007. ICORR 2007. IEEE 10th International Conference on, 2007, pp. 415.
- [64] E. D. Engeberg, S. G. Meek, and M. A. Minor, "Hybrid force-velocity sliding mode control of a prosthetic hand," *IEEE Transactions on Biomedical Engineering*, vol. 55, 2008, pp. 1572.
- [65] E. D. Engeberg and S. Meek, "Improved Grasp Force Sensitivity for Prosthetic Hands Through Force-Derivative Feedback," *IEEE Transactions on Biomedical Engineering*, vol. 55, 2008, pp. 817.
- [66] G. Matrone, C. Cipriani, E. L. Secco, M. C. Carrozza, and G. Magenes, "Bio-inspired controller for a dexterous prosthetic hand based on principal components analysis," in *Engineering in Medicine and Biology Society*, 2009. EMBC 2009. Annual International Conference of the IEEE, 2009, pp. 5022.

- [67] Z. Jingdong, J. Li, S. Shicai, C. Hegao, L. Hong, and G. Hirzinger, "A Five-fingered Underactuated Prosthetic Hand System," in Proceedings of the 2006 IEEE International Conference on Mechatronics and Automation, 2006, pp. 1453.
- [68] J. Žajdlík, "The preliminary design and motion control of a five-fingered prosthetic hand," in 10th International Conference on Intelligent Engineering Systems, INES 2006, 2006, pp. 202.
- [69] N. Tsujiuchi, K. Takayuki, and M. Yoneda, "Manipulation of a robot by EMG signals using linear multiple regression model," in 2004 IEEE/RSJ International Conference on Intelligent Robots and Systems (IROS), 2004, pp. 1991.
- [70] R. F. Weir and A. B. Ajiboye, "A Multifunction Prosthesis Controller based on Fuzzy-Logic Techniques," in Proceedings of the Annual International Conference of the IEEE Engineering in Medicine and Biology, 2003, pp. 1678.
- [71] Z. Jingdong, X. Zongwu, J. Li, C. Hegao, L. Hong, and G. Hirzinger, "EMG Control for a Five-fingered Underactuated Prosthetic Hand Based on Wavelet Transform and Sample Entropy," in Intelligent Robots and Systems, 2006 IEEE/RSJ International Conference on, 2006, pp. 3215.
- [72] Y. Dapeng, Z. Jingdong, G. Yikun, J. Li, and L. Hong, "EMG pattern recognition and grasping force estimation: Improvement to the myocontrol of multi-DOF prosthetic hands," in Intelligent Robots and Systems, 2009. IROS 2009. IEEE/RSJ International Conference on, 2009, pp. 516.
- [73] Z. Jingdong, X. Zongwu, J. Li, C. Hegao, L. Hong, and G. Hirzinger, "Levenberg-Marquardt Based Neural Network Control for a Five-fingered Prosthetic Hand," in Robotics and Automation, 2005. ICRA 2005. Proceedings of the 2005 IEEE International Conference on, 2005, pp. 4482.
- [74] R. J. Smith, F. Tenore, D. Huberdeau, R. Etienne-Cummings, and N. V. Thakor, "Continuous decoding of finger position from surface EMG signals for the control of powered prostheses." in Engineering in Medicine and Biology Society, 2008. EMBS 2008. 30th Annual International Conference of the IEEE, 2008, pp. 197.
- [75] C. Cipriani, C. Antfolk, C. Balkenius, B. Rosen, G. Lundborg, M. C. Carrozza, and F. Sebelius, "A Novel Concept for a Prosthetic Hand With a Bidirectional Interface: A Feasibility Study," *Biomedical Engineering, IEEE Transactions on*, vol. 56, 2009, pp. 2739.

- [76] L. E. Rodriguez-Cheu and A. Casals, "Sensing and control of a prosthetic hand with myoelectric feedback," in Proceedings of the First IEEE/RAS-EMBS International Conference on Biomedical Robotics and Biomechatronics, BioRob 2006, 2006, pp. 607.
- [77] G. S. Dhillon and K. W. Horch, "Direct neural sensory feedback and control of a prosthetic arm," *IEEE Transactions on Neural Systems and Rehabilitation Engineering*, vol. 13, 2005, pp. 468.
- [78] A. Panarese, B. B. Edin, F. Vecchi, M. C. Carrozza, and R. S. Johansson, "Humans Can Integrate Force Feedback to Toes in Their Sensorimotor Control of a Robotic Hand," *Neural Systems and Rehabilitation Engineering, IEEE Transactions on*, vol. 17, 2009, pp. 560.
- [79] C. Pylatiuk, S. Mounier, A. Kargov, S. Schulz, and G. Bretthauer, "Progress in the development of a multifunctional hand prosthesis," in Engineering in Medicine and Biology Society, 2004. IEMBS '04. 26th Annual International Conference of the IEEE, 2004, pp. 4260.
- [80] N. Wettels, A. R. Parnandi, J. H. Moon, G. E. Loeb, and G. S. Sukhatme, "Grip control using biomimetic tactile sensing systems," *IEEE/ASME Transactions on Mechatronics*, vol. 14, 2009, pp. 718.
- [81] E. D. Engeberg and S. G. Meek, "Adaptive object slip prevention for prosthetic hands through proportional-derivative shear force feedback," in 2008 IEEE/RSJ International Conference on Intelligent Robots and Systems, IROS 2008, 2008, pp. 1940.
- [82] A. Tura, C. Lamberti, A. Davalli, and R. Sacchetti, "Experimental development of a sensory control system for an upper limb myoelectric prosthesis with cosmetic covering," *Journal of Rehabilitation Research and Development*, vol. 35, 1998, pp. 14.
- [83] E. Mangieri, A. Ahmadi, K. Maharatna, S. A. Ahmad, and P. H. Chappell, "A novel analogue circuit for controlling prosthetic hands," in Biomedical Circuits and Systems Conference, 2008. BioCAS 2008. IEEE, 2008, pp. 81.
- [84] C. Cipriani, F. Zaccone, S. Micera, and M. C. Carrozza, "On the shared control of an EMG-controlled prosthetic hand: Analysis of user-prosthesis interaction," *IEEE Transactions on Robotics*, vol. 24, 2008, pp. 170.

- [85] Z. Z. Luo, F. Wang, and R. C. Wang, "Study of multi-freedom myoelectric prostheses with tactile sense," in Proceedings of the Annual International Conference of the IEEE Engineering in Medicine and Biology, 2005, pp. 3004.
- [86] E. Ullmann, F. Cepolina, and M. Zoppi, "Upper limb prosthesis for developing countries," in IEEE International Conference on Intelligent Manipulation and Grasping IMG 04, Genova, Italy, 2004, pp.
- [87] R. Doshi, C. Yeh, and M. Leblanc, "The design and development of a gloveless endoskeletal prosthetic hand," *Journal of Rehabilitation Research and Development*, vol. 35, 1998, pp. 388.
- [88] C. Yoonju, L. Kelvin, F. Folowosele, B. Miller, and N. V. Thakor, "Wireless Temperature Sensing Cosmesis for Prosthesis," in 2007 IEEE 10th International Conference on Rehabilitation Robotics, ICORR 2007, 2007, pp. 672.
- [89] M. R. Cutkosky, "On grasp choice, grasp models, and the design of hands for manufacturing tasks," *IEEE Transactions on Robotics and Automation*, vol. 5, 1989, pp. 269.
- [90] L. Birglen and C. M. Gosselin, "Fuzzy enhanced control of an underactuated finger using tactile and position sensors," in Proceedings of the 2005 IEEE International Conference on Robotics and Automation, 2005, pp. 2320.
- [91] H. R. Sun, P. Li, and L. H. Zhou, "A strategy of generalized predictive control based on neural network," in Proceedings of 2004 International Conference on Machine Learning and Cybernetics, 2004, pp. 483.
- [92] J. R. Noriega and H. Wang, "A direct adaptive neural-network control for unknown nonlinear systems and Its application," *IEEE Transactions on Neural Networks*, vol. 9, 1998, pp. 27.
- [93] Y. Haichen and Z. Zhijun, "Predictive Control Based on Neural Networks of The Chemical Process," in Control Conference, 2006. CCC 2006. Chinese, 2006, pp. 1143.
- [94] J. Hao, S. Tan, and J. Vandewalle, "One step ahead predictive control of nonlinear systems by neural networks," in Neural Networks, 1993. IJCNN '93-Nagoya. Proceedings of 1993 International Joint Conference on, 1993, pp. 2761.

- [95] S. Qiang, L. Fang, and R. D. Findlay, "Generalized Predictive Control for a Pneumatic System: Based on an Optimized ARMAX Model with an Artificial Neural Network," in *Computational Intelligence for Modelling, Control and Automation, 2006 and International Conference on Intelligent Agents, Web Technologies and Internet Commerce, International Conference on*, 2006, pp. 223.
- [96] P. Haley, D. Soloway, and B. Gold, "Real-time adaptive control using neural generalized predictive control," in *American Control Conference, 1999. Proceedings of the 1999*, 1999, pp. 4278.
- [97] D. Soloway and P. Haley, "Aircraft reconfiguration using neural generalized predictive control," in *American Control Conference, 2001. Proceedings of the 2001*, 2001, pp. 2924.
- [98] B. Bandyopadhyay, "Neural network based predictive controller (NNPC): An investigation into its application in Textiles," in *Computational Intelligence for Modelling, Control and Automation, 2005 and International Conference on Intelligent Agents, Web Technologies and Internet Commerce, International Conference on*, 2005, pp. 963.
- [99] O. A. Dahunsi, J. O. Pedro, and O. T. Nyandoro, "Neural network-based model predictive control of a servo-hydraulic vehicle suspension system," in *AFRICON, 2009. AFRICON '09.*, 2009, pp. 1.
- [100] M. Nrgaard, O. Ravn, N. K. Poulsen, P. M. Norgaard, and L. K. Hansen, "Neural Networks for Modelling and Control of Dynamic Systems: A Practitioner's Handbook," *Advanced Textbooks in Control and Signal Processing*, 2000.
- [101] K. Hornik, M. Stinchcombe, and H. White, "Multilayer feedforward networks are universal approximators," *Neural Networks*, vol. 2, 1989, pp. 359.
- [102] J. W. Han and M. Kamber, *Data Mining Concepts and Techniques*: Elsevier, 2006.
- [103] H. Demuth, M. Beale, and M. Hagan, "Neural network toolbox 5-User's Guide," The Mathworks.
- [104] C. Bishop, *Pattern recognition and machine learning*: Springer, 2006.

- [105] M. Norgaard, O. Ravn, and N. K. Poulsen, "NNSYSID and NNCTRL tools for system identification and control with neural networks," *Computing & Control Engineering Journal*, vol. 12, 2001, pp. 29.
- [106] N. Wettels, D. Popovic, V. J. Santos, R. S. Johansson, and G. E. Loeb, "Biomimetic tactile sensor for control of grip," in 2007 IEEE 10th International Conference on Rehabilitation Robotics, ICORR'07, 2007, pp. 923.
- [107] P. J. Kyberd, M. Evans, and S. Te Winkel, "An intelligent anthropomorphic hand, with automatic grasp," *Robotica*, vol. 16, 1998, pp. 531.
- [108] R. L. Burden and J. D. Faires, *Numerical Analysis*, 8 ed: Brooks Cole, 2004.
- [109] R. S. Johansson and G. Westling, "Signals in tactile afferents from the fingers eliciting adaptive motor responses during precision grip," *Experimental Brain Research*, vol. 66, 1987, pp. 141.
- [110] G. A. Kragten and J. L. Herder, "The ability of underactuated hands to grasp and hold objects," *Mechanism and Machine Theory*, vol. 45, 2010, pp. 408.
- [111] D. Gunji, Y. Mizoguchi, S. Teshigawara, A. Ming, A. Namiki, M. Ishikawaand, and M. Shimojo, "Grasping force control of multi-fingered robot hand based on slip detection using tactile sensor," in Proceedings of the IEEE International Conference on Robotics and Automation, 2008, pp. 2605.
- [112] J. Schuurmans, R. Q. van der Linde, D. H. Plettenburg, and F. C. van der Helm, "Grasp force optimization in the design of an underactuated robotic hand," in 2007 IEEE 10th International Conference on Rehabilitation Robotics, ICORR 2007, 2007, pp. 776.
- [113] A. Kargov, C. Pylatiuk, J. Martin, S. Schulz, and L. Doderlein, "A comparison of the grip force distribution in natural hands and in prosthetic hands," *Disability and Rehabilitation*, vol. 26, 2004, pp. 705.
- [114] "Arduino." Available: <http://www.arduino.cc/>, last update: June 28, 2010, accessed on July, 29, 2010.